OPTIMIZATION OF ACTIVATION FOIL PASSIVE NEUTRON DETECTORS

A Dissertation
Presented to
The Academic Faculty

by

Peter R. Exline

In Partial Fulfillment
of the Requirements for the Degree
PhD in Nuclear and Radiological Engineering in the
School of Mechanical Engineering

Georgia Institute of Technology
May 2019

OPTIMIZATION OF ACTIVATION FOIL PASSIVE NEUTRON DETECTORS

Approved by:

Dr. Nolan E. Hertel, Advisor
School of Mechanical Engineering
Georgia Institute of Technology

Dr. Douglas E. Peplow
Nuclear Security Division
Oak Ridge National Laboratory

Dr. Steven R. Biegalski
School of Mechanical Engineering
Georgia Institute of Technology

Dr. Wayne E. Whiteman
School of Mechanical Engineering
Georgia Institute of Technology

Dr. Margaret E. Kosal
School of International Affairs
Georgia Institute of Technology

Date Approved: March 25, 2019

[To those I have served with]

ACKNOWLEDGEMENTS

I would like to thank first the folks who gave me an opportunity to go back to Georgia Tech while still in the US Army to complete a PhD, including COL Jeffrey Becker, the commander who approved my assignment to Functional Area 52, and Mr. Rob Beimler, who worked to help me make the move and provided this opportunity.

I am grateful for Dr. Jeff Johnson and Dr. Vince Jodoin for introducing me to the AFIDS project and truly making me part of the team at Oak Ridge. Ms. Kristen Gunter was also invaluable in helping me navigate the different access and clearance processes.

The experimental portion would have been impossible without the tireless work of Ms. Christina Tabor, who went far beyond the call of duty in her radiation safety role to help me coordinate a complex set of experiments from 150 miles away. My fellow students Jacob Inman, Caleigh Samuels, Steven Mellard and Hannah Watkins also helped selflessly.

Thank you Dr. Margaret Kosal and the Sam Nunn Security Program Fellows for a very enjoyable and enlightening year. You challenge my thinking and make me better, and have made me a better Army officer over the past decade.

Thank you to COL(R) Wayne Whiteman for giving "Cadet Exline" one more chance to improve on that B+ in ME471 from Fall 2000, and for giving great advice on how to organize and communicate my research efforts, and help with my transition to a civilian institution.

Thank you to Dr. Steven Biegalski, who despite the demands of his position, always had time for detailed conversations where he provided the depth of knowledge and experience I needed in designing experiments and challenging assumptions.

Thank you, Dr. Douglas Peplow, who not only provided daily advice, guidance and mentorship on this project, but truly educated me not only on the math but on how to do research and writing correctly. His patience and effort are unmatched and greatly improved this work.

Thank you to Dr. Nolan Hertel for inviting me back to the team and giving me everything I needed to make this dream happen. Your advice, mentorship and support have made it possible for me to learn so much about nuclear engineering and have prepared me to learn even more going forward.

Thank you, Jessica and Riley, for your patience, love, and comma deletions.

TABLE OF CONTENTS

LIST OF TABLES

LIST OF FIGURES

LIST OF SYMBOLS AND ABBREVIATIONS

AFIDS	Activation Foil Integrated Detector System
Ag	silver
Al	aluminum
Al-1100	Aluminum alloy 1100 (designated by American Society for Materials)
Al-6061	Aluminum alloy 6061 (designated by American Society for Materials)
ASTM	American Society for Testing and Materials
Au	gold
Bi	bismuth
Co	cobalt
Cr	chromium
Cu	copper
ENDF	Evaluated Nuclear Data File
Fe	iron
FM	Fat Man spectrum
FORTRAN	FORmula TRANslation, a computer programming language
FUS	Fusion spectrum
Ge	germanium
Hf	hafnium
HPGe	High Purity Germanium detector
In	indium
Ir	iridium
kt	kiloton (of nuclear weapons yield)
LB	Little Boy spectrum

Mt	megaton (of nuclear weapons yield)
MCNP	Monte Carlo N-Particle code
Mg	magnesium
NAA	Neutron Activation Analysis
Nb	niobium
Ni	nickel
Pb	lead
Pd	palladium
Re	rhenium
Rh	rhodium
SCALE	Standardized Computer Analyses for Licensing Evaluation
Si	silicon
Sn	tin
t	ton (of nuclear weapons yield)
Ta	tantalum
Ti	titanium
W	tungsten

SUMMARY

Passive neutron detectors, including activation foils, use neutron absorption reactions with known cross sections to determine a level of neutron radiation received over time. Activation foils are chosen for a specific neutron measurement application based on their reaction probabilities cross section at various neutron energy levels and the properties of the activation products which result from those reactions.

Different activation foil nuclides have strongly varying neutron cross sections at different energy levels. By selecting an appropriate set of foils, the energy dependence of the neutron field can be characterized and information about the spectrum and the magnitude of the fluence can be obtained. For the Activation Foil Integrated Detector System (AFIDS), a specific set of activation wires is used to distinguish between different nuclear weapons detonation leakage spectra.

The selection of various elements for use in foils and their dimensions for AFIDS was initially based on informed judgement, but no rigorous optimization of the set was done. Since this system could be deployed in cities nationwide, cost is a key consideration alongside the ability to accurately distinguish different spectra.

This research will provide a method to optimize both the AFIDS activation detectors and the cost while maintaining feasibility and reliability for this application. A computer code has been developed to perform this optimization and it can be generalized for the use of activation detectors in many different applications and for a range of expected spectra.

CHAPTER 1. INTRODUCTION

"No threat poses as grave a danger to our security and well-being as the potential use of nuclear weapons and materials by irresponsible states or terrorists." – National Security Strategy, February 2015. [1]

Nuclear weapons are one of the gravest threats to the safety and security of the United States. In the past, only a few of the more technically advanced nations had the capacity to field such weapons potentially against the United States, and a sophisticated system of deterrence has evolved in the international sphere that serves to reduce the likelihood of a devastating nuclear exchange.

In more recent years, nuclear proliferation has spread to more states, including the rogue nation of North Korea. A small number of other nations have been working to build their own nuclear weapons, including those with close ties to terrorist groups. Instead of simply deterring the massive Russian threat, the United States now faces multiple potential actors, some of which may not be as easily deterred by the US nuclear arsenal.

A key aspect of deterrence in this new era is determining the origin of an attack. If there is no missile to track from its origin, but if, for example, the nuclear explosion originated from a stack of cargo containers in a port facility, it is of vital interest to determine the origin of the weapon, as well as information about its yield, the distribution of radioactive effects, etc. These nuclear forensics efforts depend on both nuclear and radiological analysis alongside conventional forensic and investigative techniques. There

is a demand for technology and equipment that can assist in the rapid assessment of the nature and origin of a nuclear detonation.

In the only cases of a nuclear weapon used against targets in wartime, the United States dropped two atomic bombs on Hiroshima and Nagasaki, Japan in 1945. While the origin and design of these weapons are known, the effects of the weapons over those city areas has been studied extensively for decades, incorporating a host of techniques. One technique has been looking for metals that were activated by the high flux of neutrons from the atomic bombs. Some of the nuclides in these materials reacted with the bomb neutrons to become radioactive isotopes with sufficiently long half-lives to be used as activation detectors following nuclear detonations to back calculate estimates of the neutron fluxes at various locations. These neutron fluxes can further used to compute radiation yields and other properties of the detonated bombs.

To further expound on the use of isotopes of various elements as activation detectors, the probability of such nuclides in being transformed into radionuclides are directly related to their neutron cross sections. These cross sections can be highly sensitive to the energies of the neutrons and vary greatly between different nuclides. By identifying the residual radioactivity levels in collected samples after a detonation, for example of activated building materials and structural components, coupled with knowing their precise composition and mass as well as the time elapsed since their activation, a picture can be constructed of the neutron fluence in terms of magnitude, distribution in energy, and location with respect to the weapon detonation.

A problem arises – it is difficult to determine the exact composition of materials collected from existing infrastructure post-denotation, especially when the detonation was far in the past. Suitable quantities of useful samples with activation products have to be located post-detonation to do such an analysis from existing infrastructure, and they may not be found in areas where information is needed. A possible solution for this shortcoming is put forth by the Activation Foil Integrated Detector System (AFIDS), developed at Oak Ridge National Laboratory over the past decade. This system of activation detection assemblies would be deployed prior to any event and left in place. Pictures of a previous AFIDS detector prototype are in Figure 1; the current distribution of target activation foils/wires is in Figure 2.

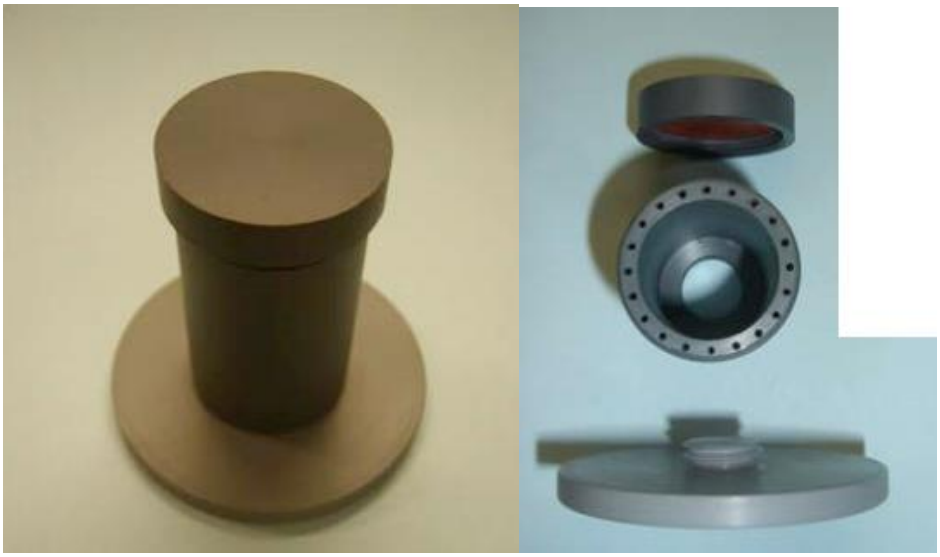

Figure 1 - PVC Model of AFIDS Detector Body (previous design iteration)

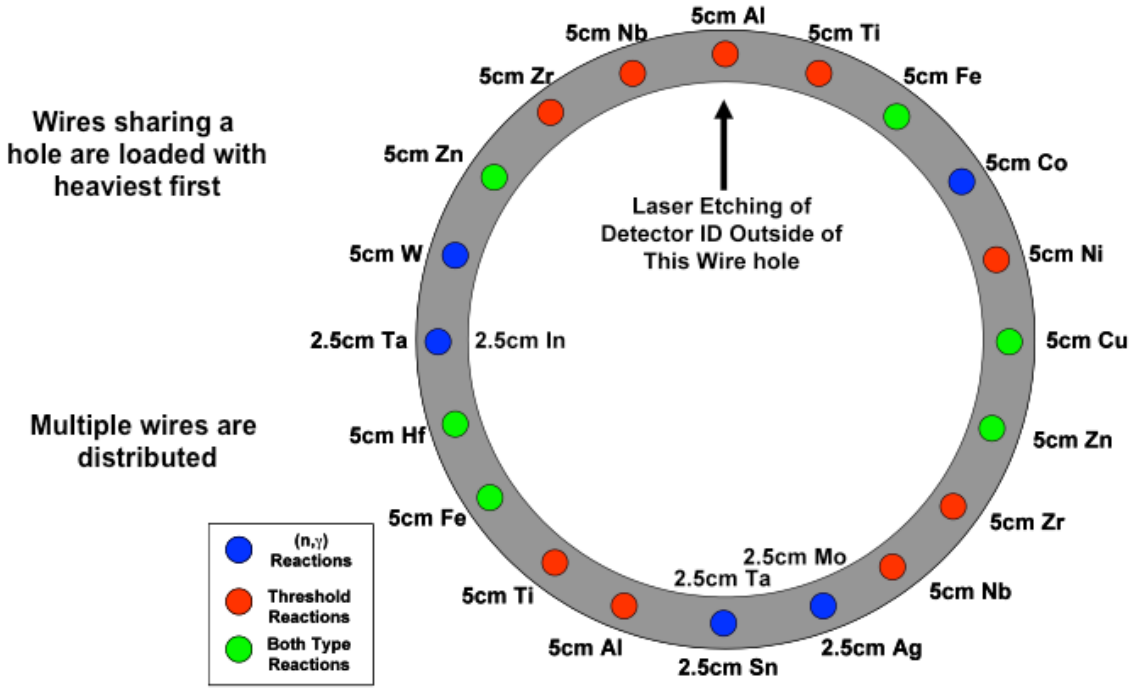

Figure 2 - Current target foil/wire configuration

The AFIDS detector solves the composition, mass, and lack of useful element issues of the activation analysis by deliberately placing high-purity metal activation foils in locations spread out in a potential target area. Since the composition, mass, and location of each target material is well-known, in the event of a nuclear detonation, the level of radioactivity present (due to neutron activation) would provide high-quality data that can be used by the Oak Ridge-developed SLEUTH[1] algorithm to determine a best fit for the nuclear weapon's leakage spectra. A screenshot of this code in Figure 3 shows how detectors may be arrayed in different locations to help piece together the event.

[1] The SLEUTH code has been superseded with newer codes, but the underlying processes are the same, and the screenshot is the best available illustration of the concept.

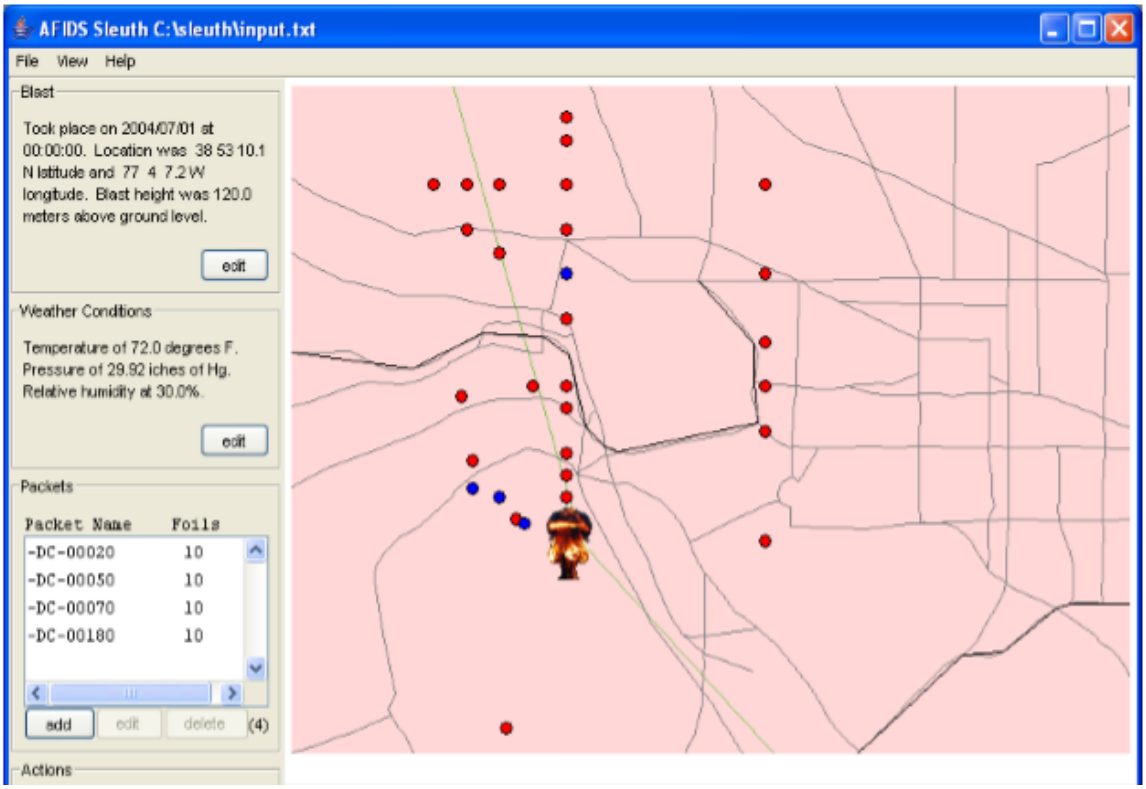

Figure 3 - Screenshot of SLEUTH Code

In the AFIDS approach to neutron detection, the neutrons activate metals and the resulting isotopes give off gamma-ray radiation over time as they decay. Gammas are easily counted by high purity germanium (HPGe) detectors, and their energies can be determined with high resolution by an HPGe detector. The activation nuclear reactions are generally well-characterized and available through the data libraries such as those in the SCALE code package.[2]

---

[2] Standardized Computer Analyses for Licensing Evaluation. The SCALE code system is a widely used modeling and simulation suite for nuclear safety analysis and design that is

While the original AFIDS detector underwent some initial radiation testing, several issues arose. The PVC holder had to be replaced with a different material due to the production of long-lived radioactive chlorine in the holder material. Aluminum is the currently proposed holder material and due for testing. Further, the choice of activation detector materials was not optimized to maximize the ability to differentiate between various nuclear weapon leakage spectra at a variety of times post-denotation while meeting cost constraints. This research presented herein is focused on this optimization and developing algorithms to both meet the needs of the AFIDS project and for general applications of activation detectors.

1.1 Objectives of Research

1.1.1 Primary Objectives

The primary objectives of the research presented in this dissertation were:

1. Creation of an algorithm for optimizing the selection of activation foil/wire materials for the AFIDS setup based on the ability to distinguish between bomb leakage spectra, provide activation products at sufficiently high levels coupled with adequate half-lives to count at various decay times post-event, and purchased at reasonable costs. Code the algorithm from objective 1 into a stand-alone, well-

---

developed, maintained, tested, and managed by the Reactor and Nuclear Systems Division (RNSD) of the Oak Ridge National Laboratory (ORNL). More information is available at https://www.ornl.gov/scale/overview.

documented software package with documented input (to include leakage spectra to be distinguished between, physical and nuclear properties of materials, etc.)

2. Optimize the current AFIDS design against unclassified nuclear weapons leakage spectra subject to cost goals.

1.1.2 Secondary Objectives

The effort presented in the dissertation had secondary objectives which include:

1. Experimentally validate the current AFIDS prototype against existing activation/count rate predictions and radiation transport modeling.
2. Test the effects of different alloys of aluminum on the current AFIDS prototype, with the goal of reducing cost if less expensive aluminum alloys are suitable.
3. Test the effects of varying size of target rods and/or using multiple copies of the same elemental rod.
4. Capture lessons learned from the experimental validation for future studies.

1.2 Relation to the Longer-Term AFIDS Project

One of the primary objectives of this research is to optimize the current AFIDS design's ability to discriminate between nuclear weapons leakage spectra subject to practical cost constraints.

The initial AFIDS design was completed during 2006 and refined in 2008 after experimentation was constrained by budget and time. The researchers at the time state "No optimization was performed to determine if all these wires were needed, if high purity was required, or whether PVC was the most optimum holder material." [2] It has since been

determined that PVC is not a feasible holder material due to radioactive chlorine byproducts when PVC is irradiated with neutrons. This research lead to modifications in the original design to optimize it and create an algorithm to allow computer-based optimization against different leakage spectra and constraints.

The initial elements selected for wires considered by the AFIDS team were based on experience, cost, and the availability. However, the 16 elements considered are only a small breadth of the practical search space that exceeds 70 elements once a few practical filters are applied.[3] By leveraging a computer-based approach, a much larger search space can be comprehensively checked for desirable combination of cross section plus activation levels versus energy and cost.[4] Further, a set of elements may be pieced together that covers a range of energy levels and decay times in a way that would be very labor intensive to do by hand. Solving this problem with specific constraints by investigating all combinations exhaustively is not feasible within reasonable computation times.[5]

A secondary objective of the research was to experimentally validate the current AFIDS prototype against the modeling previously carried out and done in more detail

---

[3] These filters include minimum melting points and the exclusion of transuranic elements. Elements that are gases or liquids at room temperature were not considered; however, elements like carbon with a solid form at room temperature were considered. Chemical compounds have not yet been considered; this may be a way to take advantage of low melting point elements that have suitable nuclear properties.

[4] The AFIDS work focuses on lower-yield nuclear weapons, in the low kt to ~20 kt range, with detectors optimized against activity levels resulting after transport from such weapons.

[5] The 27 commercially-available elements to be distributed between 20 available slots in the detector body create over 10^{28} combinations that would need to be compared.

during this research. Several simplifying assumptions were made in the initial modeling based on the geometry of the holder and the target wires. These assumptions include that the effects of self-shielding are negligible for materials that are relatively thin, and, similarly, that the effects of down-scattering on the incoming flux spectra are negligible within the detector itself since a low proportion of neutrons will have interactions with the detector or holder. After testing during this research, the decision was made to add fidelity to the model to account for detector shielding and angular effects.

Additionally, two different aluminum alloys were tested as the replacement for PVC for the holder in this work. Aluminum-1100 is a commercial high-purity alloy (99%+ Al) and aluminum-6061 is a more commonly produced alloy (~98.5%). The research will determine the difference in flux at the target rod locations between holders made of the two different alloys, with a goal of informing whether the less expensive aluminum-6061 is suitable for detection purposes.

1.3 Relation to Present State of Knowledge and Other Current Research

This research is related to the field of neutron activation analysis commonly used to identify elements in a given sample by bombarding the material to be tested with neutrons (of known energy distribution and quantity) and measuring resulting radioactivity. However, this research, as well as the AFIDS project, works the problem in the opposite direction – given well-known materials and locations, it attempts to determine the incoming neutron flux spectra.

There are standard methods for characterizing fluence based on activations outlined in American Society for Testing and Materials (ASTM) International Standards 261

(general) [3] and 526 [4] (specifically for higher energy neutrons). Those techniques only seek to find neutron fluence in very broad energy spectral ranges (epithermal, thermal, over 4.4 MeV, etc.) which is not enough to distinguish between nuclear weapon types. These standards are useful for outlining an experimental approach and listing potential sources of error to watch for in the larger search space.

Similar work to this was conducted in Japan after the atomic bombings at the end of World War II. [5] Even decades later, low-level residual radiation has been used to characterize the neutron flux from the weapons dropped on Hiroshima and Nagasaki. Part of the difficulty of this work is finding sufficient quantities of useful materials with appropriate compositions in the places that they are needed to generate a complete picture of the dose received over the cities.

The AFIDS project seeks to turn this weakness in the process into a strength by placing high purity, well-characterized target materials at specified locations in an array that can be used post-blast to quickly provide information about yield and the neutron energy spectrum of the fluence. These pieces of information can significantly inform nuclear forensic analysis and attribution. [2]

The AFIDS project currently uses an Oak Ridge National Laboratory-developed code-named SLEUTH to interpret the results of the AFIDS detector's target foils. It accounts for the distance from ground zero of each detector and can adjust the count rates by accounting for expected shaping of the flux spectra due to the local surroundings, especially in an urban environment. It then uses the count rates to determine a best fit for

the weapon's initial leakage spectrum, based on defined candidate spectra. The code uses a chi-squared goodness-of-fit test to select the best estimate.

Part of this research investigates an optimization of the system, with the goal of maximizing the target array's ability to discriminate between possible starting leakage spectra with the highest certainty possible. There is literature describing using the chi-squared test to best fit models, but there is not research readily available on working the problem in reverse – optimizing the choice of data sources to increase the ability to discriminate between competing data sets.

While the AFIDS project is not exclusively designed as a nuclear forensics tool (it is useful for consequence management and medical response planning, for instance), it complements other capabilities in this by its unique nature. It is a passive design that will be a very low-cost, deployable system with almost no maintenance requirements or maintenance costs. This will let it be deployed widely in a way that active detection systems cannot. Since it does not depend on a power supply or sophisticated circuitry, but fundamental physics, it cannot fail unless it is melted or rendered irretrievable. (Some of the detectors closest to the blast are likely to be melted, but having an affordable large array mitigates this.)

By providing gamma spectra upon being counted, the retrieval of the activation levels is based on well-developed methods. In addition, the data would still be useful in the events that errors in modeling are later uncovered or better techniques for reconstructing the spectra from the activation data are developed. At least one target wire should have a

sufficiently long half-life to leave the door open for researchers to do first-hand analysis with improved equipment years after the fact.

CHAPTER 2. BACKGROUND

2.1 Neutron Activation Analysis

Neutron activation analysis (NAA) is the process of determining information about a spectrum of neutrons (quantities and energy distribution) indirectly by counting the gamma rays emitted by the activation products the neutrons create when they interact with target materials. The neutrons interact with matter in different ways, including being captured or scattered. Typical reactions are (n,γ) for an incoming neutron being captured with an immediate gamma ray being released; (n,p) for an incoming neutron being captured and a proton being released; (n,n') for a scattering event, where the neutron exits with a different energy level than the incoming; and (n,α) where the incoming neutron leads to an alpha particle being released. There are more complex reactions as well.

2.1.1 Determining Activation Probabilities

The likelihood of any of these reactions depends on the cross section neutron cross section of the material targeted. The cross sections are dependent on the energy of the incoming neutrons, and many reactions possess resonance locations in the interaction probability where reactions are much more likely to occur. In this research, cross sections binned into 200 energy groups from the SCALE package are generally used. The cross sections are also dependent not only on element but on the individual isotopes of that element. Different isotopes of the same element can have very different cross sections due to the physics inside of the nucleus.

As reactions occur, the material becomes activated, meaning it has been transformed by the reaction into different isotopes (and sometimes different elements) that are now radioactive. Generally speaking, only a very small portion of the atoms present activate, while the vast majority remain the original isotope. This is important because it is an underlying assumption in this work that the burnup of the original isotope is so small as to be neglected when calculating the estimated number of reactions.

2.1.2 Decay of Activation Products

The activated isotopes are normally radioactive and decay subsequent to their creation. The half-lives of these decays vary from sub-microseconds to hundreds of years or more. Longer lived activation products will be slow to decay and lead to fewer gamma-ray emissions per unit time and subsequently a lower count rate when the activation detector is counted. Short lived activation products decay quickly but lead to high count rates if they can be counted after decay times on the order of multiples of their half-lives.

When the radioactive activation product decays, it emits a gamma ray (sometimes indirectly, in the case of positron emission leading to an annihilation event that produces a gamma ray). The gamma ray emitted is not correlated with the original neutron energy. Also, a single activation product may have many gamma-ray energies it can emit depending on different transitions in the nucleus as it decays. These gamma ray yields have fixed probabilities for a given radionuclide referred to as branching ratios.

2.1.3 Gamma Ray Counting

For the gamma rays to be counted in a detector, they must first escape the original target material. As previously stated, the burnup of the original nuclides of which the activation detector is composed is unchanged in a practical sense. So, the attenuation of emitted gamma rays from the activation detectors can be assumed to be the original material composition. The attenuation coefficients needed to perform this escape calculation is dependent on the energy of the emitted gamma ray and the target material composition. Since the position at which the gamma rays are emitted are random (as well as their direction of travel), transport simulations are performed for specific geometries to determine the likelihood of escape, called the escape probability.

To be detected, the gamma ray must encounter the gamma detector's active volume. This probability is based on the relative positioning and sizes of the activated target rod and the detector. It is called the geometric efficiency. Finally, the gamma ray must interact within the detector active volume, depositing its energy to create a signal. Higher energy gammas tend to have a higher probability of escaping their original material but are also likely to be harder for the detector to capture and count.

The combined geometric efficiency and the likelihood of a gamma that interacts with the detector volume being counted is called the absolute efficiency of the detector. This quantity is dependent on the energy of the gammas. A calibration must be completed to determine the absolute efficiency as a function of energy for a set activation material geometry and detector setup.

Distinguishing between gamma rays of different energies is important. It provides knowledge about which reactions are causing the gamma rays. The ability to distinguish

energy levels is a property of the detector setup called energy resolution. High energy resolution detector setups like HPGe detectors can separate gamma energies down to keV levels. There are tradeoffs – lower energy resolution detectors like sodium iodine crystals lack the same energy resolution but provide higher absolute efficiencies.

Some activation reactions that result from different nuclides can lead to the same activation product isotope (with the same gamma-ray branching ratios). This is problematic if the two different reactions start from the same element, and both reactions are somewhat likely to occur. Since the two target nuclides have different cross sections, it is impossible to figure out how many of the counted gamma rays are due to one nuclide or the other. This is called interference, and if the levels are high enough, both candidate reactions are unusable. A similar case can happen when the activation products are different but have emitted gamma rays that are very close in energy, sufficiently close that they cannot be resolved from each other, causing close peak interference. These interference situations are fairly rare but must be accounted for.

2.1.4 Neutron Activation Analysis of Nuclear Weapons Leakage Spectra

NAA is particularly suited for analysis of nuclear weapons leakage spectra, which consists of the distribution of neutrons that escape the nuclear explosion and any casing or delivery materials to interact with the surrounding environment. NAA has the advantage of not requiring powered counting equipment to be in place during the time of the neutron

flux is present.[6] Not only is this less expensive, but there is no risk of the nuclear electromagnetic pulse effects damaging the counting electronics or making the stored data unrecoverable.

NAA can be conducted on materials generally available in the environment around a nuclear detonation, most notably performed as part of the long-term studies of the effects of the two nuclear weapons detonated in Japan near the end of World War II. [5] [6] For studying the dose effects on the populations of Hiroshima and Nagasaki, NAA was used on select materials, such as europium, found in small quantities in silica rocks in the area. [7] Due to the 12.5 year half-life of the ^{152}Eu activation product, good counting statistics were still available more than 40 years after the explosions.

To do this research in Japan, the small amounts of europium had to be found and isolated from the rock samples. [7] This required sophisticated chemistry equipment and, importantly, a lot of time. The quantities involved had to be carefully measured to ensure a correct baseline for determining original activation levels.

The idea behind the AFIDS project [2] and similar detector systems [8] is to eliminate the time and cost of finding the materials best able to produce countable activation products for NAA by prepositioning intentionally selected materials in known locations in well-characterized geometries and purities. This would allow NAA to be

---

[6] For nuclear weapons, the surge of neutron emissions occurs in such a short time as to be instantaneous for purposes of modeling activations and radioactive decay. As such, references will be made to the total fluence – the time-integrated flux.

conducted in a much shorter timeframe and guarantees availability of needed target materials for activation in sufficient quantities.

The output of NAA for these nuclear forensics applications is information about the original nuclear weapon neutron leakage spectra. Rather than trying to unfold the spectrum directly, the count data from the activation products are used to calculate the number of activations in the target material immediately after the event. Then a set of library comparison nuclear weapon neutron leakage spectra are used as inputs to the Monte Carlo N-Particle (MCNP) transport code which models what the fluence striking each detector location would be for that spectrum.

That fluence is used to calculate the number of expected initial activations for each detector location and target element. The library spectra are scaled to 1 kt of yield and have an associated number of neutrons produced per kt. This allows a matching algorithm to scale the yield of the library spectra to find the best fit for all of the countable element/detector location combinations, resulting in a chi-squared matching score. [8] The yield scaling factor itself provides valuable information; a rough yield estimate would be known and if the yield scaling factor for a library spectrum were wildly different than the estimate, that spectrum would not be a good match.

2.2 Source Spectra

2.2.1 Limitations

The source spectra used in this dissertation are unclassified. This limits the spectra available to five weapons:

- “Little Boy”, the gun-type uranium fission weapon dropped on Hiroshima;
- “Fat Man”, the implosion plutonium fission weapon dropped on Nagasaki;
- “Fusion”, which is a hypothetical pure deuterium-tritium fusion device outputting only 14.1 MeV neutrons;
- “Watt-Uranium”, the Watt spectrum for U-235 fission; and
- “Watt-Plutonium”, the Watt spectrum for Pu-239 fission.

The spectra will be addressed in alphabetical order in most cases, and the following abbreviations will be used for conciseness: “FM” for “Fat Man”, “FUS” for “Fusion”, “LB” for “Little Boy”, “WPu” for “Watt-Plutonium” and “WU” for “Watt-Uranium”. The five neutron spectra are graphed in Figure 4.

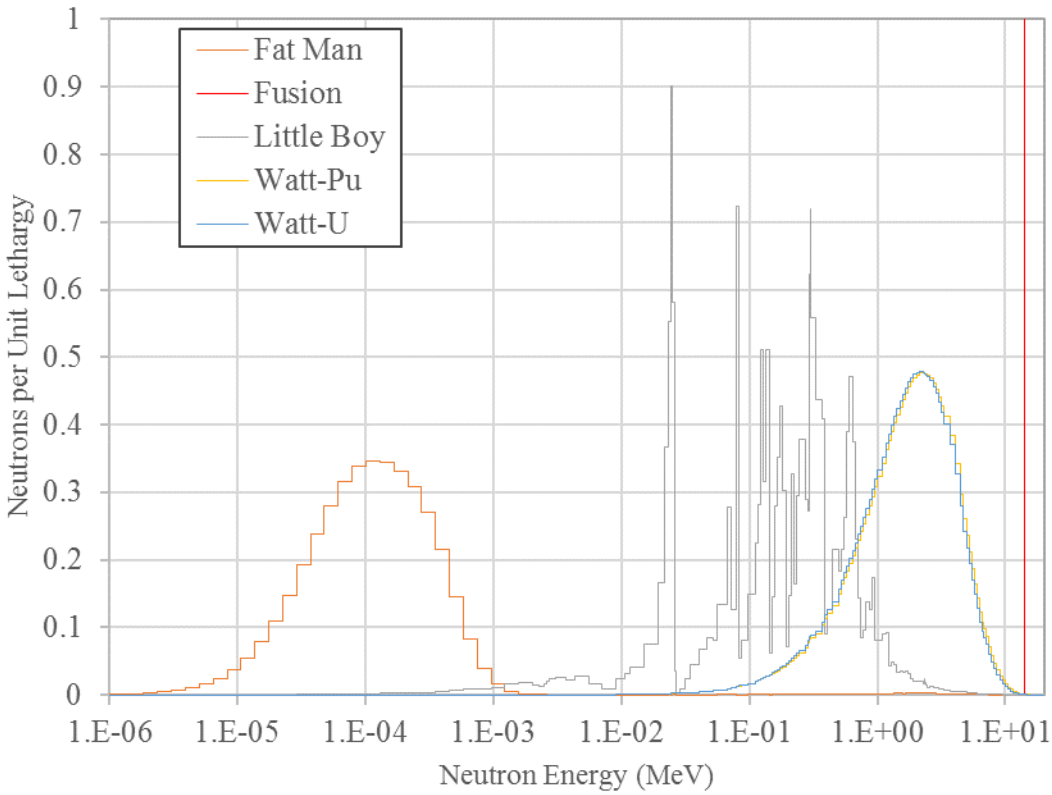

Figure 4 – Neutron Leakage Spectra, Probability vs. Energy (MeV)

Note the Fusion spectrum is a pure 14.1 MeV source, denoted by the single red line at the right side of the graph.

The analysis techniques and code written for this dissertation are carefully designed to work with a far larger data set than five spectra, to allow analysis of much larger library of spectra, if required. Test runs with up to 125 library and unknown spectra (25 repeats of same 5 unclassified spectra) were conducted successfully.

2.2.2 "Fat Man" Spectrum

The “Fat Man” nuclear weapon was an aircraft-delivered bomb dropped on Nagasaki, Japan on 9 August 1945. It was the second and currently last nuclear weapon denotated in war. The implosion design created a supercritical mass of Pu-239 by using shape charges to compress the “physics package” containing a spherical subcritical mass of plutonium and other components. The bomb casing and guidance systems were robust – the weapon weighed 4,700 kg. This affects the neutron leakage spectrum by increased attenuation.

The neutron leakage spectrum used for this research is based on the Dosimetry System 2002 (DS02) calculations performed for the re-evaluation of the doses to Japanese atomic bomb survivors. [6] This spectrum features a large number of relatively low energy neutrons, and a sharp cut off just over 10 MeV. It has no fusion component. Compared to “Little Boy”, this spectrum has a higher neutron concentration near a broad peak around 10^{-4} MeV. So, the spectrum has been significantly moderated.

2.2.3 “Fusion” Spectrum

The “Fusion” neutron leakage spectrum is not based on a real-world weapon design. It is a hypothetical weapon based solely on the deuterium-tritium fusion reaction, with a sharp 14.1 MeV peak. Real-world fusion weapons are initiated with fission physics packages and can also be multistage devices. None of this is captured in this spectrum. However, it serves as a way to determine the utility of a given element in detecting fusion weapon signatures.

2.2.4 “Little Boy” Spectrum

The “Little Boy” nuclear weapon was an aircraft-delivered bomb dropped on Hiroshima, Japan on 6 August 1945. It was first nuclear weapon detonated in war. The gun-type design created a supercritical mass of U-235 by using explosives to push one mass down a tube into contact with the other. Like the World War II era “Fat Man”, the “Little Boy” bomb casing and guidance systems were robust – the weapon weighed 4,400 kg. This affects the neutron leakage spectrum by increased attenuation.

The neutron leakage spectrum used for this research is based on the DS02 calculations. [6] This spectrum features the widest spread of neutron energies of the five test spectra, with a very broad peak centered around 50 keV and a sharp cut off just over 10 MeV. The spectrum has a lot of structure due to resonances and minima of the materials surrounding the warhead. It has no fusion component. This spectrum also produces the fewest neutrons per kt. This makes it relatively difficult to get sufficient detector counts for this spectrum.

2.2.5 “Watt-Plutonium” and “Watt-Uranium” Spectra

These two spectra are generated from the empirical Watt distribution. [9] The MCNP code uses this version of the distribution [10]:

$$f(\varepsilon) = \frac{2 * e^{-ab/4}}{\sqrt{\pi a^3 b}} e^{-\varepsilon/a} \sinh(\sqrt{b\varepsilon}) \tag{1}$$

Where:

$f(\varepsilon)$ ≡ Probability distribution function, energy dependent. [Calculated quantity]

a, b ≡ Empirical parameters

ε ≡ Energy, MeV

The parameters *a* and *b* vary with the fissionable isotope (and weakly with incoming neutron energy.) [11] The Watt spectra of U-235 and Pu-239 are very similar over much of the energy range considered. This challenges the AFIDS modeling to distinguish between two closely-related weapon types, separated only by selection of fissile isotope – an important distinction when determining the design and possible origin of a weapon. The differences between the spectra are illustrated in Figure 5 below:

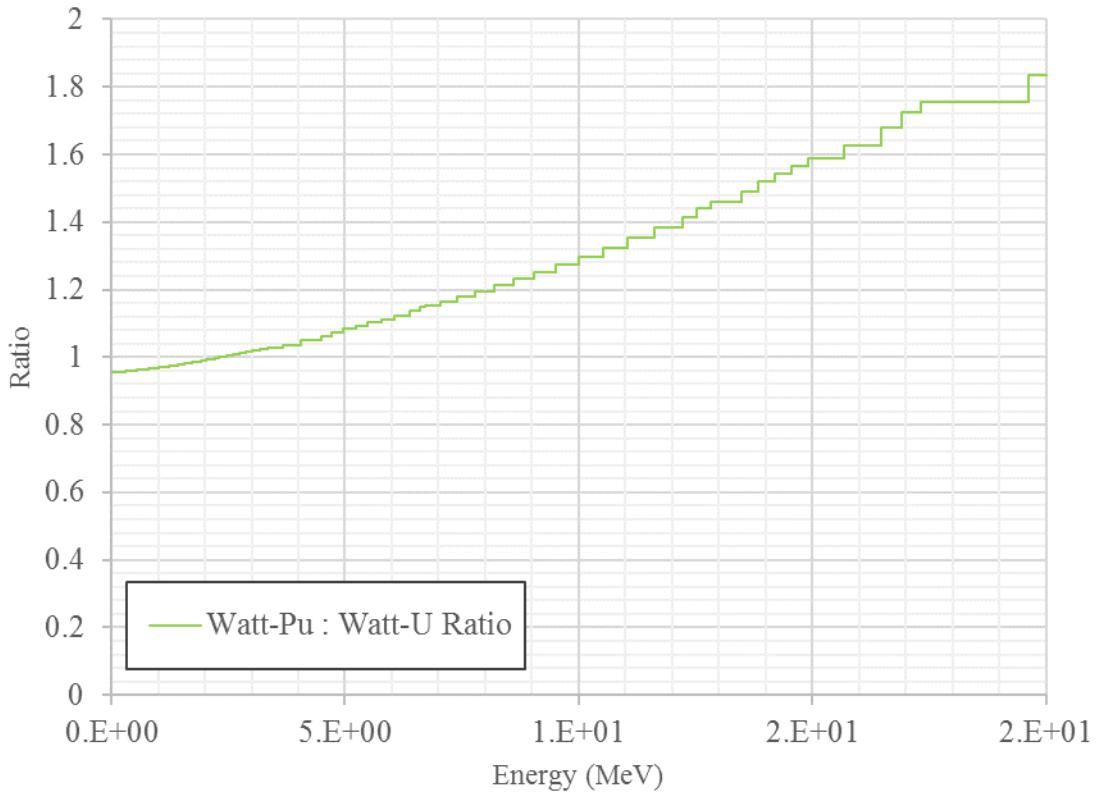

Figure 5 – Ratio of Watt-Pu:Watt-U Neutron Leakage Spectra

The Watt-U spectrum is more likely to produce neutrons in all the lower energy bins up until 2.3 MeV, where the Watt-Pu breaks even as it skews upwards to higher neutron energy levels. Elements featuring threshold reactions are expected to do well in distinguishing these two spectra. In the default scenario defined shortly, these are the two most difficult spectra to distinguish.

2.3 Default Scenario Parameters

The optimal selection and arrangement of elements for the AFIDS detectors depends on the scenarios that its design is optimized for. For instance, if the design

assumed that it would only be required to distinguish between low-sophistication fission-only device designs expected from a terrorist threat, the optimization process would likely favor elements sensitive to neutrons below the telltale deuterium-tritium 14.1 MeV peak. If the design solely sought to determine if a weapon had a fusion component, it may choose elements that are most effective at capturing that peak. Similar circumstances arise when considering low-yield versus high-yield weapons.

This research split most of these differences in trying to optimize the detector to handle a wide variety of scenarios while limiting the cost per detector, with a working limit of $250 in material cost per unit. The default scenario parameters outlined below will reflect this. Many of these parameters will be altered in the different tests subsequently run to test for both feasibility and sensitivity to these values.

The default scenario parameters are:

Yield = 15.0 kt

Delay time before starting counts = 72.0 hours

Counting time allowed, per element = 3.0 hours

Minimum counts required = 3,000

Terrain: New York City

Ground zero and detector locations: illustrated in Figure 6, with ground zero colored red. There are differences in height not pictured.

Elements: Only consider commercially-available elements with melting points greater than or equal to aluminum.

Figure 6 – Detector and Ground Zero Locations, NYC MCNP Model. (3 km x 3 km, 500 m gridlines, blue dots = detectors, red dot = detonation at Times Square) **[2]**

The default yield is similar to the Little Boy gun-type device that is a likely choice for a terrorist attack. It is also not too far from an implosion-type device that is purely

fission in nature. Higher yields lead to proportionately more neutrons which increases count rates and eases detection and distinguishing spectra, so the default yield is biased towards the more challenging scenarios involving low-yield weapons.

The delay time in the start of counting is based on judgment about how quickly detectors may be retrieved after a nuclear event. The detectors must also either be transported to a counting lab or be counted by a mobile counting lab. This parameter will be altered in the study to see which elements produce a longer-lasting signal, which is useful if the collection time exceeds 72 hours.

The counting time allowed accounts for the scarce resource of counting equipment anticipated immediately after a nuclear event and the need to provide useful results quickly. An optimized contingency plan may set different counting times for different elements to further leverage these limited resources, but this must be part of a larger plan that is beyond the scope of this work.

The required counts parameter reflects the desire to reduce the statistical uncertainty to an acceptable level and is a trade-off between uncertainty and time. The statistical uncertainty is proportionate to the square root of the number of counts, leading to diminishing returns for higher count requirements.

The selection of New York City with a detector spacing of 500 meters in a grid pattern is shown in Figure 6. New York was selected because of its high density of tall buildings that create urban canyons and lots of attenuation. This is one of the most challenging situations to get sufficient counts in and is also a very high-profile target. The

500-meter detector spacing is based on previous work done in the AFIDS research and design. [2]

Elements who are not commercially available or whose melting points are below that of aluminum will be filtered out. This filtering limits the search space to those elements feasible for use in this application. Materials that melt before the aluminum container will be uncountable and materials that are not commercially available will exceed the cost constraints of the project.

CHAPTER 3. METHODOLOGY

The primary approach to determining the optimal set of target activation detectors (target rods) is to model the expected activation of the target rods in computer codes, then conduct analysis to determine which rods contribute the most to differentiating between the library spectra. To do this, the neutron source (leakage) spectra are transported in the Monte Carlo code (MCNP) to detector locations in modelled terrain.[7] This incoming fluence is then used to calculate expected activation levels for each of the target rods at each of detector locations, 34 for this work. The initial activation levels are then decayed to allow for the delay in collection and the start of counting, and their expected count rates are calculated. The details of these calculations and processes are outlined in section 3.1.

There are several key assumptions made for this series of models and calculations which are outlined specifically in section 3.1.1. A series of experiments was executed to test the validity of some of these assumptions and that methodology is outlined in section 3.2.

Fundamental to the analysis of the results is the match chi-squared score. This score compares how similar a given library and unknown spectra are statistically and also

[7] For this research, a model of New York City is used exclusively, though the codes and methods work are agnostic to that choice. New York has pronounced urban canyons that create interesting angular distributions of the neutron fluence.

determines a scaling factor that represents the required yield of the unknown spectrum to produce the closest match. The matching process is detailed starting in section 3.3.1.

3.1 Modeling Activations, Decay, and Counting

This section will lay out the major equations used in modeling activations, decay, and counts detected, including assumptions made, inputs used, and special considerations. The code used to model will be discussed in section 3.2.

3.1.1 Assumptions

3.1.1.1 Self-shielding impact of target rods

The target rods are 1.0 mm in diameter. To simplify calculations, it was initially assumed that effectively 100% of the gamma rays emitted during radioactive decay of the activated nuclei would escape the rod itself. In other words, the number of gamma rays leaving the rod was unaffected by the small amount of intervening material. This simplified the efficiency calculation of the gamma-ray detector by limiting it to the geometric factor and the energy efficiency of the detector for each gamma ray.

This assumption turned out to be invalid, as some low energy gamma rays are strongly attenuated by the target rod material and many gamma rays key to the analysis had significant attenuation in the rod. The testing of this assumption is outlined in section 4.1.1.1. This assumption was not used in final calculations; an escape factor for each gamma ray / target rod combination was calculated and used.

3.1.1.2 Impact of Shielding of the Rods by the Walls of the Holder

The aluminum detector body's cylindrical wire holder is 0.476 cm thick. The amount of aluminum holder material between a target rod and a neutron source varies with orientation and is 0.188 cm for a rod directly facing the source versus 0.664 cm for a rod just offset from the opposite side. Previous AFIDS work modelled these situations in MCNP and calculated a net change in activations of less than 4% from a bare target rod (no holder) setup. [2] This modeling work was tested by experiment and additional modeling which is detailed in section 4.1.

3.1.1.3 Impact of the Orientation of the Detector Body

This assumption is related to the previous assumption but is listed separately because it may be valid even if the previous assumption is not valid. Previous AFIDS work showed a very small angular dependence on activations with an aluminum holder, which is one of the major reasons the material was selected. However, the modeling in the previous work focused on two target rod reactions; experimental tests which are outlined in section 4.1.1.2.3 will test for a variety of target rod materials with different neutron activation cross sections (as a function of neutron energy).

3.1.1.4 The Dominant Uncertainty in Predicted Initial Activations: Neutron Fluence

There are multiple variables with associated uncertainties in equation (2) used to calculate predicted (library) activations. Most of these quantities have very small relative uncertainties compared to the statistical uncertainty resulting from the MCNP transport modeling, with the exception of the uncertainty in gamma ray counts. For the library spectra, the MCNP transport uncertainty should dominate; for the unknown spectra, the counting uncertainty should dominate.

3.1.2 Algorithm Development

This section outlines the major equations and variables used to model target rod activations, their subsequent counting and the chi-squared matching analysis.

3.1.2.1 Library Activations

The number of activations is calculated in a target rod for a given reaction using equation (2):

$$N_{act} = \Phi_E * \ \sigma_E * \left(\frac{m * abundance}{A}\right) * N_A \qquad (2)$$

Where:

N_{act} ≡ number of activated nuclei for a given reaction present in the target rod due to the brief fluence from the detonation event, in a given energy bin. [Calculated quantity]

Φ_E ≡ incoming neutron fluence from a selected energy bin at the target rod location, neutrons per cm^2.

σ_E ≡ the effective microscopic cross section from a selected energy bin for the specific desired reaction, barns (10^{-24} cm^2).

m ≡ mass of the target rod, calculated from its density and volume, grams.

Abundance ≡ fraction of total mass of an element mass that is the specific desired isotope.

$A \equiv$ average atomic weight of the element of the target material (isotope specific), grams/mole.

$N_A \equiv$ Avogadro's Number: number of atoms per mole.

3.1.2.2 Decay of Activated Products

The number of activation product nuclei left as a function of time after its creation is calculated with the radioactive decay equation:

$$N(t) = N_{act} * e^{-\lambda t} \quad (3)$$

Where:

$N(t) \equiv$ Number of activated atoms at a given time [Calculated quantity]

$N_{act} \equiv$ Number of activated atoms at time zero, previously calculated. The is the number of atoms of the activation product immediately present after the weapon detonation.

$\lambda \equiv$ Decay constant of the product isotope of interest, hour^{-1}

$t \equiv$ Time, hours

3.1.2.3 Count Rate

The count rate equation is the time derivative of the decay equation multiplied by several terms accounting for the expected number of gammas per decay and the absolute efficiency of the gamma ray detector at a given energy level.

$$C(t) = \lambda N(t) * \frac{\gamma}{decay} * p_{esc} * \varepsilon_{abs} \quad (4)$$

Where:

C(t) ≡ Count rate at a given time, hour^{-1}. [Calculated quantity]

λ ≡ Decay constan, hour^{-1}

N(t) ≡ Number of activated atoms at a given time

γ/decay ≡ Number of gamma rays emitted per decay event; only including gamma rays from the best gamma ray selected

p_{esc} ≡ Probability that a given gamma ray escapes from the target rod

ε_{abs} ≡ Absolute efficiency of the detector for the chosen gamma ray

3.2 Modeling and Analysis Code

This section describes the overall set of FORTRAN codes that model the activations of target rods from a given set of library and unknown (perturbed) spectra. The unknown spectra represent the data that would be collected by the counting process after a nuclear event and are generated by taking the library spectra, perturbing them based on their uncertainty using a randomly-sampled gaussian distribution, and calculating the associated activation levels, decays over time, and final number of counts. This process leads to filters that eliminate elements that do not produce enough counts for good counting

statistics. The uncertainty for the unknown spectra also follows along this chain of calculations.

The code determines the radioactive decay rates and amounts, determines the optimal reactions and gamma rays to measure, and calculates predicated count rates and total counts for a given set of target rods and locations. Many key parameters are adjustable to run different scenarios and compare results. The scoring and analysis portions of the code are covered separately in section 3.3.2.

3.2.1 Overall Modeling Code Structure

The overview of the code structure is covered in Figure 7:

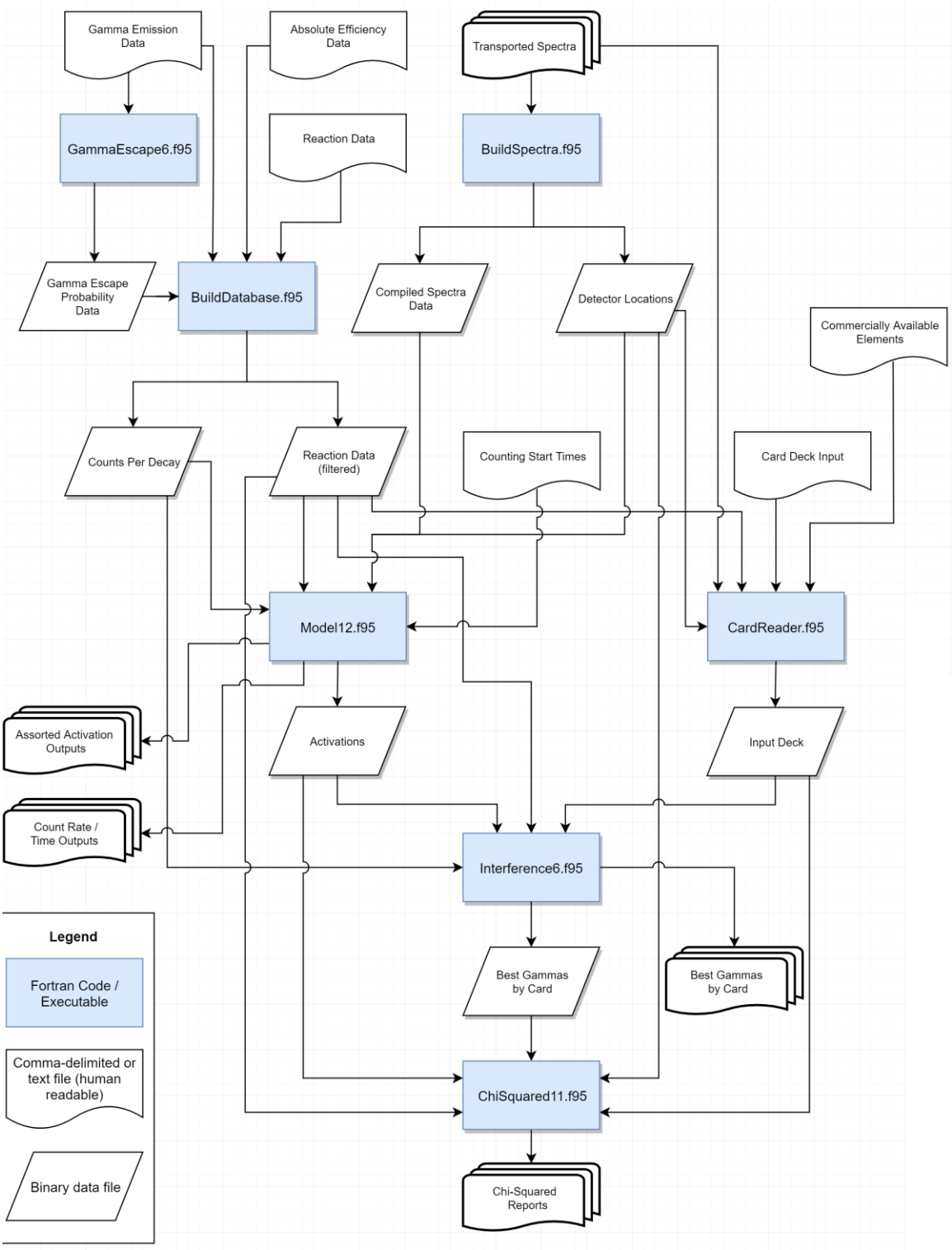

Figure 7 – Overall Code Structure

The seven subprograms are highlighted in blue; the first six will be discussed in this section, and the final scoring and analysis program will be discussed in section 3.3. The first subprogram discussed, the Gamma Escape code, is somewhat standalone in the sense that it only needs to be ran one time to generate needed input for the rest of the subprograms. Its output does not vary with the numerous parameters that are adjustable in the overall code.

3.2.2 Subprogram Descriptions and Key Algorithms

3.2.2.1 Gamma Escape Probability

This subprogram calculates the probability of a gamma ray of a given energy level escaping from an elementally-pure target rod of a given element. The input data for this subprogram include the energy-dependent cross sections for gamma rays for each element, sourced from the National Institute for Standards and Measures' Physical Measurement Laboratory [12]. The program also refers to basic elemental physical data, such as density.

The calculations for each element are independent. Thus, the code also allows command line inputs for which elements to run, allowing for simple parallelization on multi-processor-core computers, which reduced the local runtime by a factor of ten.

This subprogram assumes that the gamma ray emissions (also the location of activated nuclei and decay events) are uniformly distributed in position. It is also assumed that the gamma ray emissions are isotropic in angle. Finally, any gamma ray interaction with the target rod is considered a non-escape event and the particle is dropped from consideration.

After reading in the input data, including the number of energy bins for each element in the gamma ray cross section data, the subprogram determines if a file containing pre-calculated pathlengths exists. (These pathlengths only depend on the target rod geometry, and considerable computational time is saved by calculating a large number of them once upfront.) If the pathlength file does exist, the subprogram skips the next paragraph.

The subprogram then selects a random starting position[8], azimuthal angle, and polar angle for a gamma ray. It then calculates the path length covered until the ray would intersect either the cylindrical edge or end cap of the cylinder and selects the smaller of these two values as the path length and appends it to the pathlength file. The subprogram repeats this random generation / pathlength calculation until 3.0E+9 pathlengths are generated and appended to the pathlength file.[9]

The subprogram then loads the pathlength file. Then, for each element considered, and for each energy bin within the cross section data for that element, the subprogram calculates the escape probability for a pathlength, and maintains a running uncertainty level for all pathlengths tested so far. If the uncertainty is less than the maximum allowed, or the maximum number of pathlengths is reached, the subprogram moves on to the next

---

[8] Care must be taken to get a uniform distribution in a cylinder; the code uniformly distributes over a square cross section then throws out starting positions outside the radius of the cylinder. Similar care must be taken in sampling of starting angles.

[9] This number is an empirically-determined compromise between run time, memory available, and uncertainty reduction possible for given element/energy level escape probability calculations. Most combinations will converge in far fewer iterations.

element / energy bin combination.[10] When all elements are completed, the gamma escape probability data are saved in both comma-delimited and binary formats.

The output product for this code is a lookup table of escape probabilities for a given gamma-ray energy and element combination from the common geometry of the target rods. Later codes will use linear interpolation for gamma rays that do not match one of the energy level entries from the cross section database. An excerpt from the escape probabilities of a gamma ray from iron are shown in Table 1:

[10] To speed up the actual code, this test is not conducted for the first 10,000 pathlength iterations, and then only checked every 10,000 iterations thereafter.

Table 1 – Excerpt of Gamma Escape Probabilities for Iron

	Gamma Escape Probabilities			
Energy	Escape Probability	Absolute Uncertainty	Relative Uncertainty	Iterations
1.00E-03	1.41E-04	1.53E-07	1.09E-03	3.00E+09
1.50E-03	3.77E-04	3.77E-07	1.00E-03	1.32E+09
2.00E-03	7.90E-04	7.90E-07	1.00E-03	6.32E+08
3.00E-03	2.31E-03	2.31E-06	1.00E-03	2.15E+08
4.00E-03	5.05E-03	5.05E-06	1.00E-03	9.80E+07
5.00E-03	9.34E-03	9.34E-06	1.00E-03	5.26E+07
6.00E-03	1.55E-02	1.55E-05	1.00E-03	3.13E+07
7.11E-03	2.49E-02	2.49E-05	1.00E-03	1.91E+07
7.11E-03	3.16E-03	3.16E-06	1.00E-03	1.57E+08
8.00E-03	4.22E-03	4.22E-06	1.00E-03	1.18E+08
1.00E-02	7.56E-03	7.56E-06	1.00E-03	6.51E+07
1.50E-02	2.27E-02	2.27E-05	1.00E-03	2.10E+07
2.00E-02	5.07E-02	5.07E-05	1.00E-03	8.87E+06
3.00E-02	1.58E-01	1.58E-04	1.00E-03	2.21E+06
4.00E-02	3.28E-01	2.69E-04	8.21E-04	1.00E+06
5.00E-02	4.99E-01	2.52E-04	5.04E-04	1.00E+06
6.00E-02	6.31E-01	2.16E-04	3.43E-04	1.00E+06
8.00E-02	7.84E-01	4.87E-04	6.21E-04	1.00E+05
1.00E-01	8.55E-01	3.67E-04	4.29E-04	1.00E+05
1.50E-01	9.17E-01	2.40E-04	2.62E-04	1.00E+05
2.00E-01	9.35E-01	1.96E-04	2.10E-04	1.00E+05
3.00E-01	9.49E-01	1.62E-04	1.70E-04	1.00E+05
4.00E-01	9.56E-01	1.45E-04	1.52E-04	1.00E+05
5.00E-01	9.60E-01	1.34E-04	1.39E-04	1.00E+05
6.00E-01	9.63E-01	1.25E-04	1.30E-04	1.00E+05
8.00E-01	9.67E-01	1.12E-04	1.16E-04	1.00E+05
1.00E+00	9.71E-01	1.02E-04	1.06E-04	1.00E+05

The goal for reducing the relative uncertainty for each energy level was 1.E-3, subject to running out of pathlengths to use to continue reducing the uncertainty. Note the very low energy bins where the goal relative uncertainty is not reached did indeed run out of pathlength data, stopping the iterative convergence process in the interest of limiting

computational time required. These relative uncertainties are still low enough to not be a major factor in later calculations.

The results from the code matched well with what would be physically expected: lower energy gamma rays have lower escape probabilities and higher-Z materials are more difficult to escape from. Select results are pictured in Figure 8 below:

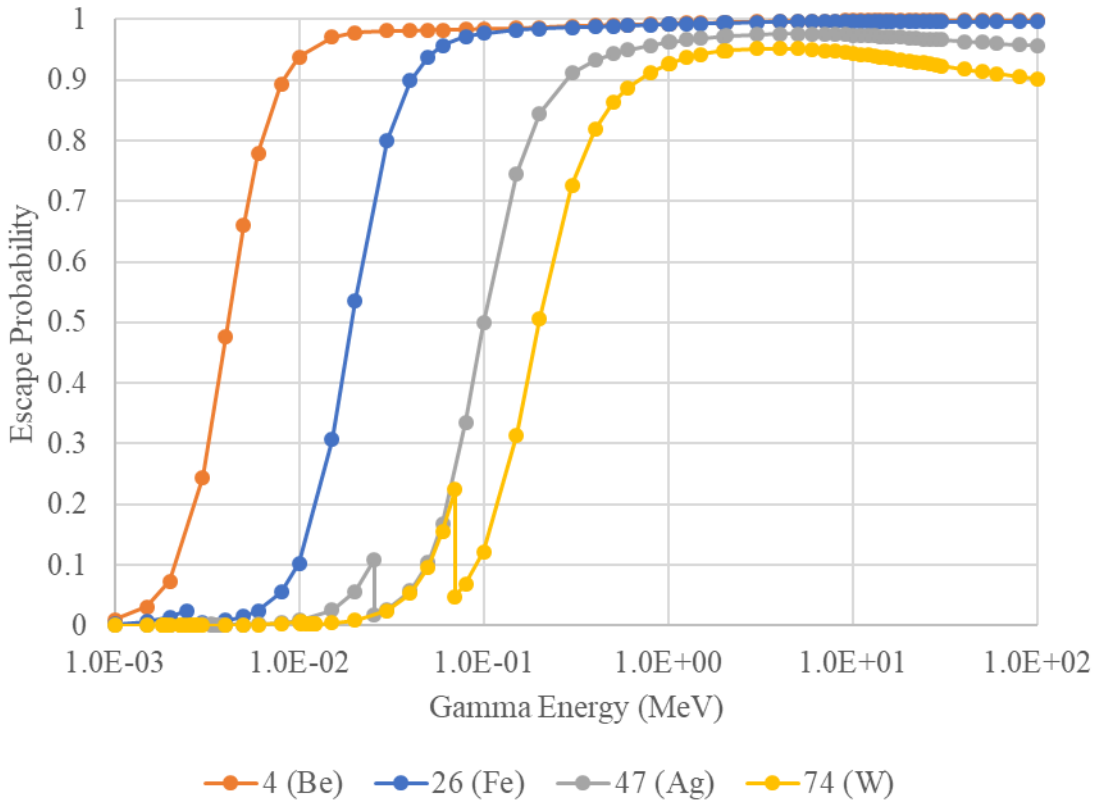

Figure 8 – Escape Probability of Select Elements

The discontinuities in Figure 8 reflect the decreased escape probabilities that are due to the effect of the K-edge of the materials in the rod. [13] Since this program considers any interaction to be a non-escape event, the escape probabilities are inversely proportional to this change. The higher-Z elements also exhibit such similar structure at lower energies at the energies required to free L and M shell electrons.

3.2.2.2 Build Database

This subprogram combines several data inputs into a cohesive reaction data structure. These inputs include the basic elemental physical data, possible neutron activation reactions and their associated 200 energy bin cross sections, and the energy-dependent absolute efficiency of the chosen gamma ray detector setup. It also calculates the expected number of counts per decay for a given gamma ray/activation product combination. Since this subprogram consist of mostly data structure and formatting for further work, it is not described in detail here.

3.2.2.3 Build Spectra Information

This subprogram reads in the raw output files of the MCNP transport calculations for each spectrum and pulls it into a useable format for use in further programs. It also extracts the detector locations and separately outputs them for further use. No calculations occur in this subprogram, but it is important because it allows for the rapid integration of new transported spectra data in the event of a nuclear explosion or intelligence about a new weapons design to be added to the libraries.

3.2.2.4 Modeling Library and Unknown Activations, Counts and Uncertainties

This subprogram combines multiple inputs and calculates the expected number of activations for each reaction, at each detector location, for each library spectra (per kt of yield). These activation amounts are then multiplied by a yield to create unknown spectra used for the counting portions of the code. These unknown spectra will later be perturbed to introduce additional uncertainty such as one would expect in a physical measurement. The subprogram calculates uncertainties for both, using a follow-on calculation of expected count rates/total counts to determine the unknown spectra uncertainty. This program also filters out reactions that provide no useful data for the given library of spectra before generating its outputs.

This subprogram uses the reaction data, gamma escape data, spectra data, and detector location data previously generated. In addition, it reads in a list of delay times to compute count rate scenarios for intermediate outputs.

This subprogram assumes that all target rods are elementally pure with an isotopic distribution equal to the naturally-occurring ratios on earth.[11] It also assumes that all uncertainty from the transported spectra is reflected in the relative uncertainties produced by MCNP (no major errors in weapon detonation location, detector locations, or gross modeling errors.)[12] The subprogram also assumes that the uncertainties associated with

---

[11] For the elements ultimately considered after preliminary filtering for melting points and commercial availability, this assumption is true to at least one part in one hundred and does not significantly alter activation results.

[12] In a real-world use of MCNP, the transport for each spectrum would be rerun with the latest information about the detonation location, detector locations, terrain, and weather data.

neutron activation cross sections are small enough to be negligible compared to other sources of uncertainty.

After reading in the appropriate input files from previous subprograms, the code then calculates the number of library activations as a function of source spectrum, detector location, energy bin, and reaction using Equation (1). This is done for each spectrum, detector location and reaction combination in each energy bin.[13] These library reactions are scaled to a 1 kt yield. The subprogram then calculates the number of unknown activations (unperturbed) by multiplying the library activations by a chosen yield, with 15 kt as default.

Absolute uncertainty in library activations is then computed by the code. A filter then drops any activation records below a cutoff threshold chosen to eliminate data that cannot possibly produce sufficient counts to impact the analysis later in the process. The code then sums the number of library and unknown activations over all energy bins for each spectrum/location combination, yielding the number of activations for each reaction in those circumstances. The subprogram also calculates diagnostic quantities including count rates at different times, the number of counts in a given timeframe, and the maximum allowable delay to start counting given set conditions. The code then appends all these

[13] Due to memory constraints, this loop actually runs for 3 spectrum/location combinations at a time before dumping data to the output files and starting with the next 3 combinations until complete.

data to the activation and diagnostic files and continues until all combinations are completed.[14] An excerpt of activation data is in Table 2 below:

Table 2 – Excerpt of Activation Data for Fusion Spectrum, Detector Location 16

	Activations by Energy Bin				
Energy	180Hf(n,γ) 181Hf	181Ta(n,2n) 180Ta	181Ta(n,3n) 179Ta	181Ta(n,γ) 182Ta	181Ta(n,p) 181Hf
2.00E+01	0.00E+00	0.00E+00	0.00E+00	0.00E+00	0.00E+00
1.96E+01	0.00E+00	0.00E+00	0.00E+00	0.00E+00	0.00E+00
1.73E+01	0.00E+00	0.00E+00	0.00E+00	0.00E+00	0.00E+00
1.69E+01	0.00E+00	0.00E+00	0.00E+00	0.00E+00	0.00E+00
1.65E+01	0.00E+00	0.00E+00	0.00E+00	0.00E+00	0.00E+00
1.57E+01	0.00E+00	0.00E+00	0.00E+00	0.00E+00	0.00E+00
1.49E+01	0.00E+00	0.00E+00	0.00E+00	0.00E+00	0.00E+00
1.46E+01	0.00E+00	0.00E+00	0.00E+00	0.00E+00	0.00E+00
1.42E+01	5.07E+06	8.35E+09	0.00E+00	1.70E+07	1.41E+07
1.38E+01	6.51E+06	1.05E+10	0.00E+00	2.16E+07	1.47E+07
1.35E+01	5.35E+06	8.27E+09	0.00E+00	1.76E+07	8.21E+06
1.28E+01	2.96E+06	4.41E+09	0.00E+00	9.60E+06	2.63E+06
1.25E+01	3.50E+06	5.07E+09	0.00E+00	1.13E+07	2.27E+06
1.22E+01	5.99E+06	8.11E+09	0.00E+00	1.92E+07	3.54E+06
1.16E+01	4.36E+06	5.32E+09	0.00E+00	1.45E+07	2.29E+06
1.11E+01	3.37E+06	3.68E+09	0.00E+00	1.16E+07	1.57E+06
1.05E+01	2.31E+06	2.20E+09	0.00E+00	8.12E+06	9.57E+05
1.00E+01	2.41E+06	1.87E+09	0.00E+00	8.56E+06	8.78E+05

[14] The activation data files scale proportionally with the number of library spectra squared; the raw activation data by spectrum/location/reaction/energy bin exceeds 16 GB for a 125-spectrum run. The run time required scales this way as well.

This excerpt shows a clean upper cutoff energy that reflects the 14.1 MeV neutrons released by the fusion process. Note that different isotopes and reactions within the same element have very different activation levels.

The primary outputs of this subprogram are the library and unknown (perturbed) spectra activity and their associated uncertainties.[15] The subprogram also outputs calculated diagnostic data for a set of fixed conditions to assist with troubleshooting and individual test cases. These diagnostic outputs include the decay rate at different times post-activation, the count rates at those time, the total counts in a given time window, and the maximum allowed delay that will let sufficient counting statistics be gathered in a predetermined time window. A later subprogram allows a multitude of conditions to be tested on individual runs for the scoring and analysis portions of the overall program. A sample of the diagnostic output is in Table 3 below:

[15] The unknown spectra uncertainties will later be recalculated with perturbed spectra and by working through the expected number of counts back to the number of original activations, to reflect the real-world processing of data and the new uncertainties introduced.

Table 3 – Select Diagnostic Data for Fusion Spectrum, Detector Location 16[16]

	Diagnostic Data				
	180Hf(n,γ) 181Hf	181Ta(n,2n) 180Ta	181Ta(n,3n) 179Ta	181Ta(n,γ) 182Ta	181Ta(n,p) 181Hf
Count Rate at 72 h (1/h)	4.59E+07	1.16E+05	0.00E+00	1.01E+09	3.73E+03
Counts, delay 72 h, 3 h count	1.37E+08	3.07E+05	0.00E+00	3.04E+09	1.12E+04
Max Delay for 1000 counts/h (h)	1.58E+04	1.28E+02	0.00E+00	5.50E+04	2.00E+03

These diagnostic calculations account for the differing half-life, output gamma rays, and associated absolute energy-dependent efficiency of the counting system. For instance, while the tungsten activation rod count rate at 72 hours post activation is barely above the 1,000 counts/h threshold, the activation product is sufficiently long lived that it maintains that approximate count rate for more than 11 days.

3.2.2.5 Read Card Deck

A thorough optimization process for the AFIDS target rod set requires testing against a multitude of independent parameters and generating dozens of output sets. To avoid changing key variables individually (whether in a text file or in the code itself), a card reader subprogram was designed to automate handling a variety of input "cards" (lines

[16] Note that these calculated quantities are based on summation over all 200 energy bins, most of which are not pictured in **Error! Reference source not found.**.

of data in a text file that set the parameters and modification for each scenario to be run) and run them in a single operation. This collection of cards is called the card "deck" (a set of scenarios to be run contained in one text file). Each card in the deck can have multiple instructions in any combination. These instructions take the form of filters and can be set to either exclude or include based on the given criteria.

The criteria for each card that may be set in the card reader input file includes: detector distance from ground zero, azimuth (angle) of detector from ground zero, x/y/z position filters, include/exclude threshold/non-threshold reactions, emitted gamma energies, commercial available elements, manually select elements to include/exclude, manually select detector locations to include/exclude, manually select reactions to include/exclude, and the ability to exclude/include all items. The criteria are executed in the order listed within the card, allowing complex filters to be constructed, such as excluding all detectors within 500m of ground zero, except in the opposite direction of the fallout plume.

Each card is assigned a label in the card deck. This label is used to generate unique filenames to organize the different outputs. Additionally, each card must specify four key parameters for the run: weapon yield (kt), the time to start counting after detonation (h), time to count (h), and the minimum number of counts required.

The code works by starting with an array reflecting all detector location and reaction combinations. By default, all combinations are enabled. The code then reads the filters and applies them using Boolean logic in sequence. When a card is complete, the

use/do not use array alongside the card's key parameters are saved as a binary input file for the subsequent subprograms.

3.2.2.6 Determine Best Gamma Rays / Avoid Interferences

The next subprogram performs two functions. The first function is to check all the gamma rays that each reactant element can produce via all its activation products against the others for interference. This interference can be caused two ways: two different reactant isotope reactions leading to the same activation product, or two different reactant element reactions having energy peaks too close together with similar magnitude in the number of expected counts, making them unresolvable. The former interference is problematic because each reaction has a different energy-dependent cross section, and if two reactions (starting from the same element) lead to the same activation product, there is no way to determine which cross sections produced what portion of the counts.[17] The latter is problematic because the counting system cannot differentiate total counts between two gamma lines too close together.

The second function of this code is to determine the best gamma rays to consider for each reaction, and then from the best gamma rays for each reaction, the best gamma ray to count for each candidate target rod element. This is a multistep process, as the latter task depends on the library spectra as well as the cross sections of each reaction. Gamma

[17] Some of these interferences could be avoided by using isotopically-pure target rods, but that is prohibitively expensive for most circumstances expected in the AFIDS program.

rays previously flagged as having any interference are excluded from this selection process. The selection of the overall best gamma ray for each candidate target rod element is determined by which gamma ray has the highest number of counts resulting from the fluence of the greatest number of the library spectra. Whichever gamma "wins" for the most spectra is selected.

Selecting to only count the best gamma ray from each element[18] simplifies the counting process for the end user without losing fidelity in the model. Each activation product has well-established branching ratios that state the probability of each possible gamma ray being emitted per activated isotope decay. The best gamma ray for an activation product is not solely the one with the highest branching ratio, but the gamma ray that results in the most counts (without interference). This requires consideration of both the probability of the gamma ray escaping the target rod (see section 3.2.2.1) and the energy-dependent efficiency of the detector.

The code starts by reading in previously generated reaction, spectra, gamma ray and activation data, alongside the input card deck.[19] Using the key parameters from the card deck, for each spectrum/detector location combination, it calculates the number of

---

[18] The decision to use a single best reaction / gamma ray for each element, instead of say, the best gamma ray for each different activation product isotope, was designed to both simplify counting, and avoid undesirable biasing in the chi-squared scoring metric that would result from an element with numerous countable activation products being counted multiple times and receiving a heavier weight in the scoring. Counting two separate reactions with different activation products is possible and would have been a reasonable decision as well.

[19] The entire code is run separately for each card in the deck, with separate outputs.

counts of each activation product at the times specified in the input deck using equations derived from equation (3). Then, for each reactant element (as opposed to isotope), it checks all the possible reactions for common products (first type of interference) and for counting peaks too close together and too similar in magnitude (second type of interference). If either interference condition is met, all offending gamma rays are flagged and not used further.

For the remaining gamma rays, the code then determines which gamma ray from a given reaction path ultimately produces the greatest number of counts per decay, after accounting for escape probability and detector efficiency. Then, within a reactant element, the best gamma ray for that spectrum/location combination is determined.[20] This process is repeated for all the spectra in the library at all the locations. Then the code predicts the counting results to determine the most frequently selected gamma ray energy for a given element across the entire library of spectra and locations. This becomes the best gamma ray for that element and will be used for that card in the matching subprogram and further analysis.

3.3 Match Scoring and Analysis Process

3.3.1 Match Chi-Squared Contribution Equation

[20] It is possible to use more than one reaction pathway; a judgement was made in favor of simplifying the counting and scoring processes by not doing this. Future work can revisit this possibility.

The match chi-squared contribution equation used in the AFIDS process is below:

$$\chi_s^2 = \frac{1}{F}\sum_{d}^{D}\sum_{j}^{J}\frac{(y_s B_{sdj} - M_{dj})^2}{y_s^2 u_{sdj}^2 + \sigma_{dj}^2} \tag{5}$$

Where:

$\chi_s^2 \equiv$ Chi-squared value, used to determine how good of a statistical fit two different spectra are. This quantity depends on 4 independent variables (library spectra activations, unknown spectra activations, detector location, and reaction) plus a scaling factor (yield) which is used to minimize the overall chi-squared value. [Calculated quantity]

$F \equiv$ Degrees of freedom – determined by the number of valid detector location/reaction combinations for the two spectra being compared. For the sample calculation, a single degree of freedom is tested. Will be referred to as "countable locations" when discussing the AFIDS system. The degrees of freedom are bounded by the upper limit of $F \leq DJ$.

$d \equiv$ Detector location index

D ≡ Number of detector locations

$j \equiv$ Reaction index

J ≡ Number of reactions considered

$y_s \equiv$ yield (in kt); used as a scaling factor to minimize the magnitude of the overall chi-squared for library source s

$B_{sdj} \pm u_{sdj} \equiv$ The library reference spectrum's activation level and uncertainty at a given detector location for a given reaction. These library spectra are produced assuming a 1.0 kt yield, allowing y_s to serve as a scaling factor to match the unknown spectrum's activations.

$M_{dj} \pm \sigma_{dj} \equiv$ The unknown spectrum's activation level and uncertainty at a given detector location for a given reaction.

3.3.2 Match Scoring and Analysis Procedure

This section describes the portion of the code used to determine match scoring and then the approach used to analyze the results. The matching subprogram is the final subprogram, shown near the bottom of Figure 7.

3.3.2.1 Matching Score Code

The matching score subprogram calculates best fit scores for each combination of unknown and library weapon spectra, and an associated best fit weapon yield for each score. In a real-world AFIDS matching test, a single unknown activation set would be tested against the entire library of possible starting spectra (and their associated activation sets). For purposes of analyzing match chi-squared scores of different detector material configurations, a full set of unknown spectra are generated by perturbing the library spectra to simulate measurement uncertainty, which are then cross-compared. This leads to a matrix comparing each spectrum against the whole library set, with the best matches occurring along the diagonal representing perturbed spectra being tested against their original form. Along this diagonal the calculated yields also track closely with a

predetermined yield used to generate the unknown spectra. By default, this predetermined yield is 15 kt.

This subprogram uses the compiled reaction data, detector location data, activation data, and interference data previously generated. It is driven by the input deck cards previously processed, as it runs each card's scenarios independently and generates output separately.

This subprogram inherits the assumptions from the previous subprograms, with the assumption that the transported library spectra only have the statistical uncertainties generated from the MCNP transport calculation. It assumes that the modelled city and terrain is sufficiently detailed and that the weapon detonation location is sufficiently certain to not add to the uncertainty.

The subprogram does not consider detector orientation relative to direction of the nuclear detonation. This original assumption is tested in section 4.1.1.2, and may require a correction factor for real-world use. For purposes of analysis, it is assumed that directional dependence will be accounted for and corrected when calculating activation levels.

The code starts by reading in all needed previous outputs, including the card deck that specifies the scenarios to run in the subprogram. The code then filters out any element/detector location combinations excluded by a scenario's input card. The subprogram then calculates the expected number of counts for each possible element (subject to filters from the input deck) that would be detected for each library spectra (scaled up to the unknown weapon's yield), incorporating the decay time until the start of

counting, allowed counting time, and minimum number of counts needed to reduce statistical uncertainty. The default parameters are a 15 kt yield, a 72 hour delay in the start of counting, a 3 hour allowed count, and 3000 total counts required.

The subprogram then filters out any element/detector location/library spectrum combinations that do not generate the minimum number of counts required. These combinations will not be considered for further analysis for this scenario. This is to prevent any activation level with too great of uncertainty to be used from influencing the match chi-squared calculations.

The code then creates the unknown spectra set by perturbing the library spectra set using a normal distribution and the reported uncertainties from the MCNP transport calculation. This perturbation is based on a single standard deviation by default; it can be scaled up for other tests if desired. The resulting unknown spectra are scaled up by the yield factor from the input deck.

The subprogram then calculates a match chi-squared score and associated yield for each unknown and library spectra combination. A golden section search is used to find the yield factor that minimizes the chi-squared score calculated from equation (5). During the process, useful summations of the match chi-squared contribution by element and detector location are compiled as well. Upon completion, each scenario's independent results are written to files before starting the next.

A sample of the primary output of the matching program generated using all default values is below in Table 4:

Table 4 – Matching Results: χ^2 and Yield Results, Default Scenario

		χ^2 value Unknown Weapon				
		FM	FUS	LB	WPu	WU
Library	FM	0.22	4105	1649	225	224
	FUS	1181	0.16	4927	1862	1575
	LB	730	4077	0.09	1454	1439
	WPu	184	4143	2649	0.13	4.14
	WU	171	4305	2531	4.14	0.10

		Yield				
		FM	FUS	LB	WPu	WU
Library	FM	15.0 kt	53.7 Mt	328.0 kt	5.0 Mt	3.2 Mt
	FUS	0.01 t	15.0 kt	0.36 t	2.7 kt	1.8 kt
	LB	0.99 t	59.1 Mt	15.0 kt	627.8 kt	384.6 kt
	WPu	0.05 t	150.1 kt	1.3 kt	15.0 kt	9.8 kt
	WU	0.07 t	231.0 kt	2.0 kt	23.1 kt	15.0 kt

Note the low matching scores along the diagonal that represent the unknown and library spectra matches, and how that diagonal's yield scores are very close to the default unknown yield of 15 kt. The Little Boy (LB) library spectrum was such a poor match for the Fusion (FUS) unknown spectrum that the code's upper yield scaling limit was reached – 10,000 times the expected value, in this case 150 Mt for a 15 kt unknown spectrum. The large yield factors for the FUS column show the program trying to match library spectra that lack the characteristic fusion 14.1 MeV neutron peak to a spectrum that originated with that large peak. The match chi-squared scores are very high, but a yield estimate that is wildly out of bounds compared to real world estimates is another indicator of a poor spectra match.

Another important set of outputs are the breakdowns of match chi-squared contributions. These are broken down for each scenario by detector location and element (and thus reaction). Two separate scenarios' differing results (summed over each of the 25 library/unknown spectra combinations for each element) are shown as examples below in Table 5 and Table 6:

Table 5 – Match Chi-Squared Contribution, Default Scenario

	χ^2 contribution		
Mg	1.41%	Rh	0.27%
Al	1.45%	Pd	0.52%
Ti	2.80%	Cd	1.61%
Cr	8.56%	Sn	0.26%
Fe	0.26%	Hf	7.39%
Co	4.40%	Ta	8.07%
Ni	5.78%	W	5.00%
Cu	11.13%	Re	9.64%
Ge	0.42%	Ir	16.28%
Zr	0.42%	Au	10.30%
Mo	2.36%	Pb	1.65%

Table 6 – Match Chi-Squared Contribution, Default Scenario plus 500 keV Threshold

	χ^2 contribution		
Mg	0.53%	Cu	0.28%
Al	0.39%	Mo	0.27%
Ti	22.20%	Rh	1.16%
Cr	0.01%	Cd	0.26%
Fe	0.97%	Re	4.12%
Co	0.35%	Au	11.10%
Ni	58.11%	Pb	0.24%

Note that changing a single parameter in the analysis significantly changed the relative importance of each element to the match chi-squared scores, and eliminated several elements altogether.

Another useful set of metrics reported by the subprogram are the countable locations for each scenario. The countable locations represent the number of element/detector location combinations for each spectrum that meet the minimum counting criteria. Sample output from the default scenario is below in Table 7:

Table 7 – Countable Locations, Default Scenario

	Countable Locations				
	FM	FUS	LB	WPu	WU
Mg	0	4	0	0	0
Al	0	4	0	0	0
Ti	0	11	0	2	0
Cr	0	18	3	10	8
Fe	0	2	0	0	0
Co	1	24	6	16	14
Ni	0	13	0	3	2
Cu	3	30	7	20	18
Ge	0	12	1	6	5
Zr	0	17	2	7	6
Mo	1	26	6	16	15
Rh	0	4	0	0	0
Pd	0	10	1	6	5
Cd	3	30	8	20	18
Sn	0	9	1	5	3
Hf	6	31	10	22	21
Ta	15	32	21	31	30
W	15	32	21	31	30
Re	19	32	24	32	32
Ir	17	32	21	32	31
Au	27	32	30	32	32
Pb	0	4	0	0	0
Total:	107	409	162	291	270

Since the default scenario includes 34 detector locations, this is the maximum number of countable locations a library/unknown spectra combination can have for a given element. Gold has a large number of countable locations across all the combinations, whereas lead is only countable in a handful of locations for a single library spectrum – FUS. Using these data alongside the match chi-squared contribution chart in selecting elements that not only have large match chi-squared contributions in general, but that cover a large portion of the spectra search space and work at a variety of detector locations. If an element only works

at detector locations very close to the nuclear explosion, it may be difficult, slow, or even impossible to recover those detectors, reducing that element's utility for the AFIDS project. Multiple scenarios will be designed to test the sensitivity of each elements' countable locations to both distance and direction from the explosion.

3.4 Analysis Procedure

This section lays out the overall plan for selecting optimal materials for the AFIDS detector. Some of the analysis plan changed during the research due to the nature of the initial results, especially the concentration of match chi-squared contribution in a limited number of elements.

3.4.1 Initial Approach and Changes

The initial approach to this analysis was to create a scoring algorithm to rate different combinations of elements for the AFIDS detector material against each other, then use a computer program to exhaustively examine the search space to determine the highest scoring combination for a set optimization criterion. This approach had several shortcomings.

First, with 27 commercially-available elements with high enough melting points to be useful for AFIDS, alongside the 20 target rod slots available in the design, the search space was very large indeed – 27^{20}, approximately $4(10^{28})$ possible combinations.[21]

[21] Re-use of the same element multiple times in a detector has value and will be considered. Multiple copies can increase the available mass, increasing the number of

Scoring each combination takes about 5 seconds of real time with the available computer power, which led to a wildly impractical runtime to complete the search. A directed optimization approach would be required.

Second, the relative match chi-squared contributions from different candidate elements was not evenly or randomly distributed. Rather it was concentrated into 4-7 elements for most scenarios, including the default scenario, with less than 1% of the remaining contribution attributable to the other ~20 elements. These two initial realizations drove a change from an exhaustive search approach for optimization to a manual optimization driven by prioritized criteria, subject to constraints of cost and the amount of time a sample remained countable.

3.4.2 Account for Cost of Target Rod Materials

The AFIDS project is subject to cost constraints, and even within the hard constraint, improving the effectiveness/cost ratio is desirable. The budget for each detector, when manufacturing at scale, is $250 for each complete detector set, including up to 20 target rods. The materials and manufacture for the detector body accounts for $50 of this, leaving a maximum of $200 for target rod elements. In Table 8 below, the approximate costs for a target rod of each of the commercially-available elements are shown, with dimensions of 1.0 mm diameter x 5.0 cm length, with the assumption of a

---

activations and eventually counts. Multiple copies can be dispersed angularly to mitigate directional attenuation effects as well.

minimum 1,000 rod purchase. If AFIDS is fully fielded, this cost will only be lower at scale.

Table 8 – Cost per Target Rod, 1mm Diameter, Minimum 1,000 Rod Purchase[22]

Cost per rod, min. 1,000 rods			Cost per rod, min. 1,000 rods		
Symbol	Element	Cost	Symbol	Element	Cost
Mg	Magnesium	$18.94	Pd	Palladium	$196.50
Al	Aluminum	$0.06	Ag	Silver	$1.06
Si	Silicon	$169.00	Cd	Cadmium	$13.40
Ti	Titanium	$0.23	In	Indium	$2.37
Cr	Chromium	$0.85	Sn	Tin	$0.13
Fe	Iron	$0.10	Hf	Hafnium	$10.50
Co	Cobalt	$42.10	Ta	Tantalum	$4.13
Ni	Nickel	$0.35	W	Tungsten	$0.59
Cu	Copper	$0.06	Re	Rhenium	$123.20
Ge	Germanium	$10.95	Ir	Iridium	$390.24
Zr	Zirconium	$1.88	Au	Gold	$97.80
Nb	Niobium	$0.89	Pb	Lead	$0.08
Mo	Molybdenum	$0.30	Bi	Bismuth	$0.33
Rh	Rhodium	$208.17			

Note that two elements, rhodium and iridium, outright exceed the total target rod budget for a single rod. However, it is possible to place half-length rods into the AFIDS detector, which would cut these costs in half and make those elements still feasible to use. They

[22] These costs are based on comparing scientific supplier catalogs offering elemental metals at >99% purity in 1mm diameter rod form for a 5 cm length. A larger scale AFIDS purchase by the US government could drive better economy of scale and pricing.

would need to provide very strong impact on the results for inclusion, however. Several of the more common metals are very inexpensive, creating a very low threshold for their inclusion if they provide useful results at all.

3.4.3 Maximize Discrimination of Incorrect Spectra

Early in the analysis of results, it was clear that the AFIDS match scoring approach would clearly delineate correct matches under the ideal conditions of the default scenario, which includes recovering all 34 detectors and counting all the target rods in each – an unlikely scenario in the real world, but a useful one for comparing element performances. There were no elements that produced false negatives – high match chi-squared scores for correct matches.

The more useful metric was how high of a match chi-squared contribution the elements each made to incorrect matches. An element that scored very low (<1) for the correct match and very high (>1,000) for most of the incorrect matches is much more useful than an element that scores low for almost every combination. The discriminatory value comes in how strongly an element rejects an incorrect match.

3.4.4 Account for coverage across spectra types

While the magnitude of discrimination discussed in the previous section is a driving factor in the selection of elements, a breadth of coverage is needed as well. An example is nickel. This element does an excellent job of discriminating between fission and fusion spectra at a very low cost. However, it is less useful in discriminating between some fission spectra, and it is unable to get sufficient counts at most detector locations for the LB

spectrum. While a very useful material, it must be complemented by an element like copper that better discriminates the different fission spectra and is countable in more locations for the LB spectrum.

3.4.5 Minor Criteria

There are several other small matters to consider when selecting the optimized target set. These are not as important as maximizing discrimination ability and ensuring wide coverage across spectra but should be accomplished if possible.

The inclusion of elements that feature neutron energy threshold activation reactions can reduce uncertainty related to local neutron scattering effects. An extreme example would be a detector placed near a swimming pool, full of highly-moderating hydrogen. A city-scale MCNP model could not capture such local details that could affect activation results. While the detectors would be placed more sensibly than that, threshold reactions are likely to have undergone fewer scattering events on the way to the detector, and the scatters they do make are more likely to be in the form of skyshine, which is less affected by the details of the urban terrain below. This creates a better signal/noise ratio.

It is desirable to have at least one element whose main activation product has a long half-life to allow follow-up counting and validation well after the 3-10 days immediately following the event. Researchers are still studying activated samples from Hiroshima and Nagasaki as new and better analysis techniques and equipment are invented. Intentionally including one long-lived activation product could aid in additional studies after the immediate aftermath.

A tertiary consideration is avoiding vandalism and theft of the detectors from those who would sell the metals inside for scrap. An AFIDS deployment would place dozens if not hundreds of detectors in a large city, and if it became known that each detector contained a significant amount of gold that could be resold, they could be targeted. While many of these detectors will be out of easy reach, it is not practical to check on them frequently, and the detectors could be missing materials without anyone being made aware. Therefore, highly-pilferable materials like gold should be avoided unless they provide very large contributions to the project. Elements like iridium, although expensive, are less easily identified and do not have a robust resell market.

3.5 Selection Methodology

The goal of the optimization is to select the target rods that clearly discriminate between the most spectra, with maximal spectra coverage, at a minimum cost.

3.5.1 Spectra Set

The optimization will consider all five unclassified spectra equally weighted. The ability to discriminate between fission and fusion, gun-type and implosion, and uranium versus plutonium, are all valuable parts of the AFIDS project. The breadth of coverage is important; certain elements excel at distinguishing between fission and fusion spectra, while others discriminate well between different fission spectra. Two examples are shown in Table 9 below:

Table 9 – Match Chi-Squared Contributions, Select Spectra, Default Scenario

Library Unknown	χ^2 contribution WPu FUS	WPu WU
Mg	7.16%	0.00%
Al	7.33%	0.00%
Ti	14.01%	0.00%
Cr	7.48%	4.20%
Fe	0.57%	0.00%
Co	2.73%	2.30%
Ni	24.16%	5.12%
Cu	5.92%	8.82%
Ge	0.52%	0.54%
Zr	0.39%	1.86%
Mo	2.48%	3.12%
Rh	1.37%	0.00%
Pd	0.72%	1.62%
Cd	0.91%	2.77%
Sn	0.49%	0.03%
Hf	2.53%	8.25%
Ta	2.61%	13.67%
W	1.42%	7.37%
Re	2.68%	8.94%
Ir	4.14%	16.18%
Au	2.10%	15.23%
Pb	8.30%	0.00%
χ^2 total	4143	4.15

In the first column, which shows the discrimination between a fission (WPu) and fusion (FUS) spectrum, elements like chromium and copper stand out, performing better than even the expensive iridium and gold target rods. Conversely, the second column shows contributions to two similar fission spectra undergoing discrimination. Iridium and gold, alongside tantalum, provide much of the chi-squared score. Copper does less but is still a

valuable contributor, especially for its price. Chromium is much less effective. Note that some elements like nickel perform equally well between these two different tests. Finding a combination of target rods that can cover the range of possible spectra is critical for reliable discrimination.

3.5.2 Yield Range

The minimum yield that will be examined is 15 kt, which is in line with a gun-type device of limited size and sophistication. This is lower end of the yield range is also the most important, because it is the hardest to obtain sufficient counts for. Some tests, focused on threshold reactions, will conducted at 150 kt, to increase the number of countable locations.

3.5.3 Minimum Distance (Melting Considerations)

The temperatures endured by a detector are primarily a function of nuclear weapon yield and distance. Previous work on AFIDS conducted a detailed analysis of what distances each material is likely to remain unmelted as a function of yield. [2] Most potential target rod materials have melting points exceeding the aluminum detector body, and the detector body itself somewhat protects target rods from the heat of the explosion. A notable exception is tin, which melts at distances further out than the aluminum detector body.

Based on the previous work, a minimum distance of 400m from the explosion will be required for the 15 kt explosions, 700m for the 150 kt, and 1 km for the 1.5 Mt.

Detectors inside these radii may be partially melted and uncountable and should not be relied on for match discrimination.

3.5.4 Angular Effects

Angular effects come in two forms: the change in neutron fluence dependent on the location of a target rod within the detector relative to the direction of the blast, and the ability to retrieve and count detectors in a timely manner disrupted due to directional fallout. The effects of the target rod location are discussed in more detail at the start of section 4.1; selecting elements with reaction thresholds >500 keV avoids the majority of these effects. However, non-threshold reactions are still usable with modeling and correction factors applied.

The fallout plume from a nuclear detonation will be created downwind of the explosion. Winds are generally unpredictable, so a detector target rod set must not depend strongly on detectors located in a particular direction for its results. To test for this, analysis will exclude 60-degree swathes of detectors in multiple directions to see if results are significantly affected.

3.5.5 Delay Time Before Start of Counting

Elements whose activation products have longer half-lives will maintain a sufficiently high count rate for a longer period. This allows for a greater delay in the collection and counting of these elements. While some shorter half-life elements can be accommodated by strategically planning the order of counting, generally speaking, elements who can maintain the minimum count rate for longer are more valuable. It is

difficult to predict how long the delay in the start of counting may be, especially in the more damaged or radioactive areas that detectors are in.

The trade-off of a longer half-life is that these activation products will tend to have lower count rates in general, even if that count rate is maintained for a longer time. Some of these elements will require a large number of initial activations to create a count rate sufficient for AFIDS purposes.

CHAPTER 4. RESULTS

4.1 Validation of Assumptions

The four major assumptions listed in section 3.1.1 are examined in this chapter, using both experimental and modeling approaches. Refinements to the approach based on these tests will be incorporated before conducting the optimization of target rods.

4.1.1.1 Gamma Self-shielding Assumption

An initial assumption was made that the gamma rays emitted from activation products would not be significantly self-shielded by the target rods themselves. To test this assumption, the Gamma Escape Probability code (section 3.2.2.1) was written to model uniformly distributed, isotropically-directed gamma rays emitted at a range of energies from each of the elements. Select results shown in Figure 8 (page 42) illustrate that this is not a valid assumption. Low energy gamma rays are significantly attenuated while escaping the 1mm diameter rods, and even higher energy gamma rays have measurable attenuation.

Fortunately, this attenuation is only a function of the element and the gamma ray's energy, so lookup tables were calculated for each element over a large range of gamma energies, with close attention paid to energy levels near discontinuities in attenuation. These lookup tables were then used in the remainder of the code as a correction factor when determining the number of initial activations based on counts taken at a later time.

4.1.1.2 Detector Body Shielding and Angular Effects Assumptions

Note that this section assumes the worst case of a monodirectional incoming neutron fluence to determine the differences in angular positioning of target rods. Actual fluence will have scattering effects that reduce the effects of angular positioning. The validations of these assumptions are combined because they are both testable using a detailed MCNP model of the main part of the detector body and the transported neutron spectra. They are also testable by physical experiment.

4.1.1.2.1 Modeling Approach

The modeling efforts will show that there are significant effects from the detector body, especially at select energy levels. There are also significant effects dependent on the target rod slot location relative to the direction of incoming radiation. A representation of the model is below in Figure 9:

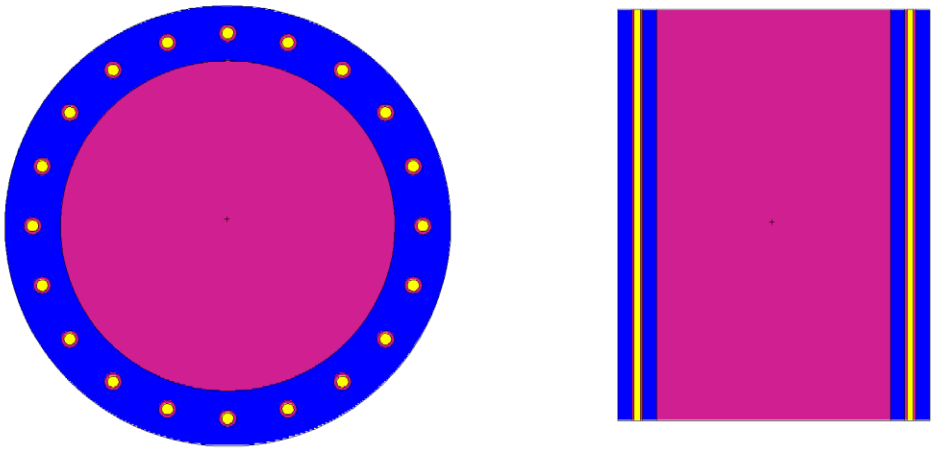

Figure 9 – MCNP Model of Detector and Target Rods

The first modeling approached used an MCNP model of the aluminum detector body, constructed out of Al-6061 alloy. Only the cylindrical portion, which is the hollow piece separate from the top and bottom of the detector body, is modelled to focus on the angular effects. Target rods are also modelled. Changing which element to use for the target rods did not appreciably change the fluences in other target rod slots, so aluminum was used by default. The source term was designed to isolate the effects of scattering and capturing in the aluminum body by incoming neutron energy level. This was accomplished by a series of 200 files, each with a monoenergetic source aligning with the 200 energy groups of the reaction cross section data. Figure 10 and Figure 11 display the normalized flux versus energy group for each target rod location, with 0 degrees representing the target rod directly facing the incoming neutrons, and 180 degrees on the very far side of the detector. The flux is normalized against what would occur in a vacuum with no detector body.

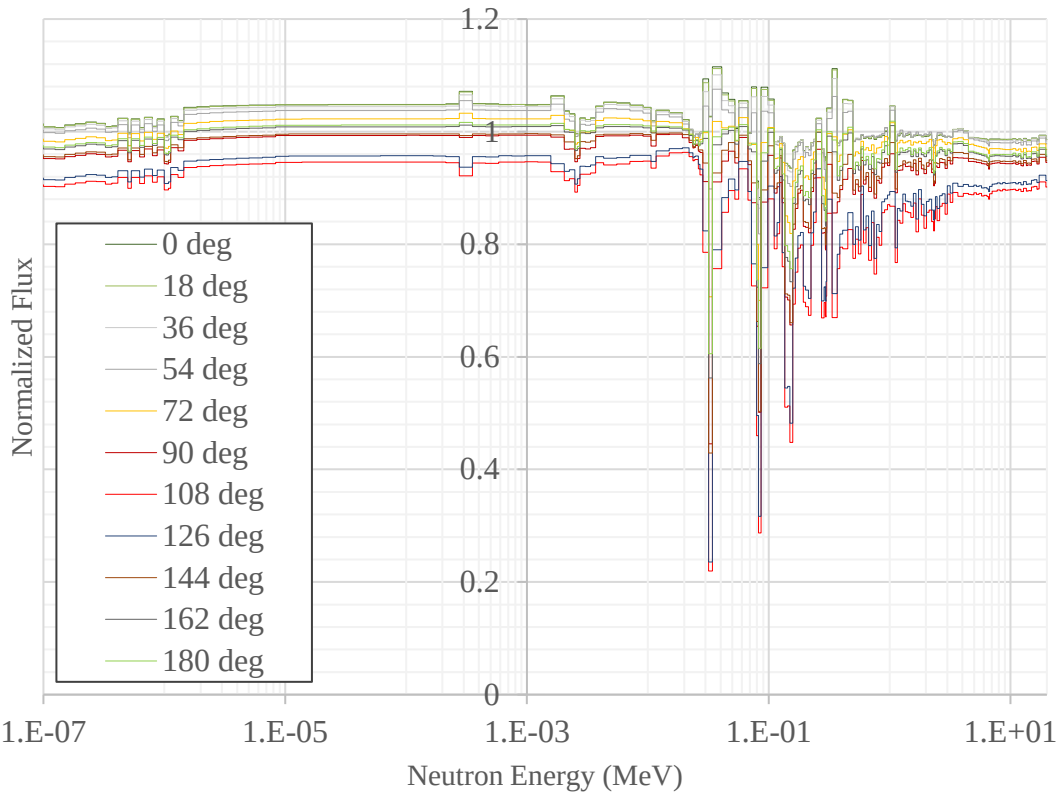

Figure 10 – Normalized Flux vs. Energy (MeV)

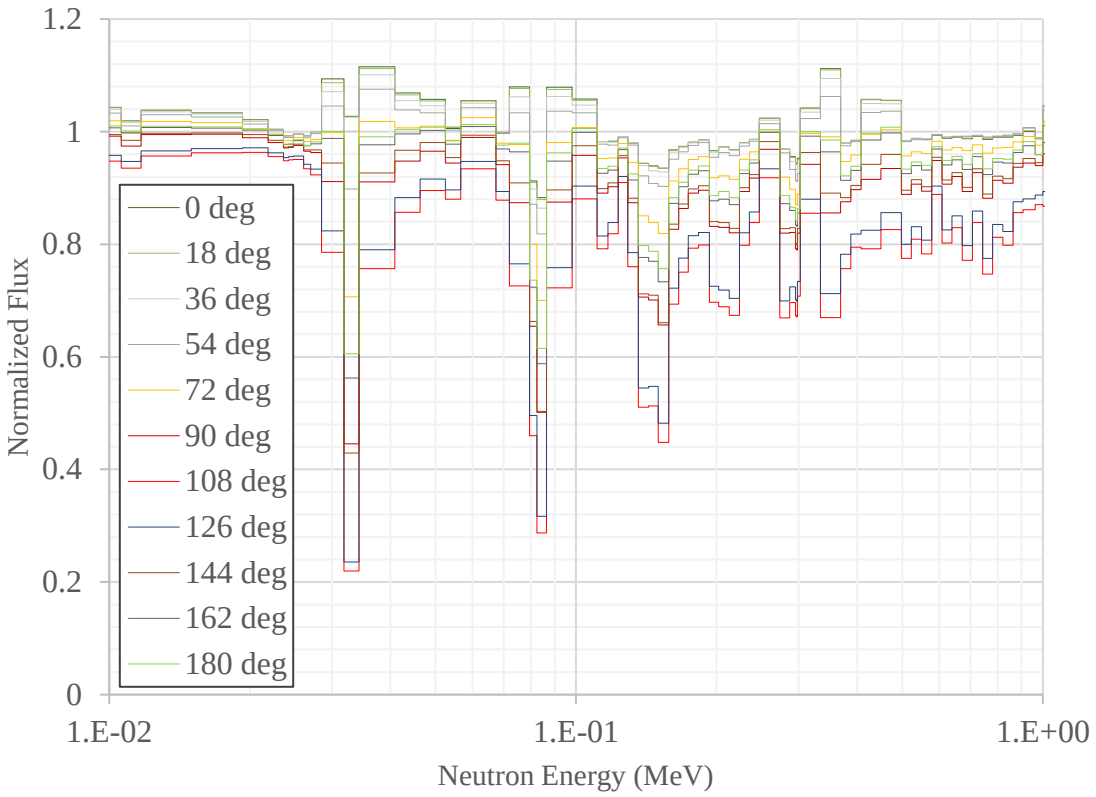

Figure 11 – Normalized Flux vs. Energy (MeV), Zoomed View

There are select energy bins, including multiple bins in the 30 keV-90 keV range, with very large reductions in flux. The maximum effect is in the 108 degree slot, which requires the incoming fluence to travel through the largest amount of material before reaching it. The largest reduction was 78% in a single energy bin. Some positions have normalized fluxes greater than 1, though this effect is not nearly as significant.

These large reductions in flux align closely with the resonances in the aluminum cross section data. In Figure 12, the Evaluated Nuclear Data File (ENDF) cross section data for ^{27}Al is superimposed on Figure 11 after normalizing against its largest peak. [14]

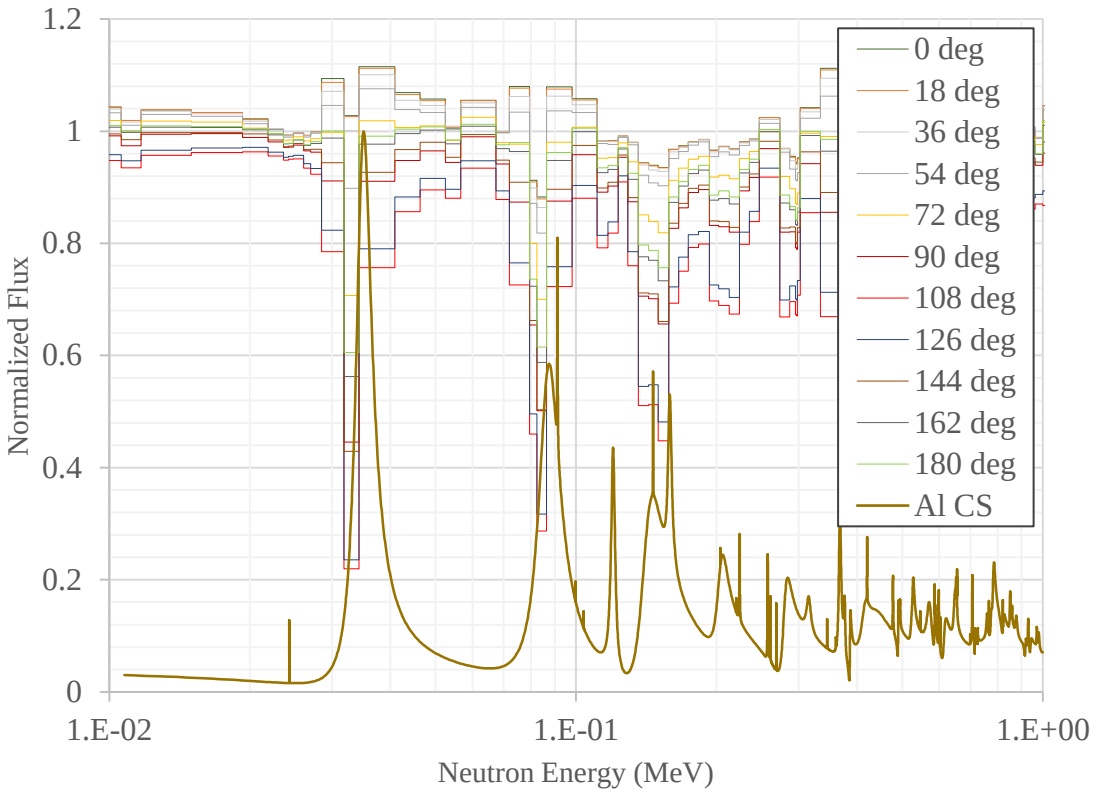

Figure 12 – Normalized Flux vs. Energy (MeV) with 27-Al Normalized Cross Section

Since the angular effects appear important, they were tested again, this time using realistic transported neutron spectra from the spectra list. The effects were not as pronounced since the majority of the incoming fluence was not contained in the absorption/scattering peaks, but the 108 degree slot did show a 15% reduction in flux in an average test case.

The effect of the detector body and angular slot position, while not overwhelming, is measurable and noteworthy. In this worst-case scenario of a mono-directional beam source the effects are not negligible; they must be accounted for and corrected in physical measurements. The real world fluence would not be mono-directional in nature, but the degree of anisotropy to expect requires transport calculations recommended for future

work. The needed correction factors can be pre-calculated using a representative unknown spectrum. The effect can also be reduced if multiple copies of the same element are dispersed along the angles of the detector body and averaged.

Although this assumption is not valid for real-world use of AFIDS, the effects are not so large that they will change the number of countable locations (countable elements) in the majority of detector locations. In the subsequent modeling, it is assumed that the correct factor has been used to adjust for angular position as part of the counting / activation determination process.

4.1.1.2.2 Effects of Impurities in Alloy

To determine if impurities in Al-6061 were causing significant effects on the flux received by the target rods, the MCNP models were re-run using pure aluminum. The results were almost identical, with the same angular effects. Therefore there is nothing to gain by using the more expensive but higher purity Al-1100 alloy.

4.1.1.2.3 Experimental Approach

A limited series of physical experiments were conducted to validate the modeling discussed in the previous section. An americium-beryllium (AmBe) source as well as a deuterium-deuterium neutron generator (2.5 MeV neutron peak) were used as neutron sources. Detector prototypes constructed of Al-6061 were used to hold target rods. To match the model, only the cylindrical portion of the detectors (no top or bottom pieces) were emplaced.

For the AmBe source, calculations determined that nickel and titanium target rods were most likely to produce enough counts for reasonable uncertainties, given the constraints on experimental and counting time. Unfortunately, liquid nitrogen supply issues interrupted the counting of these samples, leaving decayed activities too small to be useful.

For the neutron generator, copper was the target rod with the greatest predicted activation level.[23] Two targets were irradiated simultaneously as pictured in Figure 13 below:

[23] Gold target rods would have performed better, but were not available due to cost.

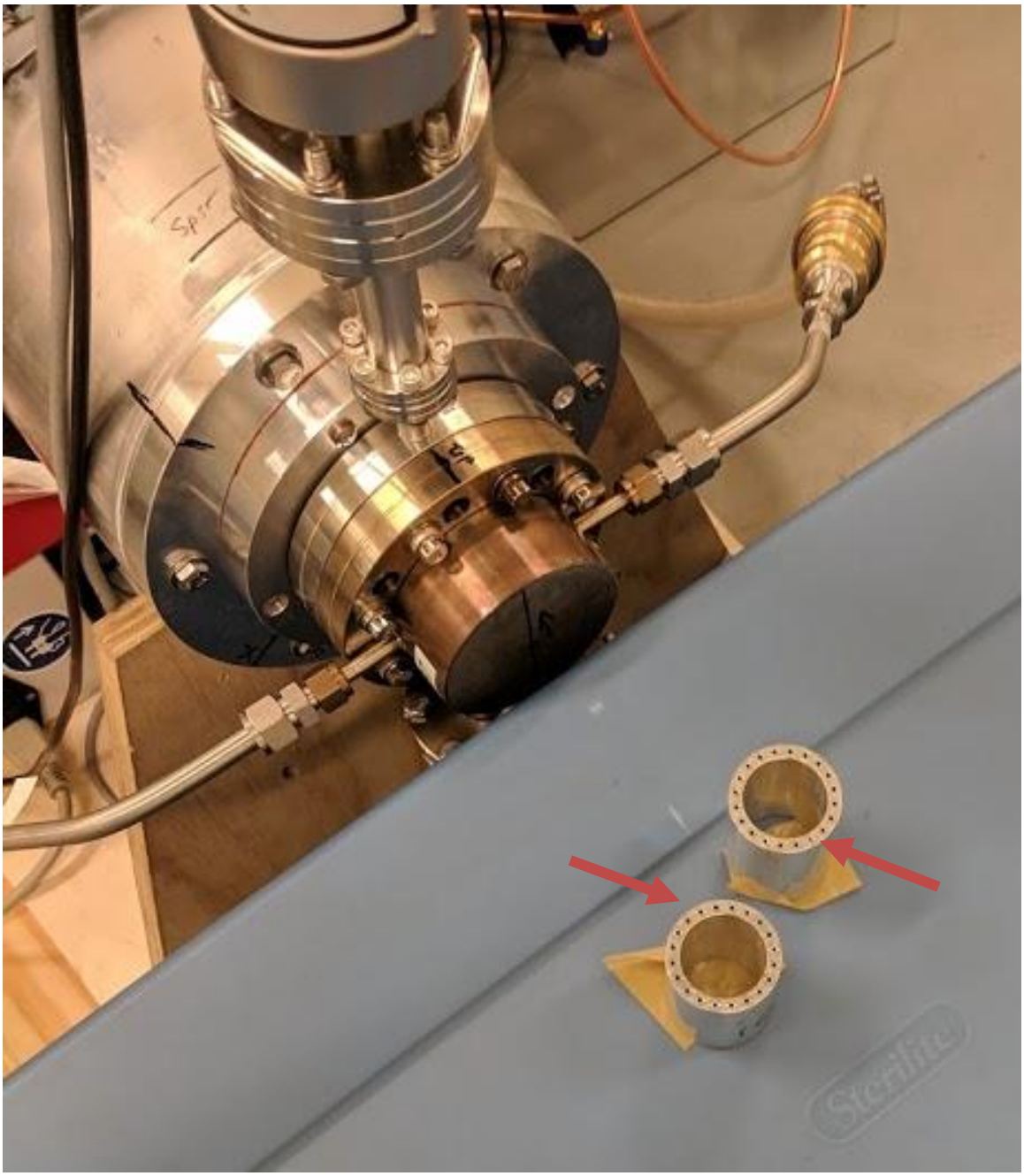

Figure 13 – Neutron Generator Experimental Setup

The “outer” position is the rightmost detector, with the copper target rod in the position 180 degrees from the front of the detector facing the neutron generator. The “inner”

position is on the left and has its target rod in the 0-degree position, with the minimal amount of aluminum holder material between the source and the target rod. Red arrows point at the slots used. Note that the target rods are equidistant from the source; only the amount of detector body in the line-of-sight to the source has been altered. The irradiation was performed simultaneously to minimize effects of the neutron generator's warm-up cycle in producing a consistent neutron fluence over time.

The expected activation reaction was $^{63}Cu(n,\gamma)^{64}Cu$, given that the neutron source was below the energy threshold for the competing $^{63}Cu(n,2n)^{62}Cu$ and $^{65}Cu(n,2n)^{64}Cu$ reactions. This reaction's activation product has a gamma line at 511 keV due to the immediate annihilation of the emitted positron, which occurs in 61% of the decay events.

The samples were both irradiated for 3 hours. The outer target was counted immediately after irradiation for 2 hours; the inner target was counted immediately after the outer target at 2.5 hours after irradiation, in order to increase the counts captured after the second target's ^{64}Cu (half-life of 12.7 hours) decayed while waiting for the detector. The HPGe counts are shown in Figure 14 below:

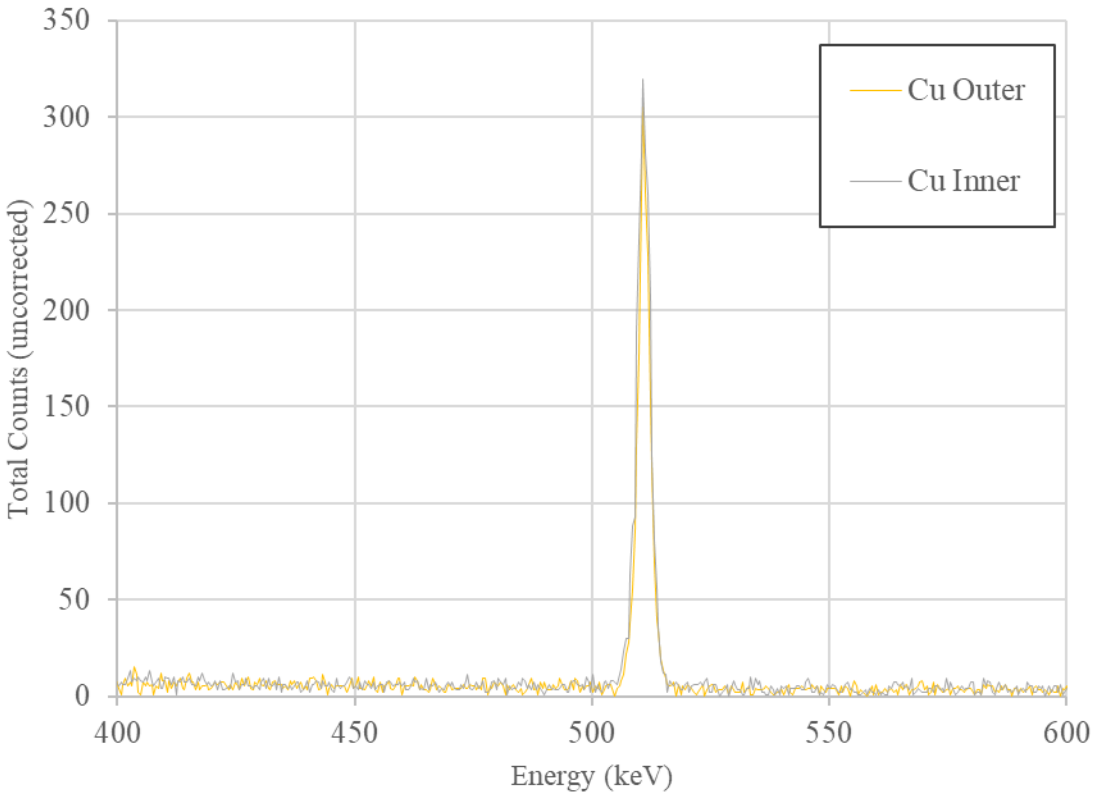

Figure 14 – 511 keV Peaks from Cu Counting

The sharp annihilation peak matches the expected reaction. Integrating the peaks for the two rods yields 1960 ± 50 counts for the outer position and 2310 ± 50 counts for the inner position. Correcting for decay and calculating the initial number of activations, the ratio of activations between outer and inner rod locations was is 0.94 ± 0.03, which is a function of the intervening aluminum thickness.

An MCNP simulation of the experiment assumed a monoenergetic, monodirectional source of 2.5 MeV neutrons arriving at the detector body. This approximation is sufficient to determine the proportionality between the outer and inner

target rod positions. The reaction rates are calculated for both the 0 and 180-degree cells using modified track length estimator tally. The ratio of the total reaction rates from the simulation was 0.9677 ± 0.0003 between outer and inner, a lower ratio than the experimental value, but within the combined margin of error. Given the simplification of the models that ignored the angular and energy spread of the neutron generator's fluence, this experimental result matches reasonably well with the models used in MCNP, giving confidence to that modeling effort.

4.1.1.2.4 Correction of Detector Shielding/Angular Dependence Assumption

Based on the experimental validation of the MCNP modeling, it is clear that there are a measurable, significant effects from both the detector body interacting with the incoming fluence, and that the effect is strongly dependent on the position of the target rod relative to the direction of the incoming radiation. The localized energy effects can be as high as 80% in a very few cases, but in practical application, the worst position (108 degrees) will receive about 20% less activations than the optimal position (0 degrees). This 20% factor assumes that the incoming radiation is monodirectional, which is not strictly true, so the real-world correction factor would be less.

To correctly account for this in real-world modeling, the MCNP transport of the library spectra to the detector locations must also tally information about the direction of the incoming neutrons, to determine how much the direction is biased. Then an additional smaller model MCNP code simulation could take that angularly-distributed incoming fluence and transport it the final distance through the detector body to the target rods to

model the relative differences in activation levels to be expected based on position. This is beyond the scope of this research effort but not difficult to account for.

For purposes of selecting the optimal target rod set, this correction factor would be applied to the modelled activations, propagated through the simulated counting process, then divided back out when determining the initial activation levels. The only effect it would have is whether a particular target rod would meet the 3,000-count threshold needed for good statistics. The desire is to err on the side of including candidate materials versus excluding them, and a 20% reduction in count rate would not affect the selection of many of the material, so this factor is ignored in the simulations in this research.

4.2 Effects of Detector and Foil Selection on Match Discrimination

In this section, multiple parameters will be varied to make new scenarios to test the ability of each elemental target rod to provide match chi-squared contributions and countable locations under a variety of conditions and restrictions. The overarching goal of the optimization remains to create the best discrimination between spectra, at the lowest cost, with enough robustness to handle a wide span of the possible design and target space of the unknown weapon.

4.2.1 Distance

The distance between the nuclear explosion and a given detector affects multiple aspects of the AFIDS system. First, detectors too close to the detector for a given yield may partially melt, leading to unusable samples. Second, detectors close to the explosion will be generally more difficult to recover, as their supporting structures such as buildings

may have been destroyed, the areas may have suffered high levels of radiation and secondary fires, and other emergency response priorities may preclude access. Third, the further a detector is from the explosion, the fewer activations it will receive in general. Detectors too far from the source will have fewer and fewer target rods sufficiently activated for counting. Conversely, these detectors are in safer areas to retrieve, so their counting would likely begin sooner, partially mitigating the loss of signal due decreasing activity with distance since the target rods will have less time to decay before counting.

In a large grid array, there will be a large number of detectors outside each minimum distance, which eventually will overwhelm the ability to count all the target rods from those locations in a timely manner. Since the activation levels and discrimination value falls off at larger distances, there are diminishing returns from counting detectors further and further away. The effects of setting a maximum distance has been tested as well. The 34 detectors modeling the default scenario have distances from the explosion ranging from 173 m up to 1,962 m.

4.2.1.1 Minimum Distance or Greater

Starting with the default scenario parameters, 14 scenarios were generated with minimum distances of 300 – 1500 m, alongside a no-minimum distance scenario for comparison. The match chi-squared contributions of the commercially-available elements are listed in Table 10 below:

Table 10 – Match Chi-Squared Contribution vs. Minimum Distance Required (km)

	χ2 contribution percentage													
	0	0.3	0.4	0.5	0.6	0.7	0.8	0.9	1	1.1	1.2	1.3	1.4	1.5
Mg	1.1	1.2	1.4	1.5	0.6	0.9	X	X	X	X	X	X	X	X
Al	1.2	1.3	1.5	1.5	0.7	0.9	X	X	X	X	X	X	X	X
Ti	2.5	2.4	2.8	2.8	2.2	2.4	1.7	1.2	0.5	0.7	X	X	X	X
Cr	10.8	10.2	8.6	6.3	4.9	3.8	2.9	2.3	1.6	1.2	0.4	X	X	X
Fe	0.9	0.7	0.3	0.0	X	X	X	X	X	X	X	X	X	X
Co	5.2	5.4	4.4	2.7	2.5	2.4	2.2	2.3	2.4	1.6	0.8	0.6	0.4	X
Ni	4.3	4.0	6.0	6.1	4.0	4.1	3.7	3.0	1.5	1.3	X	X	X	X
Cu	10.6	13.7	11.0	9.2	6.8	6.6	6.2	5.6	6.2	6.0	5.5	2.2	1.6	2.4
Ge	0.7	0.7	0.4	0.4	0.3	0.2	0.1	0.1	0.1	0.0	X	X	X	X
Zr	0.5	0.5	0.4	0.3	0.4	0.2	0.1	0.1	0.1	0.0	0.0	X	X	X
Mo	3.1	3.0	2.4	2.1	2.1	2.0	1.8	1.6	1.5	1.2	0.5	0.4	0.4	0.4
Rh	0.3	0.3	0.3	0.3	0.1	0.2	X	X	X	X	X	X	X	X
Pd	0.6	0.6	0.5	0.5	0.5	0.3	0.1	0.1	X	X	X	X	X	X
Cd	1.9	1.9	1.6	1.7	2.2	2.1	2.1	2.5	2.6	2.2	2.2	2.1	0.5	0.5
In	0.1	0.1	X	X	X	X	X	X	X	X	X	X	X	X
Sn	0.3	0.3	0.3	0.3	0.2	0.1	0.1	0.1	X	X	X	X	X	X
Hf	6.8	6.8	7.4	4.9	4.7	4.3	3.8	3.8	3.8	3.1	3.2	2.3	1.7	1.6
Ta	8.7	8.2	8.0	9.6	10.8	10.7	10.4	10.6	11.1	10.1	8.1	11.2	8.9	7.0
W	4.9	4.7	4.9	6.0	7.6	7.8	8.3	7.8	6.7	7.3	6.1	8.9	6.2	8.8
Re	9.0	8.8	9.5	11.2	13.8	13.1	14.0	15.2	14.2	14.9	17.0	17.7	13.0	11.3
Ir	14.7	14.2	16.3	16.4	17.8	18.7	19.7	19.6	19.5	20.7	17.2	14.1	14.0	15.4
Au	9.3	9.4	10.3	14.7	17.0	17.9	22.9	24.3	28.4	29.6	39.1	40.6	53.4	52.6
Pb	2.0	1.8	1.7	1.8	0.8	1.1	X	X	X	X	X	X	X	X

The “X” denotes that an element’s target rod cannot reach the minimum number of counts (default of 3,000) at that distance (given the default delay time and counting time of 72 hours and 3 hours, respectively.)

Starting at the no minimum distance scenario, the initial concentration of the match chi-squared contributions is apparent. Of the 23 elements with useful data, only 12 of the elements contribute 2% or more to the match chi-squared totals. There is a particular concentration near the higher-Z elements of hafnium through gold. None of the major

contributing elements lose their signal until 800 m away, and even then, there are no pronounced effects due to distance until 1,000 m is reached. At this distance, the signal from titanium is lost, and the signal from chromium is severely reduced in value. At 1,200 m, the signal from nickel, a key threshold reaction, is lost, and the cobalt rod is barely usable.

Meanwhile, the elements whose signals persist to longer ranges are accounting for more and more of the match chi-squared contribution. A gold target rod would single-handedly account for 39% of the chi-squared at 1,200 m and 6 elements account for 95% of the signal at that distance. Unfortunately, these tend to be expensive elements, requiring tradeoffs in the optimization plan.

The following series of tables shows the differences in the matching and yield estimate scores at select distances when major contributors start to lose their usefulness:

Table 11 – Matching Results: χ^2 and Yield at 600 m

		χ^2 value Unknown Weapon				
		FM	FUS	LB	WPu	WU
Library	FM	0.17	2114	1327	3.33	3.95
	FUS	367	0.16	3145	1023	980
	LB	427	2771	0.09	955	930
	WPu	2.02	2227	1358	0.12	3.32
	WU	1.66	2318	1292	3.10	0.15

		Yield				
		FM	FUS	LB	WPu	WU
Library	FM	15.0 kt	48.2 Mt	245.3 kt	5.2 Mt	3.4 Mt
	FUS	0.01 t	15.0 kt	0.14 t	2.4 kt	1.6 kt
	LB	1.3 kt	16.9 Mt	15.0 kt	673.6 kt	418.7 kt
	WPu	0.04 t	137.6 kt	0.70 t	15.0 kt	9.7 kt
	WU	0.07 t	211.3 kt	1.1 kt	23.2 kt	15.0 kt

Table 12 – Matching Results: χ^2 and Yield at 800 m

		χ^2 value Unknown Weapon				
		FM	FUS	LB	WPu	WU
Library	FM	0.25	860	432	2.86	3.90
	FUS	141	0.20	1327	571	537
	LB	104	1215	0.07	315	282
	WPu	2.17	924	421	0.12	3.16
	WU	1.56	958	393	2.78	0.10

		Yield				
		FM	FUS	LB	WPu	WU
Library	FM	15.0 kt	53.9 Mt	139.5 kt	5.2 Mt	3.4 Mt
	FUS	0.01 t	15.0 kt	0.06 t	1.8 kt	1.2 kt
	LB	1.7 kt	15.0 Mt	15.0 kt	843.6 kt	534.3 kt
	WPu	0.04 t	154.3 kt	0.40 t	15.0 kt	9.7 kt
	WU	0.07 t	239.0 kt	0.61 t	23.3 kt	15.0 kt

At these distances, there is not yet a major loss in the ability to discriminate most spectra (compared to the default scenario in Table 4, page 57). The ability to differentiate the WPu and WU spectrum has been reduced somewhat and this pair are the hardest to discriminate since they are the most similar. Also, of note is that the relatively low match chi-squared score between the FM and the two Watt spectra is deceiving; the yield for those near matches is several orders of magnitude off of the expected value of 15 kt. In an actual situation, the wildly inaccurate yield would indicate a poor match. Moving out to 1,200 m, the first incorrect match with a chi-squared very close to 1 appears, though its yield is very incorrect.

Table 13 – Matching Results: χ^2 and Yield at 1,200 m

		χ^2 value Unknown Weapon				
		FM	FUS	LB	WPu	WU
Library	FM	0.19	299	47.76	2.92	4.68
	FUS	36.08	0.20	182	260	244
	LB	14.92	454	0.09	80.11	67.50
	WPu	2.45	336	43.84	0.17	3.43
	WU	1.15	337	37.96	2.43	0.12

		Yield				
		FM	FUS	LB	WPu	WU
Library	FM	15.0 kt	65.1 Mt	84.9 kt	5.2 Mt	3.3 Mt
	FUS	0.00 t	15.0 kt	0.02 t	1.3 kt	0.87 t
	LB	2.8 kt	17.4 Mt	15.0 kt	1.1 Mt	712.9 kt
	WPu	0.04 t	188.3 kt	0.25 t	15.0 kt	9.6 kt
	WU	0.07 t	294.6 kt	0.38 t	23.5 kt	15.0 kt

At 1,500 m, the signal from the FM spectra is completely lost to all elements except gold, which has too small of a signal to be used. This is demonstrated by the row of X's in Table 14.

Table 14 – Matching Results: χ^2 and Yield, 1,500 m

		χ^2 value Unknown Weapon				
		FM	FUS	LB	WPu	WU
Library	FM	X	86.35	7.25	1.63	2.74
	FUS	X	0.06	37.57	99.33	90.95
	LB	X	112	0.07	15.73	12.91
	WPu	X	109	11.72	0.18	1.02
	WU	X	103	11.84	1.37	0.14

		Yield				
		FM	FUS	LB	WPu	WU
Library	FM	0.00 t	85.0 Mt	61.7 kt	5.1 Mt	3.3 Mt
	FUS	0.00 t	15.0 kt	0.01 t	0.98 t	0.63 t
	LB	0.00 t	25.1 Mt	15.1 kt	1.4 Mt	900.7 kt
	WPu	0.00 t	250.5 kt	0.18 t	15.0 kt	9.6 kt
	WU	0.00 t	393.5 kt	0.28 t	23.7 kt	15.0 kt

The FM spectra is unique in that it has a relatively low neutron energy distribution at the initial location (see Figure 4, page 21). Most of its neutrons emerge at less than 1 keV, and simply do not travel far before being absorbed or downscattered. This weapon had a very massive delivery system and casing which contributes to this attenuated spectrum. These features are less likely to be present in a terrorist weapon in a similar yield range as it would not be delivered by WWII-era aircraft bombing.

At this distance, distinguishing the WPu and WU becomes more difficult, as both the match chi-squared scores are low and the yield estimates are reasonable amounts. There are also only 5 of 34 detectors available at this distance. In a major city, there would be additional detectors at this distance that were not simulated in this work. Since the previous AFIDS work [2] established a melting danger range of about 400 m for a 15 kt weapon, the default scenario holds up pretty well if melting distance is the primary concern.

4.2.1.2 Maximum Distance or Less

A set of scenarios was run using a variable maximum distance. In keeping with the previous results and the established melting criteria, a minimum distance of 400 m was included in each scenario. Maximum distances of 600 – 1,500 m were tested.

Looking at a very restrictive case – only using the two detectors between 500 and 600 m from the explosion – reasonable matching and yield results were obtained, shown in Table 15 below:

Table 15 – Matching Results: χ^2 and Yield, 500 m < Distance < 600 m

		χ^2 value Unknown Weapon				
		FM	FUS	LB	WPu	WU
Library	FM	0.12	10842	329	681	643
	FUS	289	0.21	272	3630	1705
	LB	106	9288	0.04	595	289
	WPu	207	10150	145	0.17	5.32
	WU	191	10106	132	6.56	0.11

		Yield				
		FM	FUS	LB	WPu	WU
Library	FM	15.0 kt	150.0 Mt	447.4 kt	3.6 Mt	2.4 Mt
	FUS	0.02 t	15.0 kt	0.58 t	3.9 kt	2.7 kt
	LB	0.47 t	150.0 Mt	15.0 kt	117.1 kt	77.1 kt
	WPu	0.06 t	22.7 Mt	2.0 kt	15.0 kt	10.0 kt
	WU	0.09 t	51.7 Mt	3.1 kt	22.7 kt	15.0 kt

Between the match chi-squared scores and yield estimates, the closer-in detectors compensate for their lack of total detectors (and thus countable locations) with a very high signal. Therefore, while maximum distance will be a significant planning factor for the contingency operations plan, it does not affect the optimization of detector target rods.

4.2.2 Azimuth (Avoiding Fallout Zones)

Nuclear detonations near ground level tend to create radioactive fallout plumes in the direction of the prevailing winds in the aftermath of the explosion. These fallout areas will have high residual radiation levels for some time after the incident and will be more difficult or impossible for personnel to enter to collect AFIDS detectors.

A reasonable contingency plan would be to collect detectors that are not near the fallout plume first to start the counting process and thus more quickly obtain some results. This plan assumes that a slice of the available detectors centered in the direction of the fallout plume may be safely ignored while still producing good discrimination. The robustness of the overall plan as well as each element's contribution to match chi-squared was tested by running 13 scenarios, where 60-degree swathes of detectors are excluded (centered on the angle listed, with 0 degrees being due north). The first scenario in Table 16 below includes all detectors as a comparison.

Table 16 – Matching Results: χ^2 and Yield, 60° Angle Exclusions, > 400 m distance

	χ2 contribution percentage												
	All	0	30	60	90	120	150	180	210	240	270	300	330
Mg	1.4	1.5	1.4	1.4	1.4	1.2	1.2	1.1	1.1	1.2	1.5	1.4	1.4
Al	1.4	1.6	1.4	1.4	1.5	1.2	1.2	1.1	1.1	1.3	1.6	1.4	1.5
Ti	2.8	2.8	3.6	3.4	2.8	2.3	2.3	2.5	2.5	2.4	2.8	2.7	2.8
Cr	8.6	6.6	8.6	8.6	8.7	9.2	9.1	8.9	9.0	9.2	8.7	8.8	8.6
Fe	0.3	0.0	0.3	0.3	0.3	0.3	0.3	0.3	0.3	0.4	0.3	0.3	0.3
Co	4.4	2.5	4.5	4.5	4.3	4.6	4.6	4.5	4.5	4.6	4.3	4.5	4.4
Ni	5.8	6.4	7.0	6.7	5.7	4.7	4.7	5.3	5.4	5.0	5.6	5.8	5.7
Cu	11.1	9.7	11.2	11.2	11.0	11.7	11.6	11.2	11.4	11.6	10.9	11.0	11.1
Ge	0.4	0.4	0.4	0.4	0.4	0.4	0.5	0.4	0.4	0.5	0.5	0.5	0.4
Zr	0.4	0.4	0.4	0.4	0.4	0.4	0.4	0.4	0.4	0.4	0.4	0.4	0.4
Mo	2.4	1.8	2.6	2.5	2.4	2.5	2.5	2.5	2.5	2.7	2.3	2.4	2.3
Rh	0.3	0.3	0.3	0.3	0.3	0.2	0.2	0.2	0.2	0.2	0.3	0.3	0.3
Pd	0.5	0.5	0.6	0.5	0.6	0.6	0.6	0.6	0.5	0.6	0.6	0.5	0.5
Cd	1.6	1.8	2.0	1.9	1.7	1.5	1.5	1.6	1.7	1.8	1.6	1.6	1.7
Sn	0.3	0.2	0.2	0.3	0.3	0.3	0.4	0.3	0.3	0.3	0.3	0.3	0.3
Hf	7.4	4.5	7.6	7.8	7.5	7.5	7.6	7.3	7.2	7.3	7.3	7.4	7.5
Ta	8.1	9.3	7.9	7.8	8.1	8.2	8.1	8.3	8.1	8.1	8.3	8.1	8.0
W	5.0	6.1	5.0	5.0	4.9	4.9	4.9	5.1	5.0	4.7	4.9	4.9	5.0
Re	9.6	10.9	8.7	9.2	9.6	9.7	9.6	9.9	10.1	9.6	9.4	9.7	9.6
Ir	16.3	17.3	16.4	16.0	16.4	16.2	16.1	16.6	16.3	16.1	16.1	15.7	16.3
Au	10.3	13.3	8.2	9.0	10.1	10.7	11.0	10.7	10.5	10.4	10.5	10.8	10.3
Pb	1.7	1.9	1.6	1.6	1.7	1.5	1.5	1.2	1.3	1.5	1.8	1.5	1.7

The results here are very consistent with regards to the exclusion angle. Therefore, it is reasonable to exclude a section of detectors in a 60 degree fallout plume without adversely affecting results.

4.2.3 Height Above Ground

The detector's height above ground level in an urban environment has positive and negative effects on the AFIDS effort. Placing detectors higher in altitude can reduce

localized scattering effects, such as close-by bodies of water or buildings. The urban canyon effects, while not eliminated, are somewhat reduced. A higher proportion of the incoming fluence may be due to skyshine, which consists of higher energy neutrons that have scattered less than their low energy counterparts. Higher placement locations may also reduce the risk of theft or vandalism.

Drawbacks to higher detector positions include the greater expense of installing the detectors, as skilled personnel such as electrical line crews or cell phone tower crews may have to be hired. They are also more difficult to check on and maintain. Additionally, retrieving the detectors post-explosion will require coordination for specialized crews capable of safely climbing the supporting structures.

Scenarios were created based on the default scenario with different minimum height filters ranging from 5 m to 50 m above local ground level. The change in match chi-squared contributions was subtle but visible from some elements as shown in Table 17 below:

Table 17 – Match Chi-Squared Contribution vs. Minimum Detector Height (m)

	Percentage of χ^2 contribution									
Ht	0	5	10	15	20	25	30	35	40	50
Mg	1.4	1.4	1.4	1.4	1.4	1.7	1.7	1.2	1.1	1.1
Al	1.4	1.4	1.4	1.4	1.4	1.7	1.7	1.2	1.2	1.2
Ti	2.8	2.8	2.8	2.8	2.9	2.8	2.8	2.5	2.8	3.6
Cr	8.6	9.3	9.3	9.2	9.3	7.5	7.6	7.9	6.1	6.6
Fe	0.3	0.4	0.4	0.4	0.4	0.0	0.0	0.0	0.0	0.0
Co	4.4	4.5	4.6	4.5	4.5	2.6	2.7	3.0	2.6	2.6
Ni	5.8	6.0	5.9	6.1	6.2	6.7	7.0	6.3	7.5	9.6
Cu	11.1	11.3	11.5	11.4	11.3	10.4	11.1	12.2	8.0	7.6
Ge	0.4	0.5	0.5	0.5	0.5	0.5	0.5	0.7	0.6	0.6
Zr	0.4	0.4	0.4	0.4	0.5	0.3	0.3	0.3	0.3	0.3
Mo	2.4	2.6	2.6	2.6	2.5	2.1	2.1	2.3	2.8	2.6
Rh	0.3	0.3	0.3	0.3	0.3	0.3	0.3	0.3	0.2	0.2
Pd	0.5	0.6	0.6	0.6	0.6	0.7	0.7	0.7	0.8	0.9
Cd	1.6	1.9	2.0	2.0	1.8	1.7	1.4	1.7	1.7	1.8
Sn	0.3	0.3	0.3	0.3	0.3	0.2	0.3	0.3	0.2	0.2
Hf	7.4	7.3	7.4	7.4	7.0	4.4	4.5	4.4	4.1	4.8
Ta	8.1	8.3	8.2	8.3	8.5	9.7	9.5	9.5	8.9	9.1
W	5.0	5.0	4.9	4.9	4.8	5.6	5.5	5.3	6.2	6.6
Re	9.6	9.5	9.5	9.5	9.6	10.3	10.6	10.6	12.7	11.3
Ir	16.3	15.3	15.2	15.2	15.2	15.5	15.2	14.9	16.8	17.4
Au	10.3	9.3	9.3	9.3	9.4	12.9	12.4	12.9	14.1	10.2
Pb	1.7	1.7	1.7	1.7	1.7	2.2	2.2	1.7	1.6	1.7

Of note, the nickel detector's relative contribution increased with height. Since the best nickel reaction has a high energy threshold, this can be explained by the increased portion of high energy skyshine reaching the targets at higher altitudes. Conversely, elements with low or no threshold energy reactions gradually contribute less with minimum heights.

The highest cut off tested, 50 m, still produced good matching and yield scores as shown in Table 18 below:

Table 18 – Matching Results: χ^2 and Yield, Height > 50 m

		χ^2 value Unknown Weapon				
		FM	FUS	LB	WPu	WU
Library	FM	0.30	5000	978	5.02	4.39
	FUS	267	0.11	2207	935	718
	LB	328	4265	0.05	646	589
	WPu	3.23	9374	956	0.13	3.06
	WU	1.95	9323	951	3.97	0.07

		Yield				
		FM	FUS	LB	WPu	WU
Library	FM	15.0 kt	54.3 Mt	266.0 kt	5.2 Mt	3.4 Mt
	FUS	0.01 t	15.0 kt	0.17 t	2.5 kt	1.7 kt
	LB	1.2 kt	150.0 Mt	15.0 kt	477.8 kt	301.9 kt
	WPu	0.04 t	15.1 Mt	0.79 t	15.0 kt	9.8 kt
	WU	0.07 t	30.4 Mt	1.2 kt	23.2 kt	15.0 kt

Detectors in high locations serve the AFIDS process well. There is some decrease in the discrimination of two low-energy spectra, FM and WU, which is not unexpected since the proportion of lower energy neutrons reaching the detectors is reduced. Incorporating the yield factors makes it easy to still distinguish these spectra. The utility of detectors placed high above the ground should go into the planning process for actual positioning and deployment.

4.2.4 Threshold Reactions

Threshold reactions are neutron activation reactions that only occur when the incoming neutron energy exceeds a minimum value. Below this threshold, the cross section and thus probability of the reaction happening is zero. Most elements which have

threshold reactions also can undergo a number of non-threshold reactions. This causes these materials to generate activations and counts from low-energy neutrons, which is a double-edged sword.

Counting low-energy neutrons can help get sufficient activations and counts in borderline cases on lower yield or lower energy leakage spectrum weapons, or at further distances. For some specific weapons like the highly attenuated FM spectrum, they are the only way to get usable data. Looking at Figure 4 (page 21), the majority of neutrons from that weapons start below 1 keV. These neutrons do not travel as far without scattering or absorption as high-energy neutrons do. Also, the higher energy neutrons tend to lose energy as they scatter, with the fluence values at lower energy levels becoming noisier further from the source. Low energy neutrons are also more sensitive to very local scattering conditions.

In contrast, higher energy neutrons can travel further with fewer scattering events, are easily discernible from background noise, and are present in distinguishable quantities from most spectra. Weapons with a fusion component produce a 14.1 MeV peak that is especially noticeable, and that also produces high energy downscattered neutrons. On the downside, there may be fewer of these neutrons produced, and for most elements they are more difficult to capture. The quality of the signal they produce is high, but it is harder to obtain enough counts, especially from lower energy spectrum weapons.

All the tables up to this point have included all possible reactions without an energy threshold. In this section, the effects of filter energies including 10, 25, 50, 100, 250, 500, and 750 keV, as well as 1 and 2 MeV, will be tested. The first set of scenarios will consider

the thresholds alone (with the established 400 m minimum distance to avoid melting, which is now added to the default scenario parameters), and subsequent sets will consider the thresholds in addition to other restrictions. The threshold direct effects are shown in Table 19 below:

Table 19 – Match Chi-Squared Contribution vs. Threshold Energy (keV)

	χ^2 contribution percentage									
	0	10	25	50	100	250	500	750	1000	2000
Mg	1.4	0.5	0.5	0.5	0.5	0.5	0.5	7.8	7.8	14.4
Al	1.4	0.4	0.4	0.4	0.4	0.4	0.4	4.9	4.9	8.9
Ti	2.8	23.6	25.1	21.1	23.0	23.7	25.1	7.7	7.8	14.2
Cr	8.6	0.0	0.0	0.0	0.0	0.0	0.0	0.1	0.1	0.1
Fe	0.3	1.0	1.0	1.0	1.0	1.0	1.0	X	X	X
Co	4.4	0.3	0.3	0.3	0.3	0.4	0.3	2.7	2.6	3.9
Ni	5.8	56.7	55.2	59.2	57.3	56.6	55.2	2.2	2.2	3.2
Cu	11.1	0.3	0.3	0.3	0.3	0.3	0.3	2.4	2.4	3.6
Ge	0.4	X	X	X	X	X	X	X	X	X
Zr	0.4	X	X	X	X	X	X	X	X	X
Mo	2.4	0.3	0.3	0.3	0.3	0.3	0.3	1.0	1.0	1.1
Rh	0.3	1.2	1.2	1.2	1.2	1.2	1.2	22.8	22.7	X
Pd	0.5	X	X	X	X	X	X	X	X	X
Cd	1.6	0.3	0.3	0.3	0.3	0.3	0.3	1.2	1.2	1.4
Sn	0.3	X	X	X	X	X	X	X	X	X
Hf	7.4	X	X	X	X	X	X	X	X	X
Ta	8.1	X	X	X	X	X	X	X	X	X
W	5.0	X	X	X	X	X	X	X	X	X
Re	9.6	4.1	4.1	4.1	4.1	4.1	4.1	12.9	12.9	14.2
Ir	16.3	X	X	X	X	X	X	X	X	X
Au	10.3	11.1	11.1	11.1	11.1	11.1	11.1	33.3	33.3	33.8
Pb	1.7	0.2	0.2	0.2	0.2	0.2	0.2	1.0	1.0	1.1

Immediately noticeable are the 7 elements that do not have a threshold reaction at all. The modeling code applies the threshold by filtering out reactions that do not have a threshold above the selected energy level, so elements that have no threshold reactions are filtered out quickly. Other elements like titanium and nickel have different threshold reactions, and as the minimum threshold level rises, the code selects different reactions for those elements. In these cases, the second reaction with that higher energy requirement creates fewer activations and less signal. This is apparent for nickel which has its primary threshold reaction $^{58}Ni(n,p)^{58}Co$ give way to the higher threshold reaction $^{58}Ni(n,np)^{57}Co$ at the 750 keV filter level. This second reaction is far less useful, making a natural cut off for nickel in the 500 keV threshold range. Some elements like rhodium are consistent regardless of the neutron energy filter level, but see their relative contribution rise as other elements are excluded due to rising thresholds.

There is a sharp change in contributions between the 500 keV and 750 keV thresholds, with several contributors no longer of value in the assessment. Looking back at the energy dependence of the how the detector body affects the incoming fluence (see Figure 10, page 74), the largest effects are isolated below 500 keV. Therefore the 500 keV threshold could help improve the quality of the signal while avoiding or minimizing some of the angular effects studied earlier. This 500 keV threshold will now be applied with select other constraints to see the effects on match chi-squared scoring, yield values, and countable locations.

4.2.5 Time Delay in Start of Counts

It is difficult to predict how long of a delay will be required from the time of a nuclear explosion until a given AFIDS detector can be collected, brought to a counting lab, and counted. Not only do emergency crews have to deal with the chaos, damage, and radiation of a nuclear explosion, there could also be difficulties in reaching select detectors on places like surviving cell phone towers. There is also a limited throughput for the counting lab – only so many samples can be counted at one time – leading to additional delays. These delays can be mitigated through good planning of the order of counting, but not entirely controlled.

The default scenario uses a 72 hour delay before the start of counting. In this section, the effects on matching chi-squared contribution by varying the delay time before the start of counts are examined. Delays ranging from 12 hours to 1 year are considered, with the most attention given to the first week after the explosion.

Table 20 – Match χ^2 Contribution vs. Delay Time in Start of Counts

	χ^2 contribution percentage											
	12h	24h	36h	2d	3d	4d	5d	6d	7d	10d	30d	1y
Mg	2.3	2.4	2.1	2.4	1.4	0.6	0.1	X	X	X	X	X
Al	2.6	2.6	2.2	2.5	1.4	0.6	0.1	X	X	X	X	X
Ti	1.5	1.6	1.5	2.0	2.8	2.2	1.9	1.7	1.5	0.9	0.1	X
Cr	7.5	7.5	9.1	8.9	8.7	9.1	9.0	9.4	10.2	11.4	12.2	X
Fe	1.3	0.2	0.2	0.2	0.3	0.3	0.3	0.3	0.4	0.4	X	X
Co	3.4	3.5	4.4	4.4	4.4	4.6	4.5	4.8	5.0	5.6	6.8	14.8
Ni	1.5	2.0	2.8	3.6	6.0	6.9	7.0	7.4	7.8	8.5	6.6	1.9
Cu	16.5	15.6	19.3	16.4	11.1	8.6	6.4	5.3	3.6	X	X	X
Ge	0.7	0.7	0.7	0.5	0.4	0.3	0.1	X	X	X	X	X
Zr	0.6	0.5	0.6	0.5	0.4	0.3	0.3	0.2	0.0	0.5	X	X
Mo	2.0	2.0	2.7	2.5	2.3	2.2	2.1	2.1	2.0	1.9	0.2	X
Rh	0.0	0.1	0.1	0.1	0.3	0.3	0.3	0.4	0.4	0.4	1.9	1.2
Pd	0.8	0.8	0.8	0.7	0.5	0.3	0.1	0.1	X	X	X	X
Cd	1.4	1.4	2.0	1.8	1.6	1.7	1.5	1.5	1.5	1.1	X	X
In	0.0	0.0	0.0	X	X	X	X	X	X	X	X	X
Sn	0.2	0.2	0.3	0.3	0.3	0.2	0.3	0.3	0.3	0.3	0.1	X
Hf	4.3	4.4	6.4	6.6	7.4	8.2	6.8	7.0	7.3	7.7	9.3	5.7
Ta	4.0	4.3	6.7	7.2	8.0	9.2	8.6	8.9	9.3	10.0	13.8	27.3
W	3.2	3.2	4.9	4.7	5.0	4.6	3.6	3.3	3.2	2.1	0.2	X
Re	30.5	30.8	7.9	8.3	9.6	10.8	8.8	8.8	8.9	8.8	4.8	X
Ir	9.9	10.2	16.0	16.0	16.2	16.0	26.8	27.5	28.3	30.1	39.8	49.1
Au	4.9	5.3	8.4	9.1	10.2	11.5	10.2	10.2	9.9	10.1	4.1	X
Pb	0.7	0.8	1.0	1.3	1.7	1.4	1.1	0.9	0.7	0.2	X	X

Copper's rise and fall in matching contribution is based on the 12.7 hour half-life of its most useful activation product, ^{64}Cu. This relatively short half-life leads to an initially high decay and thus count rate immediately after the explosion. Copper contributes over 15% for any count time starting in the first 48 hours after the explosion, and actually increase to over 19% at the 36 hour mark, as very short half-life activation products of elements like rhenium decay away. At the 72 hour mark, it has undergone almost 6 half-lives, but still

contributes a healthy 11% to the overall matching score. By the end of the first week, it has almost completely decayed away and is uncountable 10 days after the explosion.

In contrast, tantalum's ^{182}Ta activation product has a 114.43 day half-life. While this long half-life reduces the decay and count rates, it retains countable activity for a reasonably long time. Initially tantalum only contributes 4.0% to the matching score totals, but steadily increases in importance as shorter-lived activation products decay away, exceeding 10% of the score contribution 10 days after the explosion. Only the very expensive iridium target rod is a greater contributor after 10 days or even at one year.

While a year long delay in counting would be impractical from an immediate nuclear forensics effort, it could be useful for long term scientific studies. Decades after the nuclear bombings of Hiroshima and Nagasaki, scientists are building ever-improving models of the radiation dose to the survivors. Technology, especially computing power for modeling, was unthinkable in the aftermath of those explosions. Likewise, the future may hold tools unimaginable today. Providing longer-lived activation products to future scientists could help survivors in unanticipated ways. While long-lived activation products are not a primary driver of the AFIDS optimization, if they can be included for a low expense and opportunity cost, they should be.

For the non-threshold reactions, copper stands out for matching contributions versus cost per target rod, though it has a somewhat short half-life and would need to be prioritized in the counting process. Rhenium and iridium complement each other with short and longer half-lives, but rhenium is very expensive, and iridium is almost prohibitively expensive – only half-length rods would fit inside the current AFIDS budget.

Chromium stands out as a longer-lived inexpensive alternative. Cobalt also offers longer half-life performance but is still significantly expensive. Tungsten only has modest performance but is an exceptional value due to its low cost.

Given the utility of reactions with neutron energy thresholds discussed in section 4.2.4 (page 96), another set of scenarios was run with a 500-keV filer on required incident neutron energy, an increased yield of 150 kt to allow more reactions to be counted[24], and the same delay time parameters. The results are in Table 21 below:

[24] The threshold reactions are most useful for either high-energy fission spectra (WPu is the only unclassified spectrum in this category) or spectra with some fusion component (only FUS in the unclassified spectrum list). To better examine the threshold reactions that are useful for more modern weapons whose spectra include these higher-energy neutrons, the yield is increased to allow appreciable counts from the WU spectrum. FM and LB are so attenuated by their large bomb casings and/or explosive charges that even a 10-fold increase in yield does not give enough counts to any threshold reactions.

Table 21 – Match χ^2 Contribution vs. Delay Time in Start of Counts, 500 keV Threshold, 150 kt Yield, only FUS, WPu, WU Spectra Matched

	χ^2 contribution percentage											
	12h	24h	36h	2d	3d	4d	5d	6d	7d	10d	30d	1y
Mg	1.7	1.5	1.2	1.0	0.5	0.4	0.2	X	X	X	X	X
Al	1.6	1.4	1.1	0.8	0.4	0.3	0.1	X	X	X	X	X
Ti	50.3	38.3	28.5	25.3	24.7	7.4	7.6	7.7	6.9	6.1	0.5	X
Cr	0.0	0.0	0.0	0.0	0.0	0.0	0.0	0.0	0.0	0.0	X	X
Fe	1.6	0.6	X[25]	0.9	1.0	1.0	1.0	1.0	1.1	1.2	2.9	X
Co	0.6	0.3	0.3	0.3	0.3	0.4	0.4	0.4	0.5	0.6	1.5	X
Ni	29.0	41.8	52.2	54.8	55.6	72.9	73.1	73.2	73.8	74.4	73.9	40.4
Cu	2.8	1.9	1.2	0.8	0.3	0.1	X	X	X	X	X	X
Mo	0.3	0.3	0.3	0.3	0.3	0.2	0.2	0.2	0.2	0.1	X	X
Rh	1.0	1.1	1.2	1.1	1.2	1.2	1.2	1.2	1.3	1.5	1.4	25.1
Cd	0.4	0.3	0.3	0.3	0.3	0.2	0.2	0.2	0.1	0.1	X	X
In	0.0	0.0	0.0	X	X	X	X	X	X	X	X	X
Re	3.1	3.6	3.8	4.0	4.1	4.0	3.9	3.8	3.6	3.0	4.8	X
Ir[26]	X	X	X	X	X	X	X	X	X	X	9.2	34.5
Au	7.3	8.6	9.5	10.2	11.1	11.6	11.9	12.2	12.4	12.9	5.8	X
Pb	0.3	0.3	0.3	0.3	0.2	0.2	0.2	0.1	0.1	0.1	X	X

Two inexpensive target rod elements stand out here – titanium and nickel. The shorter half-life (3.3 days) of titanium's primary activation product, ^{47}Sc, accounts for a significant portion of the matching score if it can be obtained quickly and counted at 12

[25] Before this gap, the contributing reaction was ^{56}Fe(n,p)^{56}Mn. At the gap, this reaction has decayed away and the new reaction, ^{54}Fe(n,p)^{54}Mn has interference. The interfering activation product dies away after this bin.

[26] Note that iridium does not have any available reactions until the 30 day test. The cause of this is an interfering gamma ray that is much stronger than the threshold reaction's gamma, until the shorter half-life interfering activation product decays away enough where it no longer causes significant interference.

hours after detonation. It maintains a very high relative contribution through the first 3 days and remains important all the way through the first week, before starting to fade in usefulness at the 10 day mark. Nickel's primary activation product, ^{58}Co, has a half-life of 70.86 days. This long-lived isotope contributes immediately after the explosion, and as shorter-lived activation products decay away, the nickel target rod starts to dominate the contribution, reaching 74% of the total contribution after 10 days. Nickel still has a usable count rate after a year. It must be noted that a large portion of nickel's contribution to the matching score is focused on fusion/fission discrimination, with smaller contributions to fission/fission discrimination.

Titanium and nickel are inexpensive and have complementary half-lives, making them an excellent potential pairing for threshold reaction selections. Magnesium has a short-lived activation product worth considering. Gold also provides a solid threshold reaction, but at a high price per target rod. An advantage for gold is that it provides more usable counts at lower yield levels, more so than any other long-lived activation product. Iron has only a modest contribution but is very inexpensive and its threshold activation product is long-lived.

4.2.6 Summary of Candidate Target Rod Elements

This subsection summarizes the observations so far by element, capturing each candidate elements' useful qualities, limitations, and costs. Half of the commercially-available elements did not significantly contribute to the matching discrimination process in any of the scenarios modelled so far and will be dropped from further consideration.

The elements dropped at this point are Si, Ge, Zr, Nb, Mo, Rh, Pd, Ag, Cd, In, Sn, Pb, and Bi. The remaining elements are summarized in Table 22.

Table 22 – Summary of Candidate Target Rod Elements

	Cost	Thresh	Prod	Half-life	Notes
Mg	$18.94	Yes	^{24}Na	15.0 h	Good fission/fusion discrimination in first 24 hours
Al	$0.06	Yes	^{24}Na	15.0 h	Very cheap low signal for 2-7 days
Ti	$0.59	Yes	^{47}Sc	3.35 d	Excellent fission/fusion discrimination for 10 days
Cr	$0.85	No	^{51}Cr	27.8 d	Cheap fission/fission discrimination for 10 days
Fe	$0.10	Yes	^{54}Mn	312 d	Very cheap threshold reaction, very long-lived
Co	$42.10	Yes	^{56}Mn	2.78 h	Too expensive and short-lived for threshold
		No	^{60}Co	5.27 y	Expensive but long-lived no threshold
Ni	$0.35	Yes	^{58}Co	70.86 d	Cheap, long-lived threshold reaction
Cu	$0.06	Yes	^{64}Cu	12.7 h	Cheap, short-lived fission/fission discrimination
Hf	$10.50	No	^{181}Hf	42.4 d	Long-lived modest contributor
Ta	$4.13	No	^{182}Ta	114 d	Very long-lived contributor for fission/fission
W	$0.59	No	^{187}W	23.7 h	Cheap, modest contributor for the first 10 days
Re	$123.20	Yes	^{186}Re	3.72 d	Modest contributor for the first month; high price
		No	^{188}Re	17.0 h	Very high contributor for first day; high price
Ir	$390.24	No	^{194}Ir	171 d	Best very long-lived contributor; extreme price

Au	$97.80	Yes	^{196}Au	6.17 d	Best for low yields, good for 30 days; high price
		No	^{198}Au	2.70 d	Best threshold reaction for 30 days; high price

4.2.7 Dimension and Number of Target Rods

In addition to narrowing down and selecting elements as target rods (the primary aim of this optimization research), improvements in performance can be gained by including two or more copies of the same element, including half-length rods (especially for expensive elements), and altering the diameter of the rod to create more mass. The current AFIDS detector body configuration allows for 20 target rod slots of 5 cm in length and 1 mm in diameter. The actual holes are 1.5 mm in diameter to allow for easy removal of the target rods.

Modestly increasing the diameter of select target rods is feasible, though it may add to the cost of the detector body as the ratio of hole width to body width increases the machining costs. An extrusion process is possible when the detector bodies are manufactured at scale which may avoid this additional cost. It is reasonable to expect that the AFIDS detector could accommodate select 2 mm diameter rods in 2.5 mm holes given the current setup.

A 2 mm diameter rod boasts 4 times the mass of a 1 mm diameter rod of the same length, and ignoring additional self-attenuation, will produce 4 times as many initial activations. This could prove very valuable for useful target rod elements that struggle to obtain enough activations from lower neutron energy spectra or lower yield weapons. This

also can make best use of the inexpensive elements where quadrupling the mass of the rod will have little effect on the overall price of a detector target rod set.

There is a non-trivial loss to the gamma escape probabilities however, leading to an optimal trade-off between increasing the total number of activations and losing gamma escape to self-absorption in the rods. Simulations of 2 mm diameter rod sizes for nickel and titanium using the gamma escape probability code from section 3.2.2.1 (page 38) are shown in Figure 15, which displays the ratio of expected counts between an increased diameter rod versus the standard 1 mm rod. The gammas from the preferred activation reactions for those two elements have the sole markers on the line.

The analysis showed that the increase in self-attenuation of emitted gammas was fairly small when only going from 1 mm to 2 mm diameter for the target elements at high enough energies, capturing more than 95% of the expected gain from the additional mass. At lower energies, the ratio would be closer to 2, because only gammas emitted near the surface would be likely to escape, and doubling the diameter only roughly doubles the surface area. Due to the energy dependence, these numbers will be specifically calculated for any elements chosen to have an increased diameter and appropriate correction factors applied.

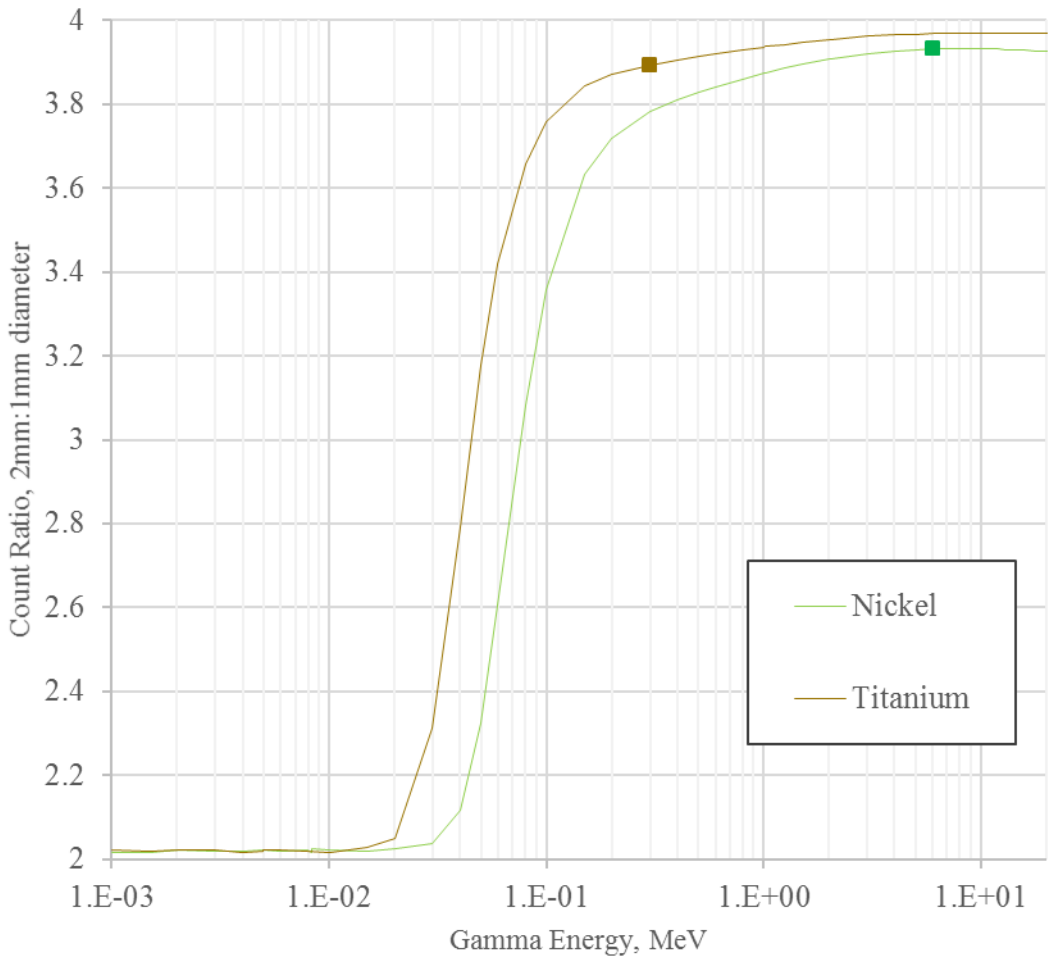

Figure 15 – Count Ratios vs. Energy for Select 2mm:1mm Diameter Target Rods

Another way to increase the number of activations and counts of the target elements is to include multiple copies of the same rod. With 20 available slots and only 14 usable candidate elements, this is a very inviting solution, especially with low-cost elements. As long as the number of duplicate rods remains reasonable in number (less than 10) the counting geometry and efficiency will not be significantly impacted. Including multiple

copies and dispersing them angularly can assist in minimizing the angular effects discussed in section 4.1.1.2 (page 71).

The final dimension considered is the length of the target rods. The cost of a target rod can be reduced linearly by reducing the length of the rod. This makes the most sense for the very expensive elements such as gold and iridium that activate well and can afford a reduction in mass while remaining countable. Cutting the length in half is the only way it would be possible to afford iridium under the budget constraint, and even then, it would financially crowd out many other options.

4.3 Selection of Target Foil Set within Cost Constraints

In this section, using previously developed goals and desired capabilities of the AFIDS detector system, an optimized set of target rod elements and associated quantities and dimensions are presented along with a distribution pattern for the angular slots in the detector. It is important to re-emphasize that these selections are based solely on the five unclassified weapons neutron leakage spectra available for this research. The rules and analysis developed here will be useful for more generalized spectra sets and larger quantities of spectra, but the final optimized result can only be as good as the data used to build it.

4.3.1 Summary of Optimization Criteria

In previous sections, the following objectives, desired capabilities, and other considerations have been developed:

1. The budget for target rod elements is limited to $200 for each detector's set, and pricing is based on a minimum order of 1,000 rods (costs are listed in Table 8, page 63).
2. The minimum weapon yield used for this study is 15 kt. Lower yields could require closer spacing of detectors than has been considered in this research. Higher yields are easier to detect as they produce more neutrons.
3. A target element must have a minimum count rate of 1,000 counts per hour after a set delay post-detonation, normally 72 hours. Achieving this count rate depends on both the initial activation level and the half-life of the activation product. This count rate also depends on the escape probabilities of the gammas rays from the rod as well as the energy-dependent absolute efficiency of a typical HPGe detector. Combinations of detector location / target element that do not meet this threshold, required for desired levels of uncertainties in the forensic analysis, are discarded. Multiple target rods of the same element can be in the holder and may be counted simultaneously to meet the detection threshold.
4. The most important part of the contribution to discrimination of different spectra is the ability to generate high matching chi-squared scores for incorrect spectra (high scores meaning that there is a poor match.) This was determined to be more useful and important than how low the scores are for a correct match.
5. The target rod set needs to be able to discriminate strongly between fission and fusion spectra.
6. The target rod set needs to be able to discriminate strongly between different fission spectra, especially closely-related spectra like WPu and WU.

7. The target rod set needs to have at least on target rod with sufficient activity after 10 days to be counted. It is desired but not required to have target rods that would have sufficient activity to be counted much longer times after the event than 10 days.
8. The target rod set needs some rod(s) that have threshold reactions to help mitigate the noise in the lower neutron energies due to the complexity of urban terrain. These reactions are also less susceptible to the angular effects detailed in section 4.1.1.2 (page 71).
9. When determining how many elements effectively cover a given spectrum, a single target element should not depend on less than 4 detector locations for its signal if at all possible. While even single countable locations will be used in the AFIDS effort, a single detector cannot be relied upon to ensure coverage for a given spectrum. Not every detector is likely to be recovered quickly, even outside of the melting zone and the fallout plume. Having multiple countable locations generated from a variety of unknown spectra is necessary to not waste precious counting time and to ensure a good signal is found.
10. It is desired but not required to have multiple copies of key target rods dispersed in the angular slots of the detector to minimize the angular effects discussed in section 4.1.1.2 (page 71).

4.3.2 Second Candidate Element Screening

The two questions that a complete target rod set must answer are "which elements to include?" and "how much of each element?" This section seeks to answer the first

question, with the subsequent section further optimizing the set by answering the second question.

Looking at Table 22 (page 106), a few candidate elements are appreciably more expensive than the remaining elements. To justify the cost under a constrained budget, these pricey elements must perform significantly better than their inexpensive peers. In the case of iridium, the most expensive element, it is the very best element at providing a large matching score contribution very long times (1 month, 1 year) after the weapon detonation. However, tantalum covers a very similar performance space at just over $1/100^{th}$ of the cost. Therefore, iridium can be inexpensively replaced and will not be used in the optimized system.

Rhenium, the next most expensive element, proves only to be a modest performer for threshold reaction, and, while it is a strong contributor during the first day for non-threshold reactions, it is unlikely that many detectors will be recovered quickly enough to obtain good Re count rates. Further, elements like tungsten can perform this task, if not as well, for $1/200^{th}$ of the price. So, rhenium is also eliminated.

Gold is the next most expensive element. It is by far the easiest element to activate and maintain good count rates on, especially for low neutron energy spectra and low-yield weapons. There is something to be said for including the element that provides the greatest number of countable locations over a range of testing conditions when anticipating working in a very difficult environment. The ease with which it activates makes it a candidate to be used in half the standard rod height to save money. Per Table 23, gold still performs well with half the mass:

Table 23 – Countable Locations vs. Mass Multiplier, Au

	Countable Locations vs. Mass Multiplier, Au											
	0.5	1	2	3	4	5	6	7	8	12	16	24
FM	24	27	29	30	30	30	30	30	30	31	32	32
FUS	32	32	32	32	32	32	32	32	32	32	32	32
LB	29	30	30	31	31	32	32	32	32	32	32	32
WPu	32	32	32	32	32	32	32	32	32	32	32	32
WU	32	32	32	32	32	32	32	32	32	32	32	32

This table shows how many (out of a possible 32 detector locations located outside 400 meters from the detonation) gold would register sufficient counts on in the default scenario. The mass multipliers ranging from 0.5 (one half of a 1 mm diameter by 5 cm standard target rod) to 24 (the equivalent of 24 standard rods, most likely by having 6 rods of 2 mm diameter) show how countable locations are gained with additional mass. In this case, gold reaches the maximum much sooner, but most elements do not. Since gold performs exceptionally well at providing countable locations even at low mass, it will be considered for the final optimized set, despite its cost.

The next most expensive element is cobalt. At less than half the price of gold, a single cobalt rod would still absorb more than one fifth of the budget for an individual detector. While its threshold reaction would not be worthwhile, the analysis of its non-threshold reaction shows the longest half-life of all the remaining activation products at 5.27 years. A look at cobalt's countable locations versus mass multiplier is in Table 24 below:

Table 24 – Countable Locations vs. Mass Multiplier, Co

	Countable Locations vs. Mass Multiplier, Co											
	0.5	1	2	3	4	5	6	7	8	12	16	24
FM	0	1	2	2	3	3	3	3	4	6	6	6
FUS	21	24	28	28	30	30	30	30	30	31	31	32
LB	5	6	6	7	8	9	10	10	10	10	12	14
WPu	14	16	18	18	21	21	21	21	21	22	25	27
WU	10	14	17	17	18	19	20	21	21	21	22	25

Cobalt does not greatly benefit from additional mass beyond the standard rod – certainly not for the increases in cost that would occur. It has a healthy number of countable locations for 4 of the 5 spectra and only very expensive amounts would increase that number. Since it potentially offers good performance with the equivalent of a single rod, it remains in consideration.

Next on the price list is magnesium. Less than half the price of cobalt, it is the most expensive element that would be considered for multiple rods. However, its 15 hour half-life only contributes significantly to fission/fusion discrimination on the first day. Its lack of longevity combined with price leave better alternatives and it will be omitted from further consideration.

Hafnium is available for just over $10 per standard rod. While its overall contributions to activation are modest, the products are long-lived. An examination of hafnium's countable locations is below in Table 25:

Table 25 – Countable Locations vs. Mass Multiplier, Hf

	Countable Locations vs. Mass Multiplier, Hf											
	0.5	1	2	3	4	5	6	7	8	12	16	24
FM	3	6	6	6	8	9	10	10	10	12	14	15
FUS	30	31	32	32	32	32	32	32	32	32	32	32
LB	10	10	14	15	16	16	16	17	17	18	18	21
WPu	21	22	27	28	29	30	30	30	30	30	30	31
WU	20	21	25	27	28	28	28	29	30	30	30	30

Much like gold, it has a large number of countable locations even at the standard rod size. There is a noticeable improvement in picking up the low energy spectra (FM, LB) when going up to 2 standard rods, which mostly levels off after 3 rods. It is a candidate for inclusion.

For the remaining elements, cost is less of a concern. Even using 20 standard rods' worth of tantalum (the next most expensive rod) would not use half of the original budget. Therefore, the remaining discussion focuses on utility of the elements and the opportunity cost of target rod slot availability, especially on elements that would benefit from higher mass multipliers.

Tantalum provides great discrimination between similar fission spectra and its activation product of interested is long-lived. The degree of freedom analysis is in Table 26.

Table 26 – Countable Locations vs. Mass Multiplier, Ta

	Countable Locations vs. Mass Multiplier, Ta											
	0.5	1	2	3	4	5	6	7	8	12	16	24
FM	12	15	17	18	19	20	21	21	21	21	24	26
FUS	32	32	32	32	32	32	32	32	32	32	32	32
LB	18	21	21	22	24	26	27	27	27	28	29	30
WPu	30	31	32	32	32	32	32	32	32	32	32	32
WU	30	30	31	32	32	32	32	32	32	32	32	32

This element has excellent number of countable locations with one standard rod. Given its utility, it is a likely candidate for the final optimized set.

The next element, chromium, costs less than a dollar per standard rod. It provides inexpensive fission spectra discrimination over the first 10 days. Its countable locations are in Table 27.

Table 27 – Countable Locations vs. Mass Multiplier, Cr

	Countable Locations vs. Mass Multiplier, Cr											
	0.5	1	2	3	4	5	6	7	8	12	16	24
FM	0	0	0	1	1	1	1	1	1	3	3	3
FUS	16	18	21	21	22	25	26	26	27	28	29	30
LB	3	3	5	6	6	6	6	6	6	7	8	10
WPu	7	10	14	14	16	17	17	17	17	18	20	21
WU	6	8	10	12	14	14	17	17	17	17	18	20

Chromium shows gradually increased performance with increased mass multipliers and then plateauing after 4 standard rod equivalents. It does not have the large number of

countable locations that gold does, but it provides a healthy amount of data on 4 of the 5 spectra and will be included.

Titanium is the first threshold reaction that combines a reasonable cost with coverage that lasts the initial 10 days after the blast. Like other threshold reactions, countable locations are a concern, since low energy neutrons cannot activate its preferred reaction. A breakdown is in Table 28 below:

Table 28 – Countable Locations vs. Mass Multiplier, Ti

	Countable Locations vs. Mass Multiplier, Ti											
	0.5	1	2	3	4	5	6	7	8	12	16	24
FM	0	0	0	0	0	0	0	0	0	0	0	0
FUS	9	11	13	15	17	18	19	20	20	20	21	22
LB	0	0	0	0	0	0	0	0	0	0	0	0
WPu	0	2	3	4	4	4	4	4	4	5	6	8
WU	0	0	2	3	4	4	4	4	4	4	4	5

With a single standard rod, titanium can only detect the fusion spectra. While discriminating fission and fusion is its strength, increasing its mass multiplier dramatically allows it to perform on more fission spectra. This may be practical using 2 mm diameter rods due to its low cost. Titanium and nickel complement each other well and both will be included.

Tungsten also provides coverage over the first ten days, and is a non-threshold reaction, allowing for better performance on the lower energy spectra as shown in Table 29.

Table 29 – Countable Locations vs. Mass Multiplier, W

	Countable Locations vs. Mass Multiplier, W											
	0.5	1	2	3	4	5	6	7	8	12	16	24
FM	12	15	17	18	20	21	21	21	21	21	24	26
FUS	32	32	32	32	32	32	32	32	32	32	32	32
LB	18	21	21	23	24	26	26	27	27	28	29	30
WPu	30	31	32	32	32	32	32	32	32	32	32	32
WU	30	30	31	32	32	32	32	32	32	32	32	32

A single rod of tungsten sufficiently activates at numerous detector locations. Combining this with its low cost and longer half-life lead to its inclusion.

Nickel provides the next threshold reaction. While it does not contribute as much matching score as titanium initially, it does excellent fusion discrimination and has a long half-life. It also has limited countable locations as shown in Table 30.

Table 30 – Countable Locations vs. Mass Multiplier, Ni

	Countable Locations vs. Mass Multiplier, Ni											
	0.5	1	2	3	4	5	6	7	8	12	16	24
FM	0	0	0	0	0	0	0	0	0	0	0	0
FUS	11	13	17	19	20	20	20	21	21	22	23	26
LB	0	0	0	0	0	0	0	0	0	0	0	0
WPu	2	3	4	4	4	4	5	5	5	8	8	10
WU	0	2	4	4	4	4	4	4	4	5	7	8

Nickel can barely detect the WPu and WU spectra (in addition to FUS) with one standard rod. However, dramatically increasing its mass to 12 or 16 standard masses allows it to work with both WPu and WU, contributing to the higher energy fission spectra. It is a candidate for multiple 2 mm diameter rod use due to its low cost.

Iron is the next element considered. It is exceptionally cheap and its activation product has a very long half-life. A look at its countable locations is in Table 31.

Table 31 – Countable Locations vs. Mass Multiplier, Fe

	Countable Locations vs. Mass Multiplier, Fe											
	0.5	1	2	3	4	5	6	7	8	12	16	24
FM	0	0	0	0	0	0	0	0	0	0	0	0
FUS	0	2	3	4	5	6	6	6	6	7	8	10
LB	0	0	0	0	0	0	0	0	0	0	0	1
WPu	0	0	0	1	2	2	2	3	3	3	5	6
WU	0	0	0	0	1	1	2	2	2	3	3	4

Iron has a major flaw – it has very few countable locations, even with a large mass multiplier. While paying for multiple 2mm rods would be inexpensive financially, the opportunity cost of having to use four slots for a pretty marginal performance is too much. Despite its cost, iron does not provide enough performance for inclusion.

The remaining elements, aluminum and copper, suffer from the same issue – a lack of activations leading to the need to use heavy mass multipliers to create sufficient countable locations. Further, both of their half-lives are not long-lived and their matching

chi-squared contributions even during the short time they are countable is not impressive. They are both dropped from consideration.

After this second, more detailed screening, the remaining candidate rod elements are gold, cobalt, nickel, chromium, tungsten, titanium, hafnium, and tantalum. The next section presents the number and dimensions of each rod, drawing from the analysis in this section.

4.3.3 Determining Optimal Quantities and Sizes of Rods

The two major constraints in this process are the overall budget and the number of slots in the AFIDS detector, which cannot be arbitrarily increased, both for mechanical reasons and due to the eventual counting throughput limitations that become more difficult with an increasing number of separate elements to count.[27] The most difficult to solve problem for the more expensive elements is the budget constraint.

Starting with the most expensive remaining candidate, gold, a decision must be made on its inclusion. Excluding it would provide much more budget room for other elements. However, in the previous section it was found that most of the other expensive elements were not exceptional performers, nor did they benefit greatly from large mass

[27] It may be feasible to count different elements that have activation product gamma rays with very different energies and no other interfering gamma rays; a more detailed contingency operations counting plan could find those efficiencies. They are not considered further here, although the ability to simultaneously count multiple rods of the same element is accounted for.

multipliers. The elements that most benefited from multiple rods in the assembly were very inexpensive threshold reaction elements like titanium and nickel. Weighing the cost against the irreplaceability of gold to provide quality data in low energy, low yield scenarios at even great distances away, the optimal decision is to include a single standard rod of it. To partially mitigate the angular effects of slot position, the gold will be split into two half-length pieces placed 180 degrees part from each other.

Another expensive element is cobalt. While it does not have the exceptional performance of gold, it has an unmatched activation product half-life, which provides long-lasting data for the better analysis that comes with large counting times in optimum conditions. It is also half the cost of gold and does not need a mass multiplier to obtain a sufficient number of countable locations. To keep costs down and to complement gold's half-length approach, a single rod of cobalt will also be split and placed with the gold target rods.

With the expensive elements accounted for, the remaining elements are unlikely to strain the budget. Now the bigger constraint becomes the number of slots remaining, currently 18 of 20 slots. The two elements that benefit most from mass multiplication are titanium and nickel, the set of threshold reaction elements who half-lives complement each other. Both of these elements benefit greatly in countable locations by have 16 times the normal mass, which is accomplished by including 4 rods each of 2 mm diameter (quadruple the mass for somewhat less than quadruple the cost per the ordering catalogues). These key threshold performers take up 2 sets of 4 slots each, leaving 10 remaining slots. They will be placed at 90 degree intervals.

The next element needing mass multiplication for optimum countable locations in chromium. Unlike the threshold reactions of titanium and nickel, chromium's non-threshold reaction does well at the lower levels of the energy spectrum. It will be given a 4 times standard rod total mass, taking up 4 more slots with 1 mm diameter rods. It would not benefit greatly from increased diameter. This leaves remaining 6 slots.

The remaining non-threshold reactions from hafnium, tantalum, and tungsten do well without the mass multiplication desired in the previous few elements. In the interest of providing angular diversity, they will each receive two standard rod slots, split by 180 degrees.

The total costs of this set of detector rods is $182.06, meeting the budget limitation. If the budget were higher, an additional gold rod would be considered in lieu of the cobalt. The optimized set is summarized in Figure 16 and Table 32.

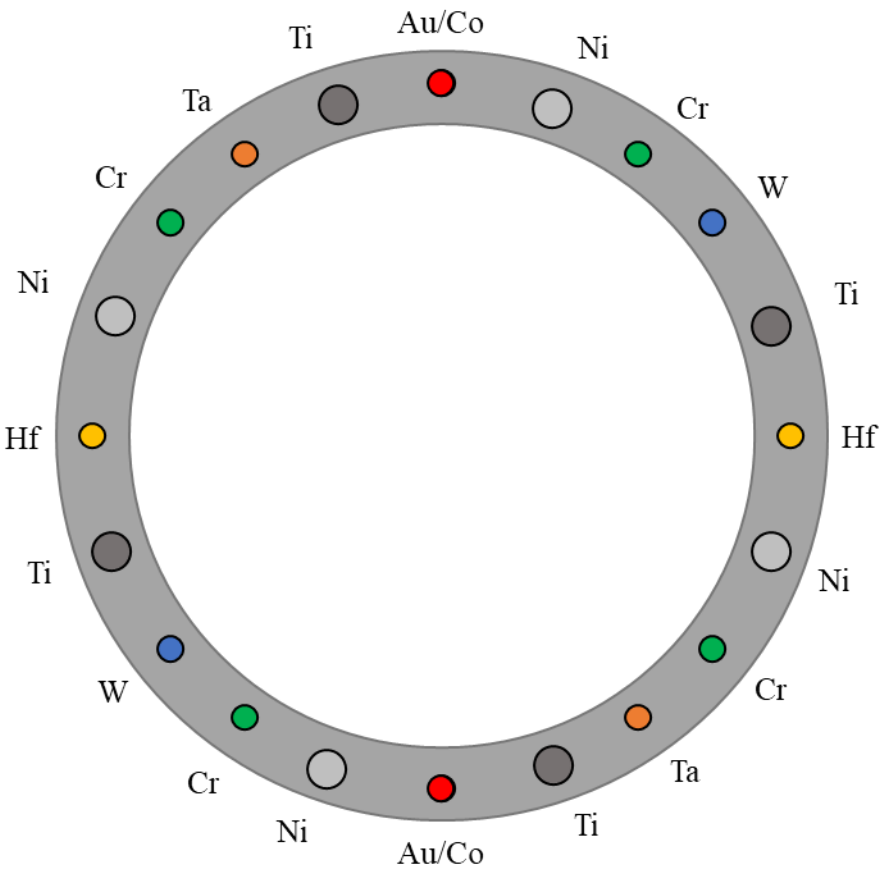

Figure 16 – Optimized Detector Target Rod Set

Table 32 – Optimized Detector Target Rod Set

	Target Rods			
Position	Element	Dia. (mm)	Length (cm)	Cost
0 deg	Au/Co	1	2.5	$69.95
18 deg	Ni	2	5	$1.16
36 deg	Cr	1	5	$0.85
54 deg	W	1	5	$0.59
72 deg	Ti	2	5	$0.93
90 deg	Hf	1	5	$10.50
108 deg	Ni	2	5	$1.16
126 deg	Cr	1	5	$0.85
144 deg	Ta	1	5	$4.13
162 deg	Ti	2	5	$0.93
180 deg	Au/Co	1	2.5	$69.95
198 deg	Ni	2	5	$1.16
216 deg	Cr	1	5	$0.85
234 deg	W	1	5	$0.59
252 deg	Ti	2	5	$0.93
270 deg	Hf	1	5	$10.50
288 deg	Ni	2	5	$1.16
306 deg	Cr	1	5	$0.85
324 deg	Ta	1	5	$4.13
342 deg	Ti	2	5	$0.93
			Total:	$182.06

The performance of this set of target rods will now be tested in a few scenarios.

4.3.4 Performance of Optimized Target Rod Set

As a baseline, the performance of the optimized detector target rod set is tested against the default scenario (with 400 m minimum distance to avoid melting), with results in Table 33 and Table 34.

Table 33 – Matching Results: χ^2 and Yield, Optimized Detector Target Rod Set, Default Scenario

		χ^2 value Unknown Weapon				
		FM	FUS	LB	WPu	WU
Library	FM	0.16	5854	1518	250	258
	FUS	1041	0.12	4411	4338	3889
	LB	693	3399	0.06	2033	1937
	WPu	149	6597	2473	0.12	8.61
	WU	139	6685	2269	8.27	0.12

		Yield				
		FM	FUS	LB	WPu	WU
Library	FM	15.0 kt	141.5 Mt	320.6 kt	4.9 Mt	3.2 Mt
	FUS	0.01 t	15.0 kt	0.35 t	2.6 kt	1.8 kt
	LB	1.1 kt	114.6 Mt	15.0 kt	1.0 Mt	533.1 kt
	WPu	0.05 t	472.7 kt	1.3 kt	15.0 kt	9.7 kt
	WU	0.07 t	777.5 kt	2.0 kt	23.3 kt	15.0 kt

Compared to the default scenario (Table 4, page 57) that included 27 elements regardless of price or ability to conduct so many counts, the 8 element optimized set performs exceptionally well. The optimized set performs significantly better than the default set on distinguishing the two closest spectra, WPu and WU, doubling the discrimination score in a range that is very important. It also improves discrimination between the fission and fusion spectra, doubling the score in some cases. This is due to the yield scaling being less affected by elements that fail to interact with high energy neutrons. The only significant decrease in matching discrimination is for the unknown FM spectra against the library WPu and WU spectra, where the chi-squared score is reduced by 30%. However, these scores are still two orders of magnitude greater than the correct match and do not cause any uncertainty as to the correct match.

Table 34 – Countable Locations, Optimized Set, Default Scenario

	Countable Locations				
	FM	FUS	LB	WPu	WU
Ti	0	21	0	6	4
Cr	1	22	6	16	14
Co	1	24	6	16	14
Ni	0	23	0	8	6
Hf	6	32	14	27	25
Ta	17	32	21	32	31
W	17	32	21	32	31
Au	27	32	30	32	32

The benefits of increasing the total mass, especially titanium and nickel, are reflected in Table 34. Every element is capable of working with the FUS, WPu, and WU spectra, which are the most representative of likely real-world modern threats, whether from nation-states or terrorist organization. The very heavy bomb casings, explosive systems, and flight systems of FM and LB are just not going to be recreated with modern technology, even by an asymmetric threat, which would not have access to a heavy capacity bomber to deliver such weapons.

Looking deeper into the matching score contributions, each element of the optimized set provides at least 6% of the total matching score, and the greatest contributor of the 8 contributes less than 23%. The standard deviation was under five percentage points. This distribution is very different than the previous iterations where a few elements dominated and most were meaningless. The mass multiplication through multiple and

larger diameter rods helps with this, and also makes the time spent counting each element more productive.

The next test combines a few of the previous parameter restrictions such as setting an artificially high minimum distance of 800 meters, blocking out a 60-degree swatch of detectors in the direction of a notional fallout plume (centered on 30 degrees east of due north), and increasing the delay in the start of counting to 10 days from the standard 3 days. The matching results and countable locations are in Table 35 and Table 36.

Table 35 – Matching Results: χ^2 and Yield, Optimized Detector Target Rod Set, 800 meter Minimum Distance, 60 degree Angle Exclusion, 10 Day Delay in Counting

		χ^2 value Unknown Weapon				
		FM	FUS	LB	WPu	WU
Library	FM	0.56	3962	296	3.11	3.16
	FUS	75.87	0.19	980	599	283
	LB	78.44	2185	0.05	283	229
	WPu	2.41	4739	321	0.20	3.68
	WU	1.84	4604	274	2.24	0.17

		Yield				
		FM	FUS	LB	WPu	WU
Library	FM	15.0 kt	100.2 Mt	144.3 kt	5.2 Mt	3.4 Mt
	FUS	0.01 t	15.0 kt	0.06 t	2.0 kt	1.3 kt
	LB	1.7 kt	138.3 Mt	15.0 kt	682.9 kt	427.5 kt
	WPu	0.04 t	290.8 kt	0.41 t	15.0 kt	9.7 kt
	WU	0.07 t	450.7 kt	0.62 t	23.2 kt	15.0 kt

This set of triple restrictions does reduce the matching chi-squared scores of the incorrect spectra (demonstrating less discrimination), especially between FM and the two Watt spectra. However, note that the yield scaling factor still reflects that FM is a terrible match for the two Watt spectra. The chi-squared score does not stand alone; the yield factor sometimes clearly distinguishes what chi-squared cannot.

The long delay in counting makes distinguishing these spectra dependent on the sensitive non-threshold reactions, and only tantalum and gold are able to contribute on all five spectra, though they do so with a healthy number of countable locations as seen below in Table 36:

Table 36 – Countable Locations, Optimized Set, 800 meter Minimum Distance, 60 degree Angle Exclusion, 10 Day Delay in Counting

	Countable Locations				
	FM	FUS	LB	WPu	WU
Ti	0	10	0	0	0
Cr	0	13	0	8	7
Co	0	15	0	9	7
Ni	0	14	0	2	0
Hf	0	20	7	17	15
Ta	10	20	13	20	20
W	0	20	2	13	11
Au	13	20	17	20	20

The inclusion of gold is especially valuable in scenarios like this where activations are more difficult to obtain and count rates more difficult to obtain for longer decay times. In

the fog and friction in the aftermath of an unexpected nuclear event, gold provides a backstop to maximize the amount of usable, reliable data available from AFIDS. The increased masses of hafnium, tantalum, and tungsten allow them to contribute as well.

Another way to test the robustness of the optimized target rod set is to increase the amount of perturbation applied when generating the unknown spectra. By default, and in every scenario up until now, the perturbation has been made using a gaussian distribution based on one standard deviation of injected random error. This error could be negative or positive, and the magnitude follows a bell curve, which larger errors becoming increasing less likely. In the following scenarios, that error will be increased by multiple standard deviations.

Table 37 – Matching Results: χ^2 and Yield, Optimized Detector Target Rod Set, 2 Standard Deviation Perturbation

		χ^2 value Unknown Weapon				
		FM	FUS	LB	WPu	WU
Library	FM	0.66	5854	1515	250	259
	FUS	1033	0.50	4408	4337	3889
	LB	698	3399	0.22	2034	1933
	WPu	147	6597	2469	0.50	9.19
	WU	137	6685	2266	8.80	0.50

		Yield				
		FM	FUS	LB	WPu	WU
Library	FM	15.1 kt	141.4 Mt	320.4 kt	4.9 Mt	3.2 Mt
	FUS	0.01 t	15.0 kt	0.35 t	2.6 kt	1.8 kt
	LB	1.1 kt	114.6 Mt	15.0 kt	1.0 Mt	532.8 kt
	WPu	0.05 t	472.4 kt	1.3 kt	15.0 kt	9.7 kt
	WU	0.07 t	777.1 kt	2.0 kt	23.3 kt	15.0 kt

Doubling the amount of perturbation does not significantly affect the matching scores or reliability for the optimized detector target rod set. The noise does appear in the slight increase of matching score for the diagonal of correct matches.

Table 38 – Matching Results: χ^2 and Yield, Optimized Detector Target Rod Set, 5 Standard Deviation Perturbation

		χ^2 value Unknown Weapon				
		FM	FUS	LB	WPu	WU
Library	FM	4.07	5856	1508	253	265
	FUS	1011	3.11	4400	4335	3892
	LB	716	3401	1.38	2039	1923
	WPu	143	6599	2459	3.12	12.37
	WU	134	6686	2257	11.95	3.09

		Yield				
		FM	FUS	LB	WPu	WU
Library	FM	15.2 kt	141.1 Mt	320.0 kt	4.9 Mt	3.2 Mt
	FUS	0.01 t	15.0 kt	0.35 t	2.6 kt	1.8 kt
	LB	1.1 kt	114.6 Mt	15.0 kt	1.0 Mt	531.9 kt
	WPu	0.05 t	471.6 kt	1.3 kt	15.0 kt	9.8 kt
	WU	0.07 t	775.8 kt	2.0 kt	23.3 kt	15.1 kt

Increasing the amount of intentionally introduced error to 5 standard deviations expected begins to have an effect on the diagonal of correct matches. Each of the scores is in the single digits, but all are now above 1, which is the rough threshold for a very close match. The combination of chi-squared with the yield scaling factors is still sufficient to discriminate between the spectra, albeit with less confidence than before.

Table 39 – Matching Results: χ^2 and Yield, Optimized Detector Target Rod Set, 10 Standard Deviation Perturbation

		χ^2 value Unknown Weapon				
		FM	FUS	LB	WPu	WU
Library	FM	16.08	5861	1499	262	279
	FUS	979	12.46	4388	4335	3898
	LB	750	3406	5.55	2051	1910
	WPu	142	6605	2444	12.43	22.38
	WU	134	6691	2244	22.33	12.32

		Yield				
		FM	FUS	LB	WPu	WU
Library	FM	15.3 kt	140.6 Mt	319.3 kt	4.9 Mt	3.2 Mt
	FUS	0.01 t	15.0 kt	0.35 t	2.6 kt	1.8 kt
	LB	1.2 kt	114.7 Mt	14.9 kt	1.0 Mt	531.2 kt
	WPu	0.05 t	470.4 kt	1.3 kt	15.1 kt	9.8 kt
	WU	0.07 t	773.8 kt	2.0 kt	23.4 kt	15.1 kt

With a 10 standard deviation error range, the chi-squared scores start to suffer, especially in distinguishing the two Watt spectra. These two spectra can be distinguished at this point, but with less confidence than before since their correct match scores now exceed 10 and are more than half of the nearby incorrect matches.

Table 40 – Matching Results: χ^2 and Yield, Optimized Detector Target Rod Set, 30 Standard Deviation Perturbation

		χ^2 value Unknown Weapon				
		FM	FUS	LB	WPu	WU
Library	FM	137	5924	1487	359	396
	FUS	896	112	4351	4378	3962
	LB	940	3441	50.45	2130	1899
	WPu	205	6668	2404	111	120
	WU	191	6745	2213	127	109

		Yield				
		FM	FUS	LB	WPu	WU
Library	FM	16.2 kt	139.4 Mt	317.3 kt	5.0 Mt	3.3 Mt
	FUS	0.01 t	15.0 kt	0.34 t	2.7 kt	1.8 kt
	LB	1.3 kt	115.8 Mt	14.9 kt	1.1 Mt	537.1 kt
	WPu	0.05 t	468.0 kt	1.3 kt	15.3 kt	10.0 kt
	WU	0.08 t	769.3 kt	2.0 kt	23.8 kt	15.4 kt

At this point, the matching chi-squared analysis breaks down, producing no reliable results due to the excessive noise. The failure is most pronounced between the two Watt spectra as well as FM. Thirty standard deviations create a truly high error level. Even at this extreme, the optimized set reliably discriminates between fusion and fission spectra.

A parallel analysis of the relative contributions of each element was conducted; the relative contributions remained steady as the noise increased. No element was particularly good or bad at handling noise.

Considering the magnitude of noise progressively introduced in the spectra, the optimized detector target rod set was fairly robust up through 5 standard deviations of noise. This is very satisfactory performance. The optimized set for this particular set of

weapons leakage spectra will function well in a wide variety of circumstances while meeting all budget limits and other constraints.

It is again worth stating that this optimized set is not a generalized solution for all neutron spectra or all nuclear weapons neutron leakage spectra. A generalized approach for optimizing for a larger and more varied spectra set is discussed in the conclusions chapter.

CHAPTER 5. CONCLUSIONS

This research effort thus far has demonstrated an approach to optimizing the detector target rods selected for an AFIDS-type detector, for the specific case of 5 unclassified weapons neutron leakage spectra. For these 5 spectra, most analysis could be conducted over 5 x 5 matrices with a manageable 25 data points for a typical scoring table. At this scale, the optimization can largely be completed manually with individual attention paid to each combination of spectra.

5.1 Differences for Real-World Applications

For real-world applications of AFIDS and other neutron activation detectors, the spectra search space will be significantly larger. The US Government has developed and deployed over 70 nuclear weapon warhead designs in its history, with 7 types currently deployed as of 2016. [15] The former Soviet Union / modern day Russia also had a robust weapons development program and there are multiple other declared nuclear weapons states.

Anticipating this larger search space, all techniques and codes were built and tested against a matrix of 125 x 125 spectra (consisting of the 5 unclassified spectra repeated 25 times each with slightly different names). In multiple parts of the modeling and analysis code, the computational time required goes up with this squared matrix value, but still runs in less than a day on a personal computer.

The biggest difference is not computing time, however. When optimizing for a much larger set of spectra, it will not be practical to analyze every single cell by hand. Even the matching chi-squared tables will take multiple pages to print unless they are reduced to a heatmap. Therefore, the built-in analysis tools of the code, such as summing of chi-squared score contributions by element, detector location, and spectra combinations are critical to creating an optimized detector target rod set that covers a much larger search space.

The spectra themselves will not only be more numerous, but also different qualitatively. There are pure fission weapons to consider, but also fusion boosted weapons and staged weapons that combine fission, fusion, and fission stages. [15] The spectra will have a greater mix of energy distributions, and will lack the clear difference between a pure hypothetical 14.1 MeV peak that the unclassified FUS spectrum modelled. However, more weapons will have high energy neutrons that threshold reactions will be able to capture. Automated tallies and summations must be used to determine the utility of each element in this more varied search space.

5.2 Generalized Approach to Optimization

5.2.1 Additional Optimization Criteria

The analysis that led to the optimization criteria detailed in section 4.3.1 (page 110) will hold true for the larger and more varied spectra data sets. In addition, some new criteria are added:

11. The spectra library set should be narrowed down to only the spectra that it is important to distinguish between. For example, the US nuclear warhead designated B61 had a total of 12 modifications (Mods). Each Mod incorporated the same base design but "incorporated a few different components that changed the operational characteristics of the weapon in a significant way". [15] The reasons for these Mods include incorporating the warhead into different delivery systems. Distinguishing between minor modifications is not as important and should not be considered valuable in the optimization process.[28] (These spectra must be culled carefully, as a change of delivery system could affect the leakage spectrum significantly.)
12. Special attention must be paid to any spectra that leads to a limited number of countable locations, either in absolute numbers, or only creating sufficient counts for a single target element. This could drive optimization decisions to increase the mass multiplier of other elements in order to increase the breadth of coverage.
13. Matching chi-squared scores should show rough degrees of similarity between spectra that are related but different. For instance, a pure fission gun-type device should have a very different score than a modern US thermonuclear staged weapon. However, two fission gun-type devices with similar materials but different components and casings should produce a much lower score.

[28] Trimming unnecessary spectra search space also allows for easier manual analysis and reduced computational time, memory and storage requirements.

14. The angular effects from the detector body shielding should be mitigated to the extent possible by placing multiple copies of the same element in offset angular locations within the detector body. Single target rods should be split in half and set 180 degrees apart to create some diversity in angle.
15. To address the likely bottlenecks in the counting process, unnecessary elements should not be included just for the sake of variety or to fill up all the slots. Alternatively, inexpensive materials of lower value can be included but have a low priority for counting. Additionally, duplicates of good materials can lead to faster counting times.

5.2.2 Element Screening and Selection Method

The thought process behind the screening of potential elements discussed in sections 4.3 (page 110) can be generalized for larger and different spectra sets. For an AFIDS-style optimization problem, the two major constraints are budget and target rod slots available (and the closely-related problem of counting throughput).

The budget constraint is most important for a handful of expensive elements like iridium, rhenium, gold and cobalt. The utility of each of these elements versus their cost should be determined first and decisions made on whether to include them and in what quantity. If the decision is not clear, then multiple courses of action can be considered with or without those specific expensive elements. The decisions made here narrow the budget space in a way that needs to be made upfront. They do not tend to take up many target slots.

Next, elements with high utility but that would benefit greatly from additional mass in order to reach higher numbers of countable locations should be considered. Tables similar to Table 30 (page 120) should be generated, with summation tallies used to show the overall effect of each additional mass portion. Plateaus should be sought out, and additional mass added only in sufficient quantity to capture the largest gains in degree of freedom with the minimal slot usage. If spare slots and money are available at the end of the process, these tables can be revisited to distribute the remaining space and material costs optimally to capture as many gains as possible.

With the number of available slots reduced, the remaining elements should be handled in an order that focuses on covering the gaps in utility left by the currently selected elements. These could be gaps in distinguishing low or high energy spectra, providing threshold reactions, or providing long-lasting counts from activation products with longer half-lives, or any combination of the above. There could also be a few specific spectra types that are difficult to count or distinguish that could be targeted by specific remaining elements.

When the available target rod slots are exhausted, increases in mass by increased diameters should be considered, subject to budget constraints and diminishing returns. There is certainly value in designing an optimized set below budget, but overall utility should be prioritized.

5.2.3 Testing of Optimized Sets

If a single optimized set is decided on, it should be tested via scenarios that push the limits on the conditions in which it can reliably distinguish spectra. If multiple courses

of action are being considered, these same tests can help determine the best course of action by finding which optimized set is able to perform with the most restrictions and the most injected noise.

Tests should include distance, angle, and time constraints similar to Table 36 (page 130). Any noticeable deficiencies in this test should be corrected by changing elements and mass multipliers to the extent possible. Further tests should inject increasing amounts of noise in a fashion similar to those done starting in Table 37 (page 131). A key decision criterion between competing optimized sets is how much noise they can handle while still successfully distinguishing spectra. Again, localized failures should be examined and mitigated if small changes in the overall optimized set can fill the gaps.

CHAPTER 6. RECOMMENDATIONS

This chapter contains recommendations for future work and studies to be conducted. These recommendations focus on both improving the information used to model and optimizing the AFIDS-style neutron activation detectors and topics generated from this research that are outside of its immediate scope but useful to improving the overall AFIDS system.

6.1 Angular Dependence of Flux

As described, modelled, and experimentally verified in sections 3.1.1.3 (page 32) and 4.1.1.2 (page 71), there is a measurable impact on the incoming flux spectra determined by the angular position of a target rod versus the direction the radiation is primarily coming from. While these effects have been modelled and correction factors generated, the model used makes the assumption that the flux in monodirectional from a nearby planar source. In reality, many of the neutrons will scatter and change directions before reaching the detector. These scatters are accounted for in the pre-calculated transport of the spectra from the detonation site to the detector sites; however, these transported spectra do not provide any information about the directional distribution of the flux.

Due to the size and complexity of the city model, it was impractical to re-run the MCNP transport without use of a supercomputer. The transport data provided were sufficient to conduct this research; further refinement and understanding of the angular effects, including both improved modeling and mitigation, will require these runs to be recomputed with a tally system that captures the directional distribution of the flux.

6.2 Optimizing Detector Placement to Minimize Noise

Part of this research considered the effects of height above ground on the flux received by the detectors. The theory is that detectors placed further from the ground and possibly above the majority of the urban terrain will have less noise introduced into the flux that reaches them – the flux will generally undergo fewer scattering events. While there will still be urban terrain effects for some detectors, especially if the detector is in the "shadow" of a building near the detonation, those effects will be less complex, less numerous, and easier to accurately model.

There are certainly trade-offs incurred by placing detectors in high places. They are more expensive to install, requiring specialized crews to be hired to install in places like cell phone towers and skyscrapers. They are more difficult to check on during a maintenance cycle. Importantly, they may be especially difficult to recover in the immediate aftermath post-blast. However, if the quality of their signal is significantly better than detectors close to the ground, these costs may be worth it.

Moving the detector locations (as opposed to filtering by height) was beyond the scope of this research. It would also require calculating additional city-level MCNP transports to new locations, requiring a supercomputer. But this work could determine the efficacy of placing detectors in high places and drive planning that will improve AFIDS performance in a manner distinct from picking the optimum target rod set.

Nothing in the AFIDS approach requires permanent, static installations. Detectors could be brought and temporarily emplaced at high-profile events at a minimal cost. They could even be fielding with military units overseas to collect data in the event of a nuclear

strike. Only their locations at the time of the strike are required to do the transport calcuations.

6.3 Determining the Optimal Counting Parameters

During this research, an optimized set of target rods was developed that proved to be very robust against intentionally introduced noise in the unknown spectra, performing well with five standard deviations of noise randomly added. The research assumed a static counting criterion of 3 hours with a minimum of 3,000 total counts.

The total count quantity is driven by reducing the statistical error in counting, which is proportional the square root of the number of counts. The 3 hours is an estimate based on maintaining throughput at the limited counting setups available to handle perhaps dozens of detectors recovered with up to 20 rods each. The 3 hour limit serves to both limit decay of short-lived activation products and to provide results to national authorities in as timely of manner possible.

Given the robustness demonstrated in this study, both the number of minimum counts and the time allowed bear reconsideration and further study. Reducing the minimum number of counts required increases potential statistical error, but also increases the number of countable locations, especially for threshold elements in low yield scenarios. Changing the time limit to a shorter quantity would allow greater throughput, though shortening the time also reduces the number of countable locations.

One possible solution, especially with a target rod set containing fewer numbers of different elements, would be to have a counting plan that is not static. Rather, the counting

is actively monitored, and samples reaching the minimum counts required early are pulled out and the next samples are placed in. In this setup, the time to reach the minimum counts is used to calculate the initial activation levels instead of the counts in a static time. This active monitoring may also help filter out elements that are clearly not on pace to reach the minimum count requirement in the time available, freeing up the counting system to focus on elements with countable quantities remaining.

Another approach would incorporate higher-efficiency detectors like sodium iodine. While sacrificing energy resolution, the gain in absolute efficiency could both speed the counting and allow some isotopes to have additional countable locations. Sodium iodine detectors are also less expensive, do not require cooling, and are available in greater quantities at universities with nuclear programs. They could also be used to triage incoming target rods to be counted, to eliminate those that will be uncountable and prioritize those that need to be counted quickly before losing their count rate.

A coincidence counting system could also help improve counting throughput at a lower cost, especially if a mobile counting laboratory is fielded for AFIDS. Using coincidence allows for good signal to be derived with far less shielding than would otherwise be required, reducing weight and cost requirements.

Finally, agreements with institutions like research universities that have sophisticated counting laboratories could bring those assets to bear on the counting throughput problem. There would be some cost, training, and testing associated with this, but the return would be high versus the investment required.

APPENDIX A. SAMPLE CALCULATIONS

This appendix shows sample calculations for each major computation executed in the FORTRAN codes supporting the inverse optimization process. Assumptions are stated before each problem, and explored, discussed, and validated after the problem when appropriate.

A.1 Post-Detonation Activation Level in Target Rod

This computation takes a known neutron fluence (in a specific energy group) that has already been transported to the location of the target rod and calculates the number of activations that will occur from that energy bin. To calculate the total activity, it is then necessary to sum all energy bins for that fluence and material.

A.1.1 Variables

N_{act} ≡ Number of activations present in the target rod after the brief fluence from the detonation event in a specific energy group, number. [Calculated quantity]

Φ ≡ Incoming neutron fluence from a selected energy bin (already transported from the detonation site to the target rod site), number of neutrons.

σ ≡ The effective microscopic cross section from a selected energy bin for the specific desired reaction, barns (10^{-24} centimeters^2).

m ≡ Mass of the target rod, calculated from its density and volume, grams.

Abundance ≡ Portion of mass that is the specific desired isotope, fraction.

$A \equiv$ Average atomic weight of the element of the target material (isotope specific), grams/mole.

$N_A \equiv$ Avogadro's Number: number of atoms per mole.

A.1.2 Assumptions

1. The self-shielding effect of the target rod is negligible: a central or far-side atom is as likely to have a reaction as the leading edge since very few neutrons of the incoming fluence are consumed in the reactions prior to reaching the middle and far sides.
2. The time in which the fluence is delivered to the target material is very short compared to the target reactions half-life for gamma emission.

A.1.3 Givens

For this sample calculation, an unclassified spectrum from the "Fat Man" nuclear explosion at Nagasaki is used for some source data. Specifically, detector location 16 is selected, with the ^{186}W(n,g) reaction and the 6703200 eV energy bin used for the sample calculation. A 15-kt yield is assumed.

Φ = 1.99223e8 neutrons/(centimeter^2*kt)

σ = 0.05202200102 barns

d = 0.10 centimeters

l = 5.00 centimeters

m = 0.7559458 grams

Abundance = 0.2843

$A \equiv$ 185.95 grams/mole

$N_A \equiv$ 6.022140857e+23 atoms/mole

A.1.4 Physics / Equation

The major equation in this step of the calculation relates the number of activations to the other variables:

$$N_{Act} = \Phi * \ \sigma * \left(\frac{m * abundance}{A}\right) * N_A$$

A.1.5 Results

Substituting in given values and conducting unit conversions yields:

$$N_{Act} = \left(1.99223e8 \ \frac{\text{n}}{\text{cm}^2 * \text{kt}}\right) * (15 \text{ kt}) * \left(0.05202200102\text{b} * \ \frac{10^{-24} \text{ cm}^2}{\text{b}}\right)$$
$$* \left(\frac{00.7559458 \ \text{g} * \ 0.2843}{185.95 \text{ g/mol}}\right) * 6.022140857e23 \text{ atoms/mol}$$

Cancelling units and calculating results in:

$N_{Act} =$ 108203.19 activations in this energy bin

This matches the output of the FORTRAN program. The FORTRAN program then sums over all the discrete energy bins to total the activation of the target rod.

A.1.6 Assumption Validation

1. The total number of neutrons passing through the target rod is roughly given by:

$$N = \left(1.99223\text{e}8\ \frac{\text{n}}{\text{cm}^2} * 0.1\ \text{cm} * 5.0\ \text{cm}\right)$$

$$N = 9.96115\text{e}7\ \text{neutrons}$$

$$(N >> N_{act})$$

The number of neutrons interacting (causing activations) with the target rod (for this particular reaction) is much less than the amount of incoming fluence, so the assumption is valid.

2. The times for arrival of prompt neutrons are measured in milliseconds or microseconds; the half-lives of all elements considered are much larger than this, so decay during the initial fluence is negligible.

A.2 Remaining Activation Level at a Given Time

The number of activated products immediately after the time of detonation must be adjusted for the radioactive decay that occurs before counting begins.

A.2.1 Variables

$N(t)$ ≡ Number of activated atoms at a given time [Calculated quantity]

N_0 ≡ Number of activated atoms at time zero, previously calculated.

λ ≡ Decay constant of the product isotope of interest (1/hour)

$t \equiv$ Time (hour)

A.2.2 Givens

N_0 = 108203.19 activations

λ = 0.028881133 1/hour

t = 24.0 hours

A.2.3 Physics / Equation

$$N(t) = N_0 * e^{-\lambda t}$$

A.2.4 Results

Substituting in given values yields:

$$N(t) = (2.484\text{e}10 \text{ activations}) * e^{-\left(0.028881133\frac{1}{\text{hour}}\right)*24.0 \text{ hours}}$$

Result:

N(t) = 1.242e10 activations at time = 24.0 hours

A.3 Count Rate at a Given Time

The primary directly-measured quantity post-detonation is the count rate of the individual target rods at a given time. This count rate is a function of the activity level of the target rod, the number of gammas per decay for the gamma ray being counted, the probability that gamma ray escapes from the target rod, and the absolute efficiency of the detector setup used at that energy level.

A.3.1 Variables

$C(t)$ ≡ Count rate at a given time (counts/hour) [Calculated quantity]

λ ≡ Decay constant (1/hour)

$N(t)$ ≡ Number of activated atoms at a given time

γ_i ≡ Number of gamma rays emitted per decay event; only including gamma rays from the best gamma ray selected

p_{esc} ≡ Probability that a given gamma ray escapes from the target rod

ε_{abs} ≡ Absolute efficiency of the detector for the chosen gamma ray

A.3.2 Givens

λ = 0.028881133 1/hour

$N(t)$ = 1.242e10 activations at time = 24.0 hours

γ_i = 0.1355

p_{esc} = 0.811923 at this gamma energy for this Z target rod

ε_{abs} = 0.272595 at this gamma energy

A.3.3 Physics / Equation

$$C(t) = \lambda N(t) * \gamma_i * p_{esc} * \varepsilon_{abs}$$

A.3.4 Results

Substituting in given values yields:

$$C(t) = \left(0.02888113\ \frac{1}{hr}\right)(1.242\text{e}10) * 0.1355 * 0.811923 * 0.272595$$

Result:

C(t) = 1.0757e7 counts/hr

The negative sign indicates that the number of activated particles is decreasing with time.

A.4 Maximum Delay Time to Start Counting

This calculation determines how long of a delay can pass while still allowing the minimum count threshold to be reached in the allotted counting time. This calculation is done on a by-reaction basis, which then can be used to determine the overall maximum delay for a starting element. (Within the reaction, the best product gamma ray is selected for analysis.)

A.4.1 Variables

t_{md} ≡ Maximum delay time before counting starts that yields the minimum required counts. [Calculated quantity]

C_{min} ≡ minimum allowed counts in counting time t_c

N_{act} ≡ Number of activated atoms at time zero, previously calculated

λ ≡ Decay constant of the product isotope of interest (1/hour)

γ_i ≡ Number of gamma rays emitted per decay event; only including gamma rays from the best gamma ray selected

p_{esc} ≡ Probability that a given gamma ray escapes from the target rod

ε_{abs} ≡ Absolute efficiency of the detector for the chosen gamma ray

A.4.2 Givens

C_{min} = 1000 counts

N_0 = 2.484e10 atoms

λ = 0.028881133 1/hour

γ/decay = 0.1355

p_{esc} = 0.811923 at this gamma energy for this Z target rod

ε_{abs} = 0.272595 at this gamma energy

A.4.3 Physics / Equation

$$t_{md} = \frac{\ln\left[\frac{N_{act} * \gamma_i * p_{esc} * \varepsilon_{abs}}{C_{min}} * \left(1 - e^{-\lambda t}\right)\right]}{\lambda}$$

A.4.4 Results

Substituting in given values yields:

$$t_{md} = \frac{\ln\left[\frac{2.484e10 * 0.1355 * 0.811923 * 0.272595}{1000} * \left(1 - e^{-0.028881133\left(\frac{1}{hr}\right)(1.0hr)}\right)\right]}{0.028881133\left(\frac{1}{hr}\right)}$$

Result:

t_{md} = 344.934 hours

A.5 Counts in a Given Time

This calculation determines the expected number of counts from radioactive decays from a given reaction, given a set delay time and counting time. Within the reaction, the best product gamma ray is selected for analysis.

A.5.1 Variables

C(T,t) ≡ Counts registered, starting at time *T* post-detonation and counting for *t* hours. [Calculated quantity]

N_0 ≡ Number of activated atoms at time zero, previously calculated

λ ≡ Decay constant of the product isotope of interest (1/hour)

γ_i ≡ Number of gamma rays emitted per decay event; only including gamma rays from the best gamma ray selected

p_{esc} ≡ Probability that a given gamma ray escapes from the target rod

ε_{abs} ≡ Absolute efficiency of the detector for the chosen gamma ray

A.5.2 Givens

T = 72.0 hours

t = 3.0 hours

N_0 = 2.484e10 atoms

λ = 0.028881133 1/hour

γ_i = 0.1355

p_{esc} = 0.811923 at this gamma energy for this Z target rod

ε_{abs} = 0.272595 at this gamma energy

A.5.3 Physics / Equation

$$C(T,t) = (N_0 * \gamma_i * p_{esc} * \varepsilon_{abs})(e^{-\lambda T})(1 - e^{-\lambda t})$$

A.5.4 Results

Substituting in given values yields:

$$C(T,t) = 2.484\text{e}10 * 0.1355 * 0.811923 * 0.272595)(e^{-0.028881133*72.0})(1 - e^{-0.028881133*3.0})$$

Result:

$C(T,t)$ = 7.7284e6 counts

A.6 Chi-Squared Calculation (local value)

This calculation determines the chi-squared contribution of a given library spectra, measured spectra, detector location, reaction, and energy bin combination. This is the fundamental quantity used in scoring spectra against each other and is summed over all the detector location/target element combinations that are countable locations. The Chi-Squared value depends on a scaling factor equal to the yield of the measured spectra, which is searched for using a Golden Section Search in the code. The search seeks to minimize the total Chi-Squared value for a given library spectra / measured spectra combination; for purposes of the sample calculation, a single value is tested.

A.6.1 Variables

$\chi^2_s \equiv$ Chi-Squared value, used to determine how good of a statistical fit two different spectra are. This quantity depends on 4 independent variables (library spectra activations, measured spectra activations, detector location, and reaction) plus a scaling factor (yield) which is used to minimize the overall Chi-Squared value. [Calculated quantity]

$F \equiv$ Degrees of freedom – determined by the number of valid detector location/reaction combinations for the two spectra being compared. For the sample calculation, a single degree of freedom is tested. Note than F is bounded by $F \leq D*J$.

$d \equiv$ detector location index

$D \equiv$ number of detector locations

$j \equiv$ reaction index

$J \equiv$ number of reactions

$y_s \equiv$ library spectrum yield (in kt); used as a scaling factor to minimize overall chi-squared

$B_{sdj} \pm u_{sdj} \equiv$ The library reference spectrum's activation level and uncertainty at a given detector location for a given reaction. This library spectra are produced assuming a 1.0 kt yield, which lets y_s serve as a scaling factor to match the measured spectrum's activations.

$M_{dj} \pm \sigma_{dj} \equiv$ The measured spectrum's activation level and uncertainty at a given detector location for a given reaction.

A.6.2 Givens

This sample calculation uses the Watt-Pu spectrum (s=4) as the library spectrum and the Fusion spectrum (s=2) as the measured spectrum.

F = 1 (to just look at the contribution to chi-squared from one measured target rod/reaction for this sample calculation; summation of multiple degrees of freedom is a trivial calculation.)

d = detector location 32

D = 34 detector locations

j = Reaction 1433, (186W(n,γ)187W). (Note: the vast majority of possible reactions will have 0 contribution to Chi-Squared due to being filtered out.)

J = 1691 reactions (not used)

y_s = 42400 kt (large quantity due to two very different spectra)

$B_{sdj} \pm u_{sdj}$ = 1.6461e7 ± 1.7016e5 activations

$M_{dj} \pm \sigma_{dj}$ = 3.0158e9 ± 1.54484e6 activations

A.6.3 Physics / Equation

$$\chi_s^2 = \frac{1}{F}\sum_{d}^{D}\sum_{j}^{J}\frac{(y_s B_{sdj} - M_{dj})^2}{y_s^2 u_{sdj}^2 + \sigma_{dj}^2}$$

A.6.4 Results

Substituting in given values yields:

$$\chi_s^2 = \frac{1}{1}\sum_{32}^{32}\sum_{1433}^{1433}\frac{((42400\ kt)(1.6461e7) - 3.0158e9)^2}{(42400\ kt)^2(1.7016e5)^2 + (2.5011e7)^2}$$

Result:

χ^2_s = 9277.5

This Chi-Squared score indicates that the library and measured spectra have very different activation levels for the reaction/detector location combination, signifying a non-match.

A.7 Uncertainty in Measured Activations

This calculation determines the absolute uncertainty of the number of measured activations. In this context of this program, the measured activations are originally produced by perturbing the library spectra activations and then multiplying by the yield. However, in a real scenario, the measured activations would not come from neutron transport calculations, but from the number of measured counts from the activated target rods. Therefore, uncertainty for the measured activations is propagated from the number of counts at a set time post-detonation and that quantity's uncertainty.

A.7.1 Variables

$\sigma \equiv$ Absolute uncertainty in measured activations [Calculated quantity]

$C(T,t) \equiv$ Counts registered, starting at time T post-detonation and counting for t hours

$T \equiv$ Time elapsed post-detonation before counting begins (hours)

$t \equiv$ Time allowed for counting (hours)

$\lambda \equiv$ Decay constant of the product isotope of interest (1/hours)

$\gamma_i \equiv$ Number of gamma rays emitted per decay event; only including gamma rays from the best gamma ray selected

$p_{esc} \equiv$ Probability that a given gamma ray escapes from the target rod

$\varepsilon_{abs} \equiv$ Absolute efficiency of the detector for the chosen gamma ray

A.7.2 Givens

This sample calculation uses the Fusion spectrum (s=2) as the measured spectrum, and the ($^{186}W(n,\gamma)^{187}W$) reaction, with the associated best gamma selected. Detector location 32 is used.

$C(T,t)$ = 938294 counts

T = 72.0 hours

t = 3.0 hours

λ = 0.028881133 1/hr

γ_i = 0.1355

p_{esc} = 0.811923 at this gamma energy for this Z target rod

ε_{abs} = 0.272595 at this gamma energy

A.7.3 Physics / Equation

$$\sigma = \frac{\sqrt{C(T,t)} * e^{\lambda T}}{\gamma_i * p_{esc} * \varepsilon_{abs} * \left(1 - (e^{-\lambda t})\right)}$$

A.7.4 Results

Substituting in given values yields:

$$\sigma = \frac{\sqrt{938294} * e^{(0.028881133\ 1/hr)(72.0\ hr)}}{0.1355 * 0.811923 * 0.272595 * \left(1 - (e^{-(0.028881133\ 1/hr)(3.0\ hr)})\right)}$$

Result:

σ = 3.113372e6 activations (uncertainty)

N_{act} = 3.0158e9 ± 3.1134e6

APPENDIX B. CROSS SECTION PLOTS

This appendix includes the cross section plots of the 27 commercially-available candidate elements. The cross sections displayed are for the reaction of most interest when applicable; some elements have both their best threshold and no threshold reactions displayed separately. All data comes from the ENDF database. [14]

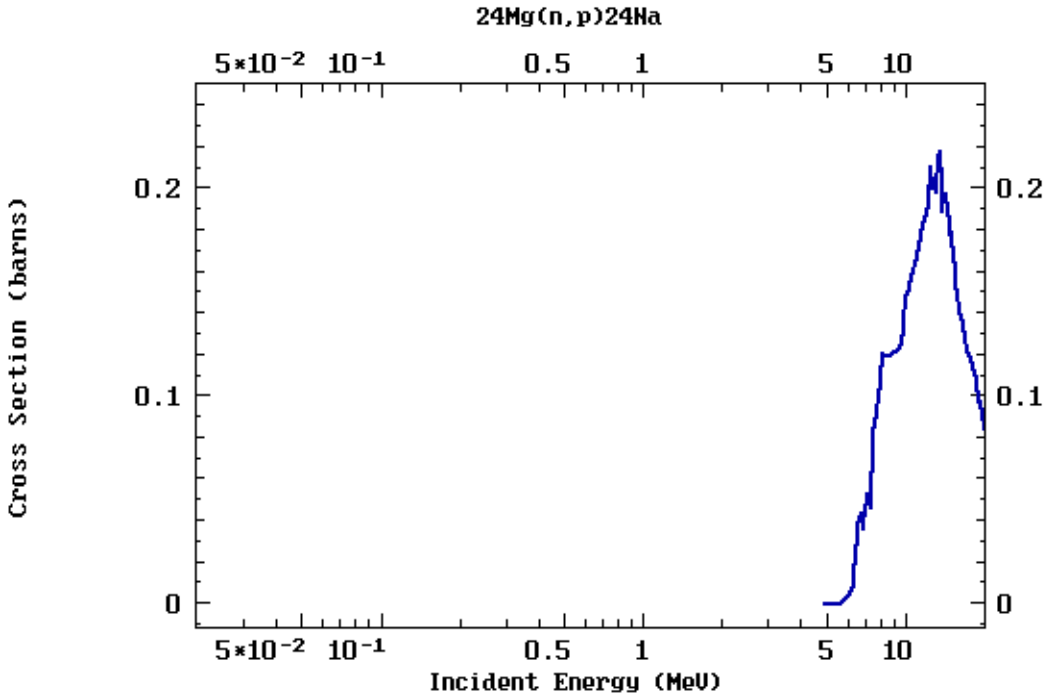

Figure 17 – Mg Cross Section (lin/log)

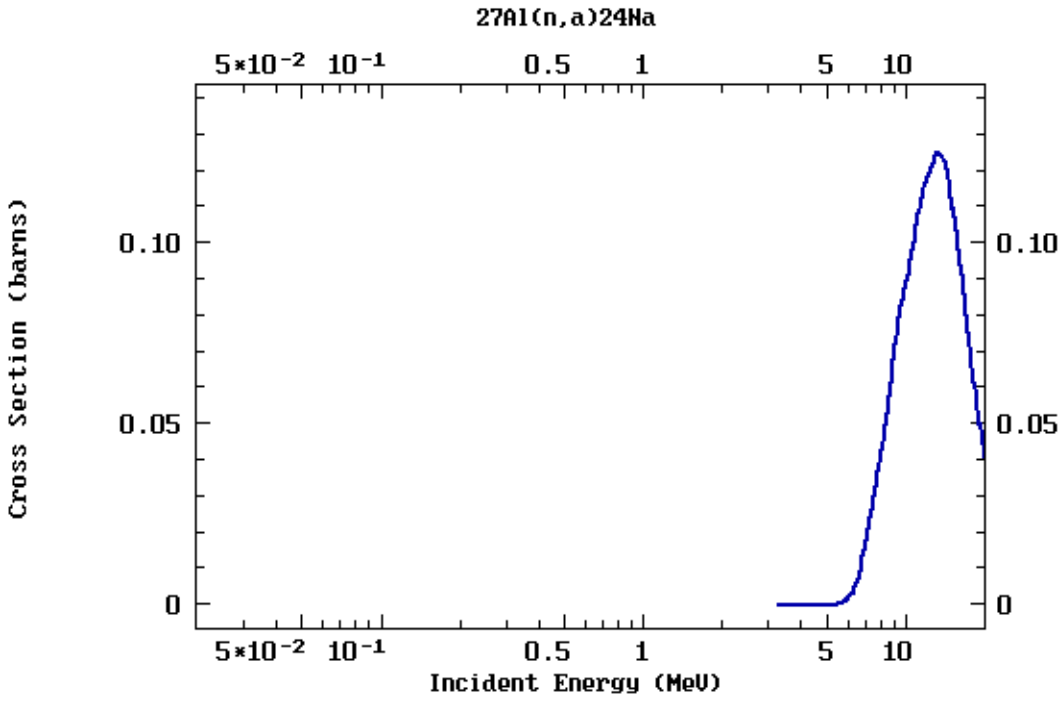

Figure 18 – Al Cross Section (lin/log)

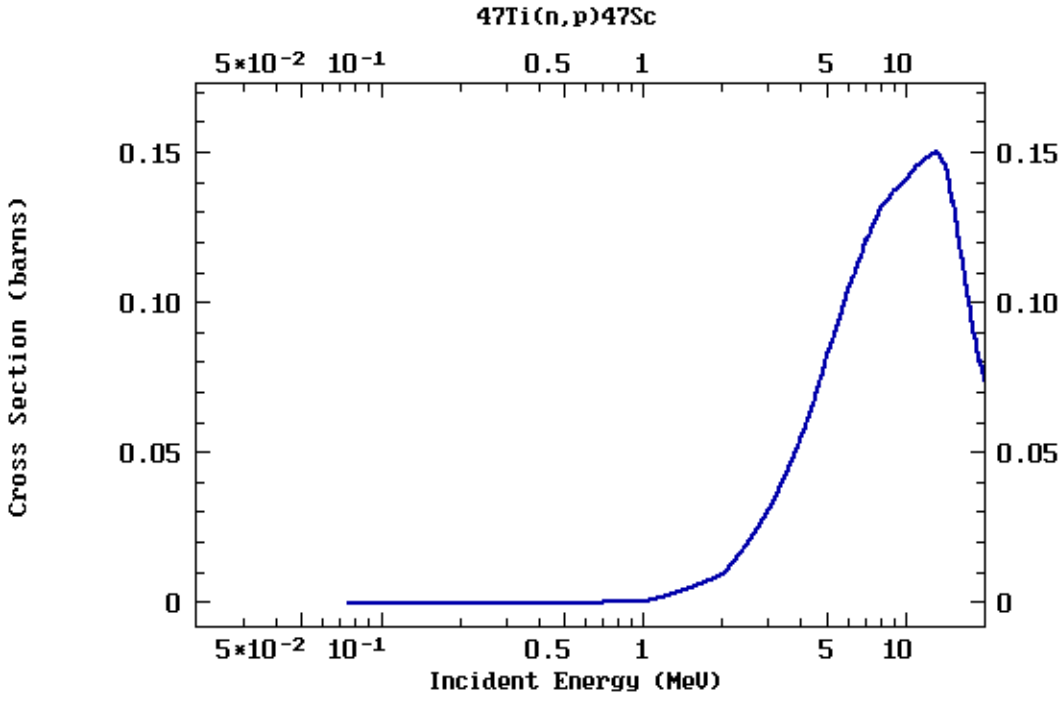

Figure 19 – Ti Cross Section (lin/log)

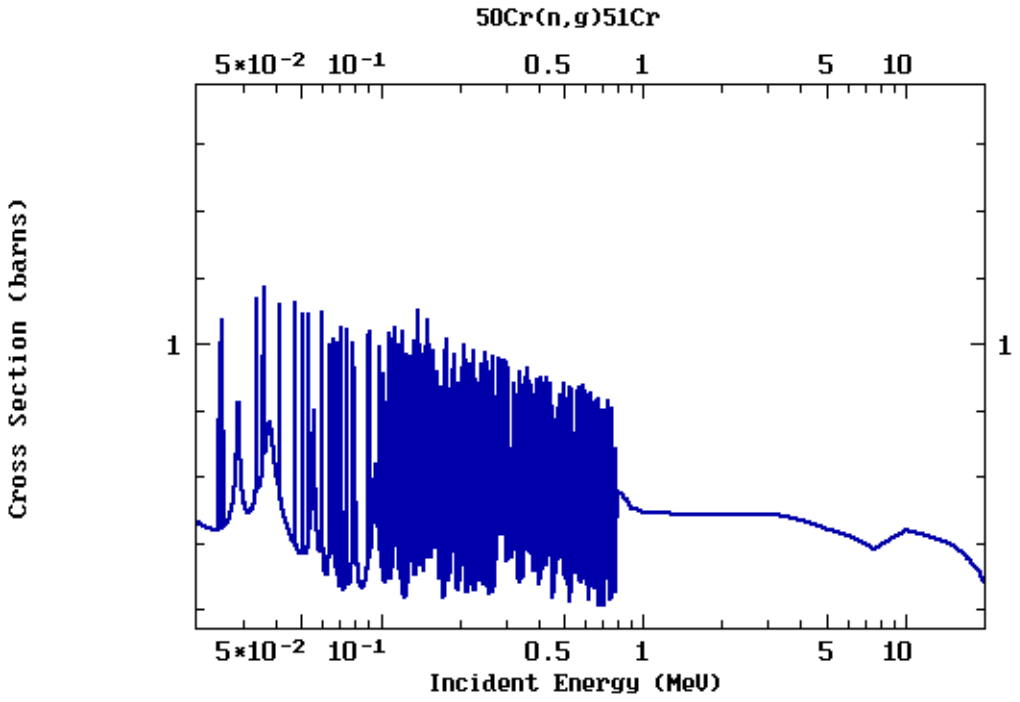

Figure 20 – Cr Cross Section (log/log)

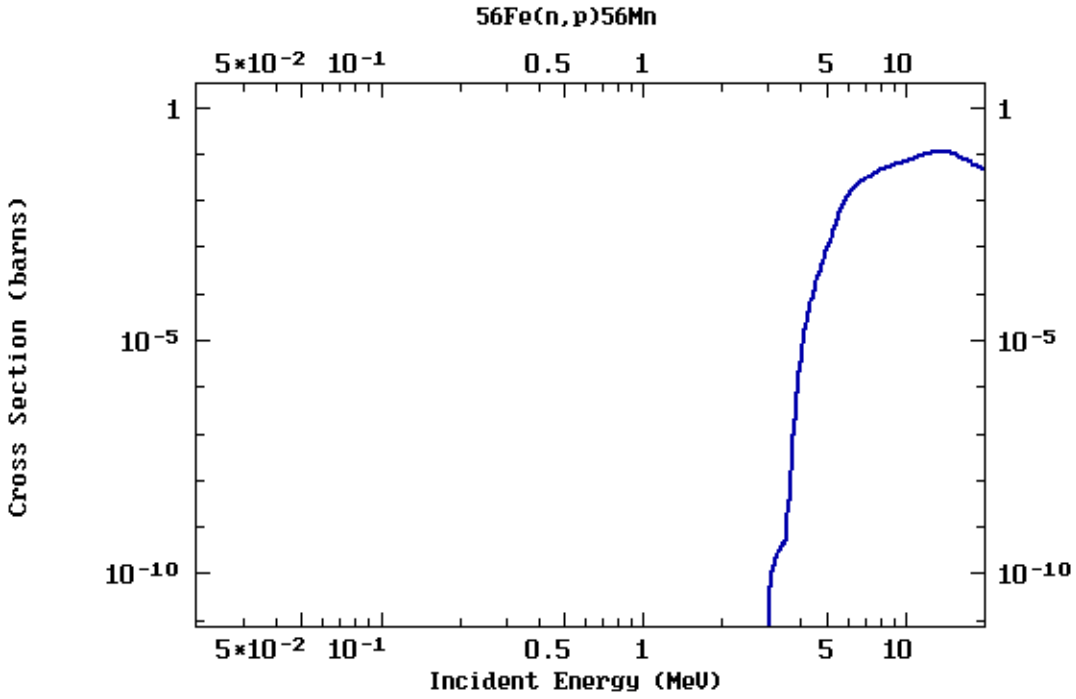

Figure 21 – Fe Cross Section (log/log)

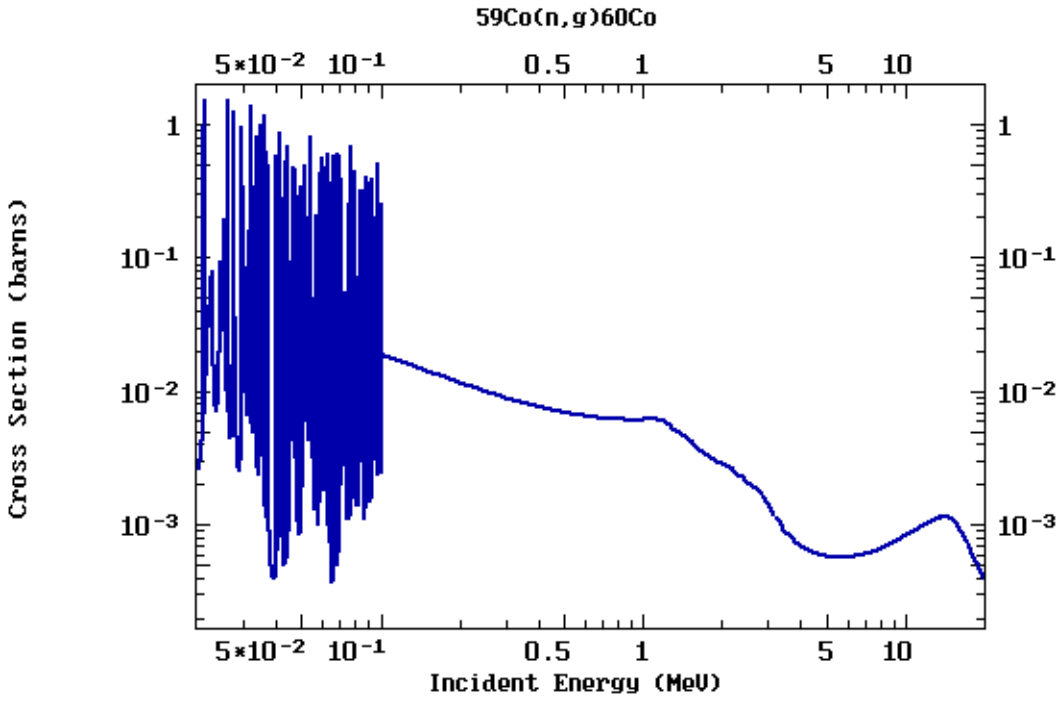

Figure 22 – Co Cross Section (log/log)

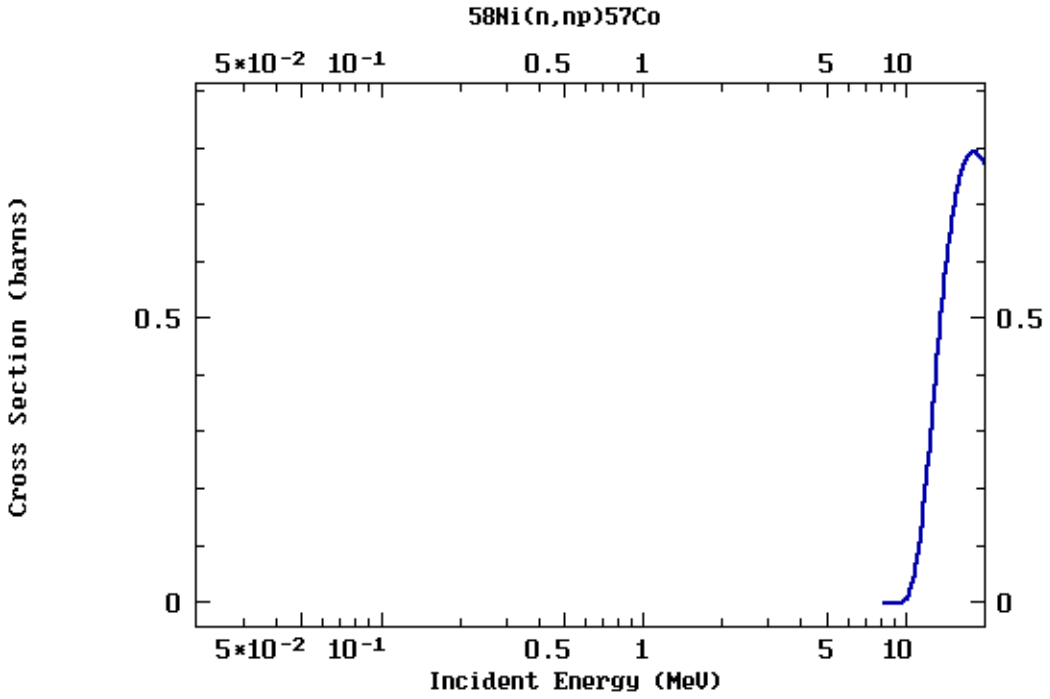

Figure 23 – Ni Cross Section (lin/log)

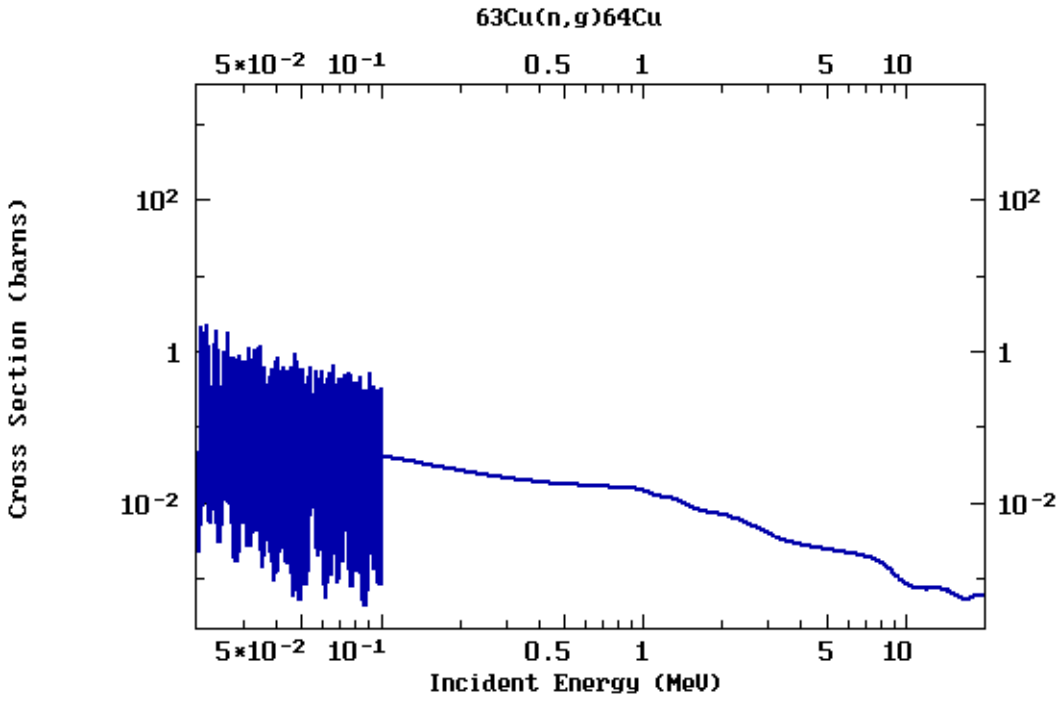

Figure 24 – Cu Cross Section (log/log)

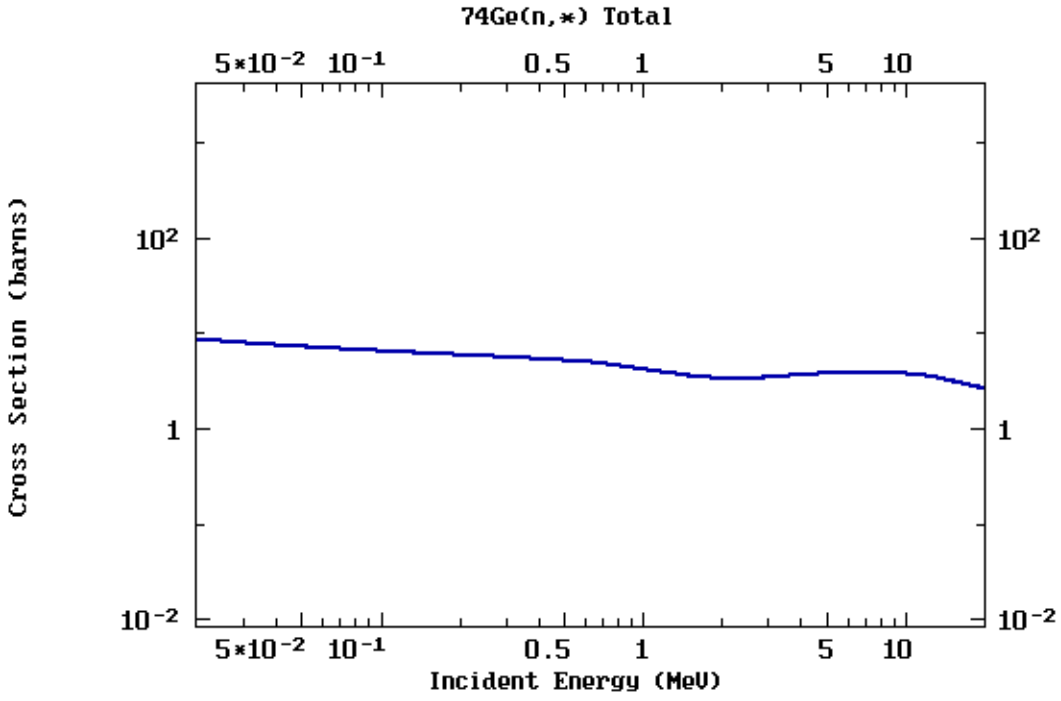

Figure 25 – Ge Cross Section (log/log)

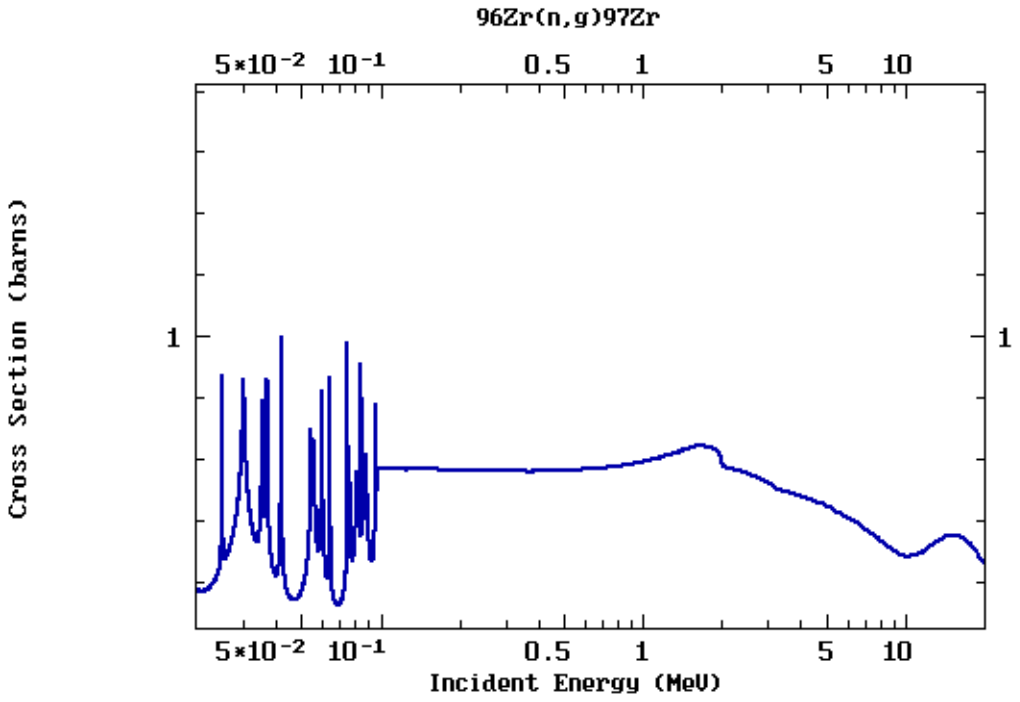

Figure 26 – Zr Cross Section (log/log)

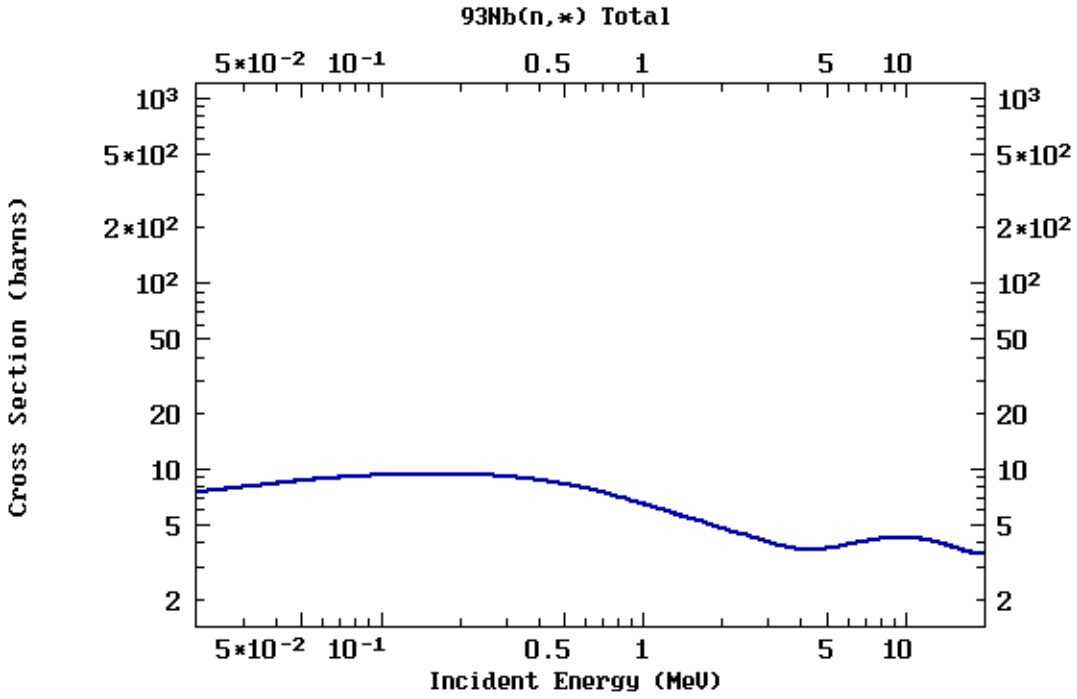

Figure 27 – Nb Cross Section (log/log)

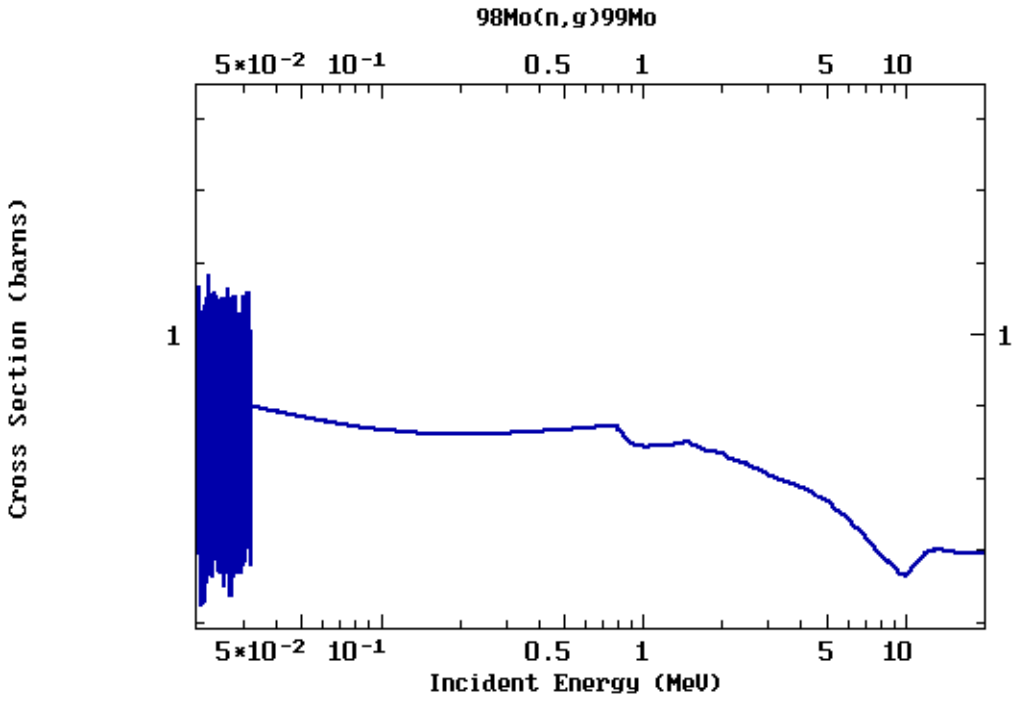

Figure 28 – Mo Cross Section (log/log)

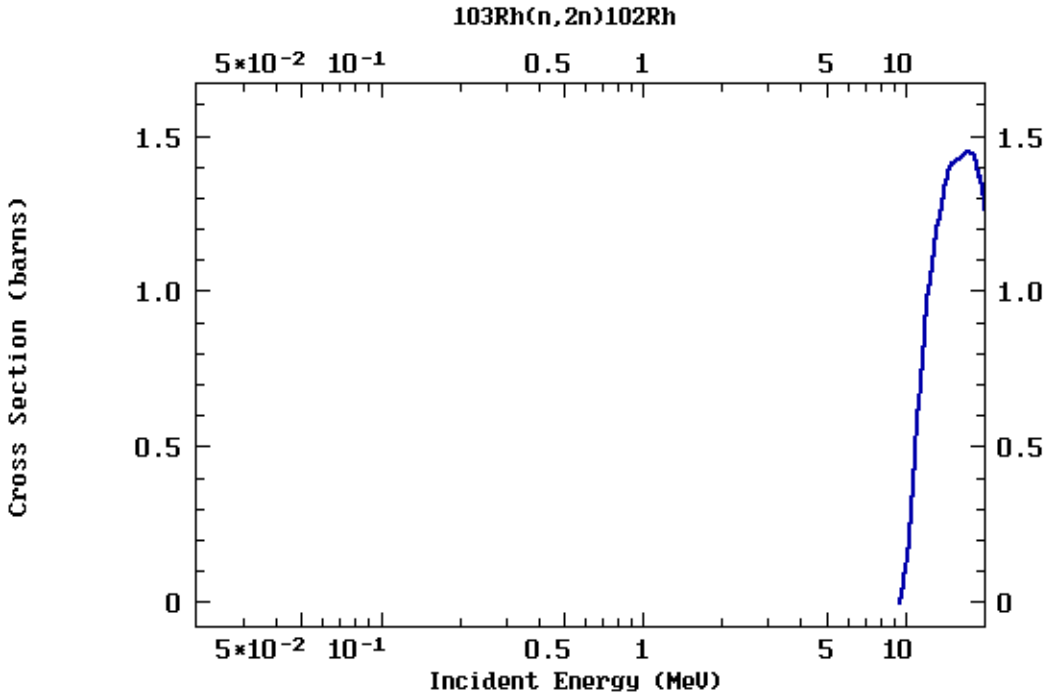

Figure 29 – Rh Cross Section (lin/log)

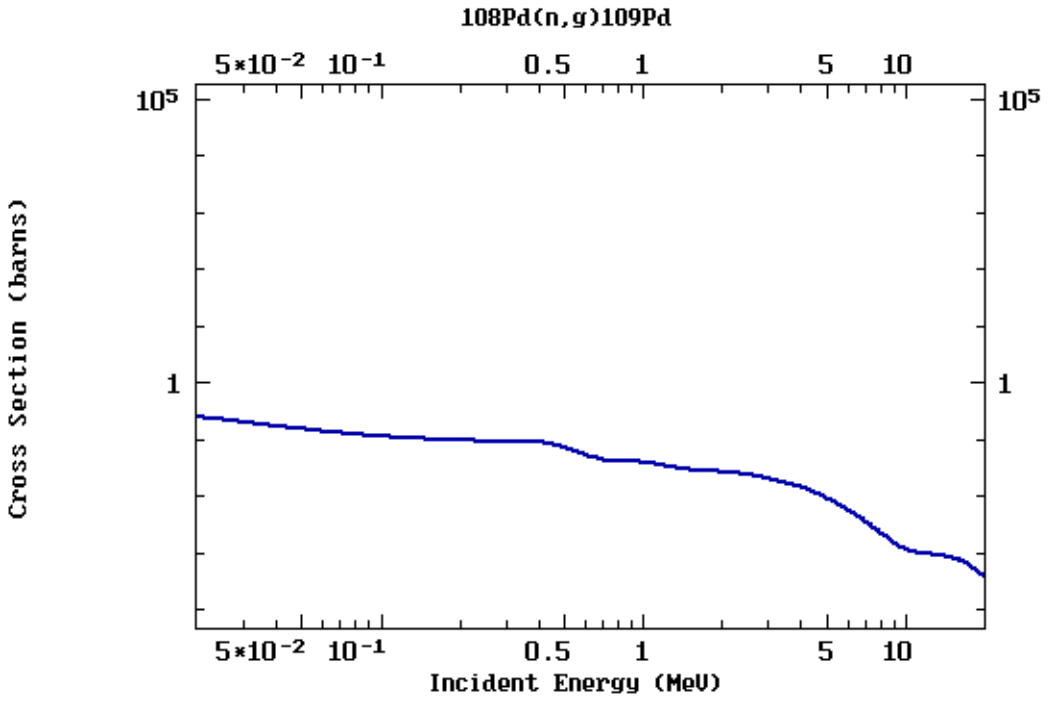

Figure 30 – Pd Cross Section (log/log)

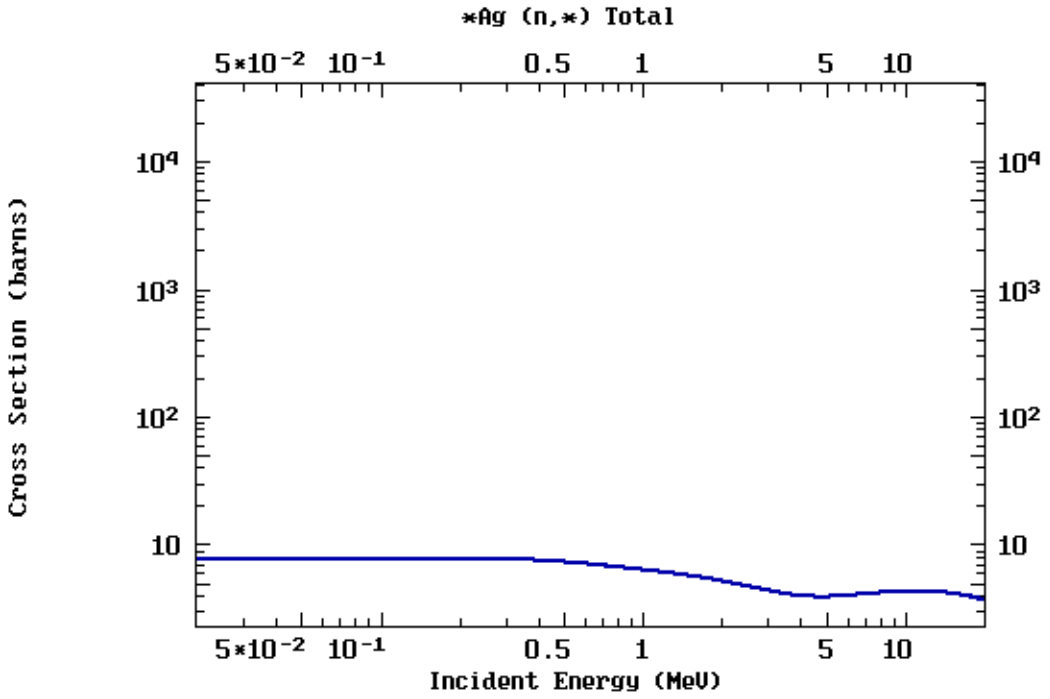

Figure 31 – Ag Cross Section (log/log)

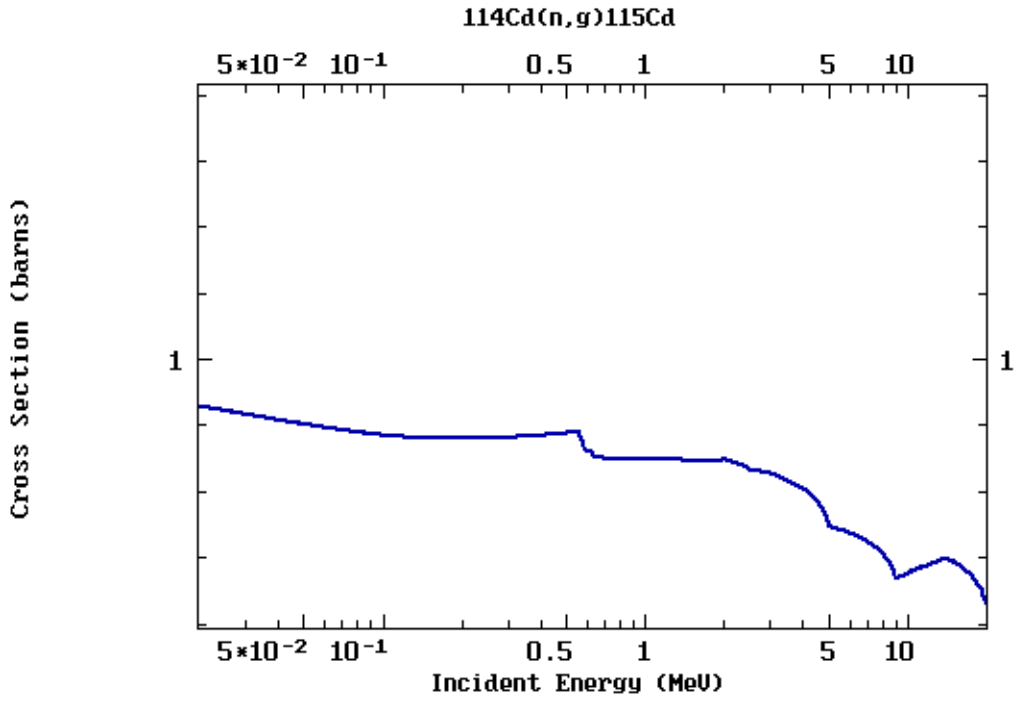

Figure 32 – Cd Cross Section (log/log)

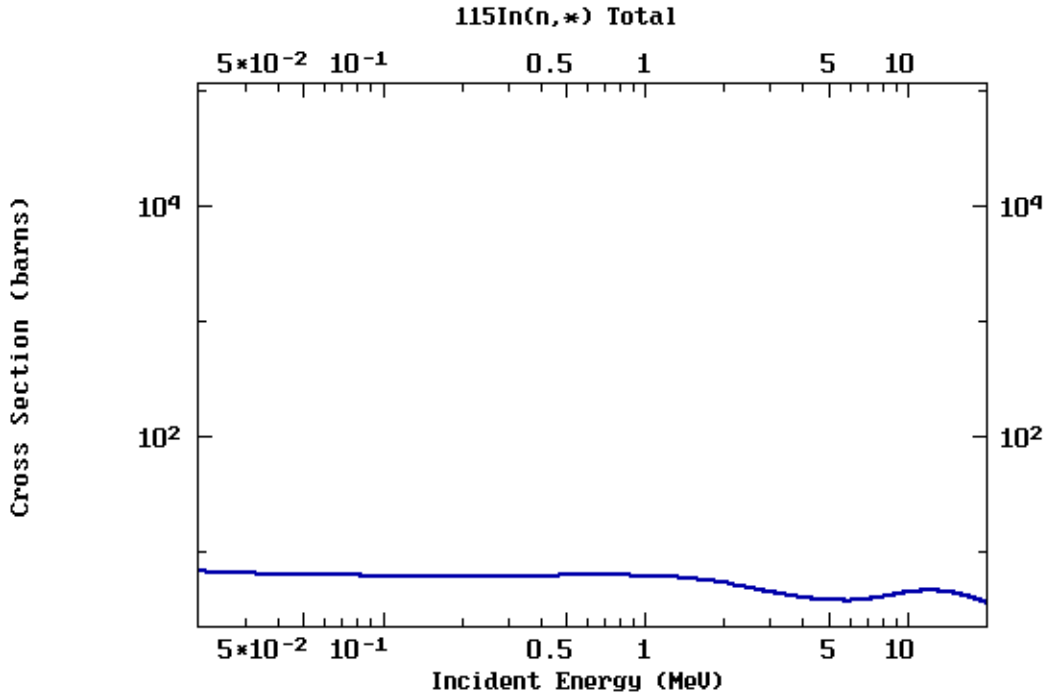

Figure 33 – In Cross Section (log/log)

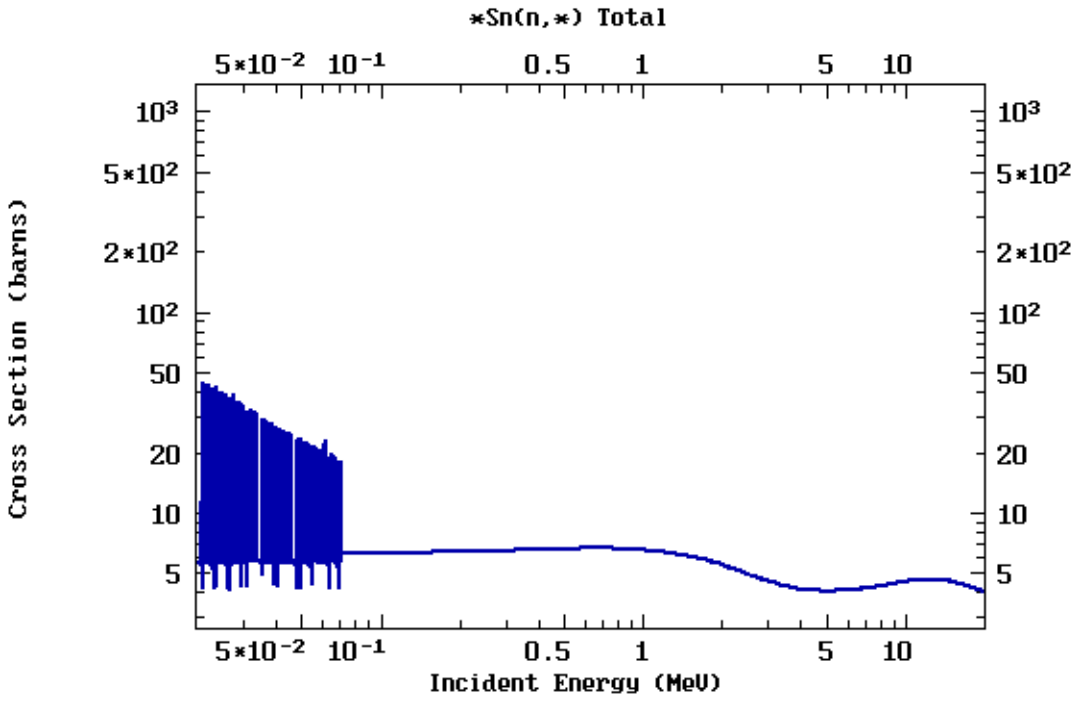

Figure 34 – Sn Cross Section (log/log)

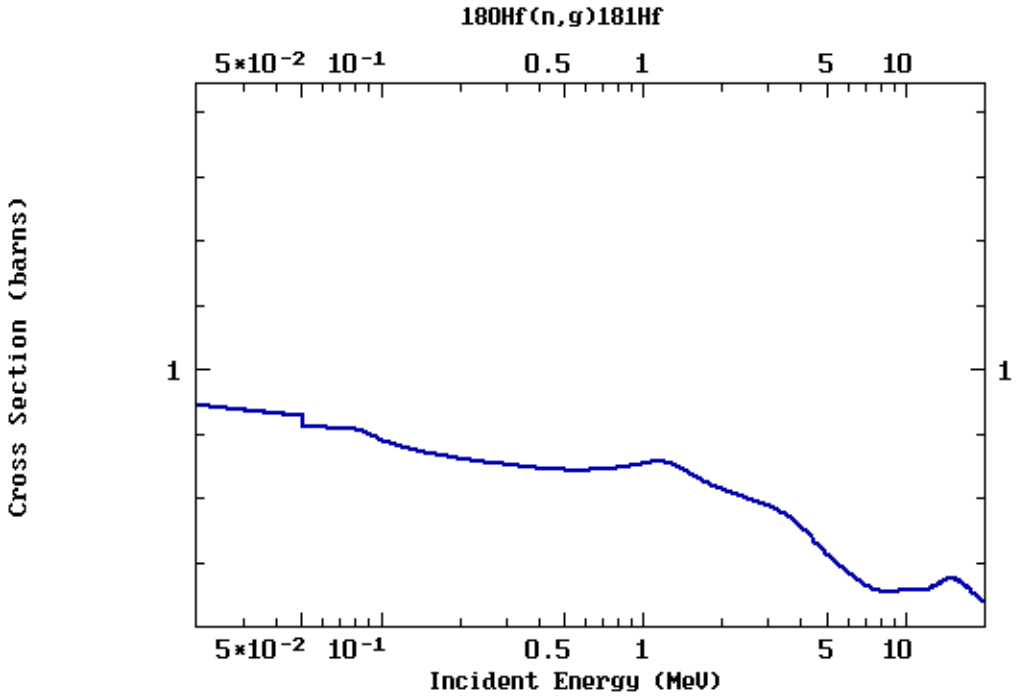

Figure 35 – Hf Cross Section (log/log)

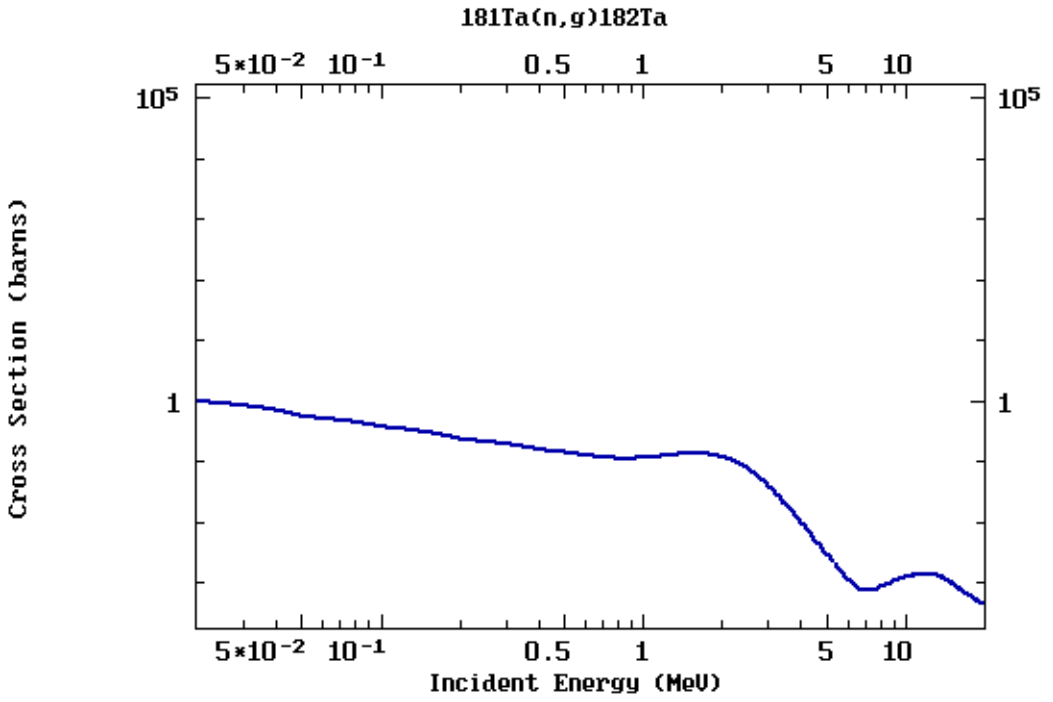

Figure 36 – Ta Cross Section (log/log)

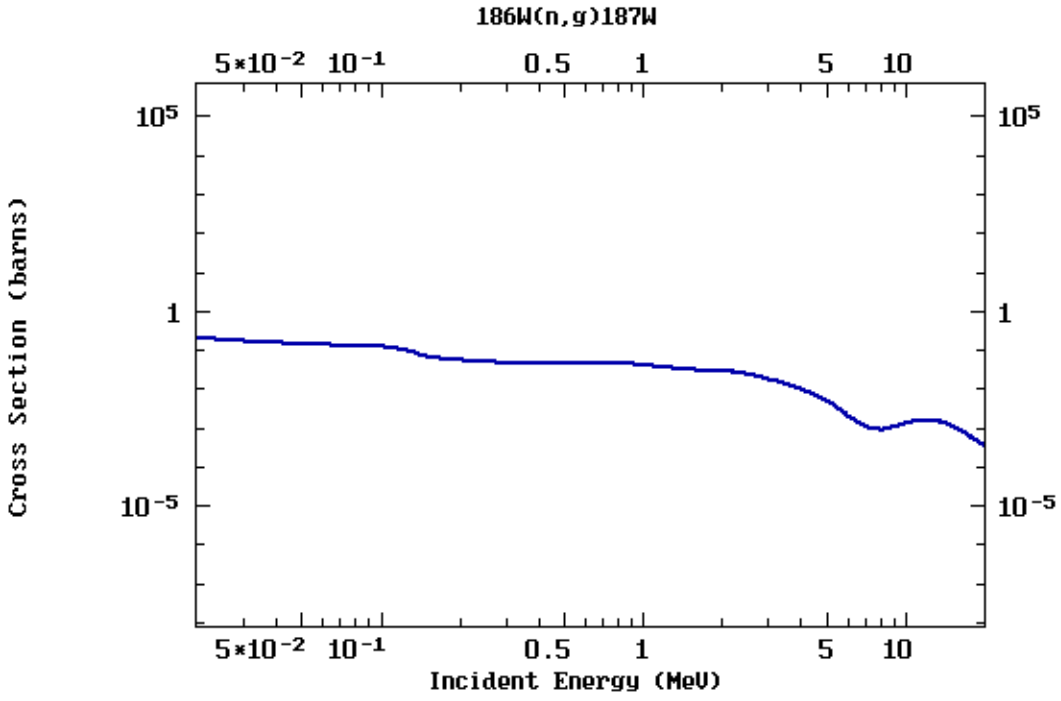

Figure 37 – W Cross Section (log/log)

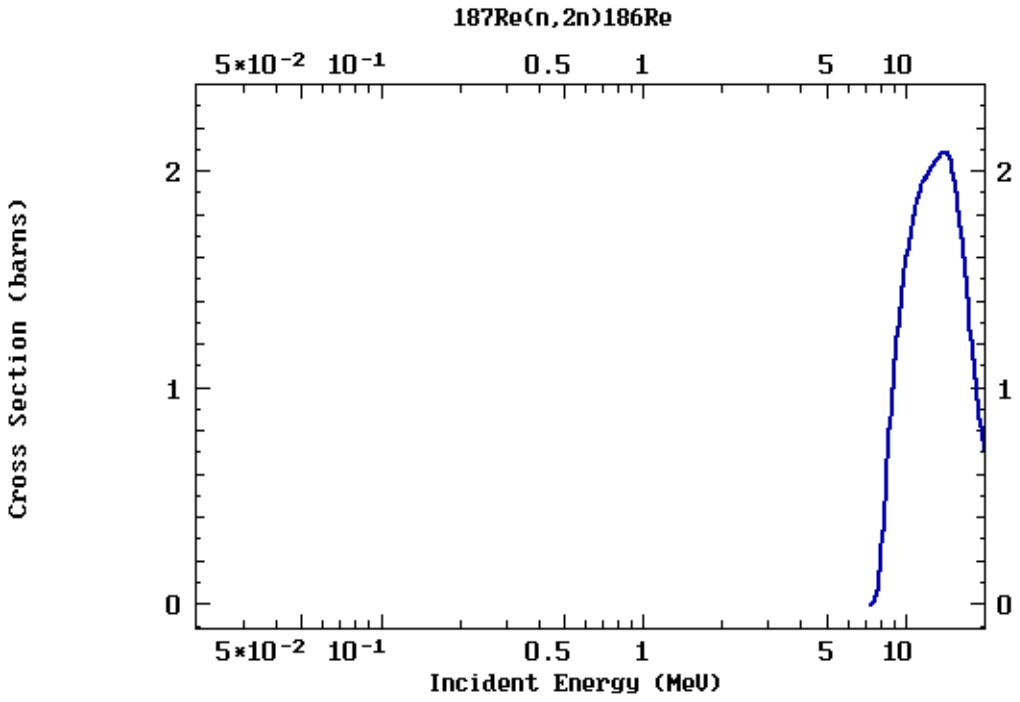

Figure 38 – Re (Threshold Reaction) Cross Section (lin/log)

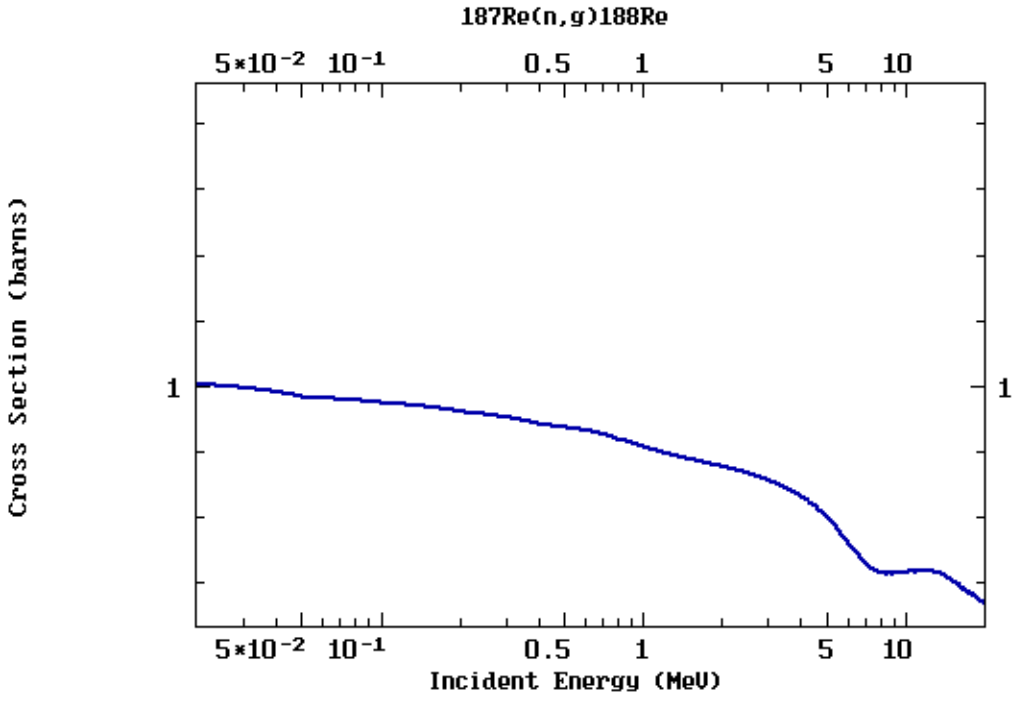

Figure 39 – Re (No Threshold Reaction) Cross Section (log/log)

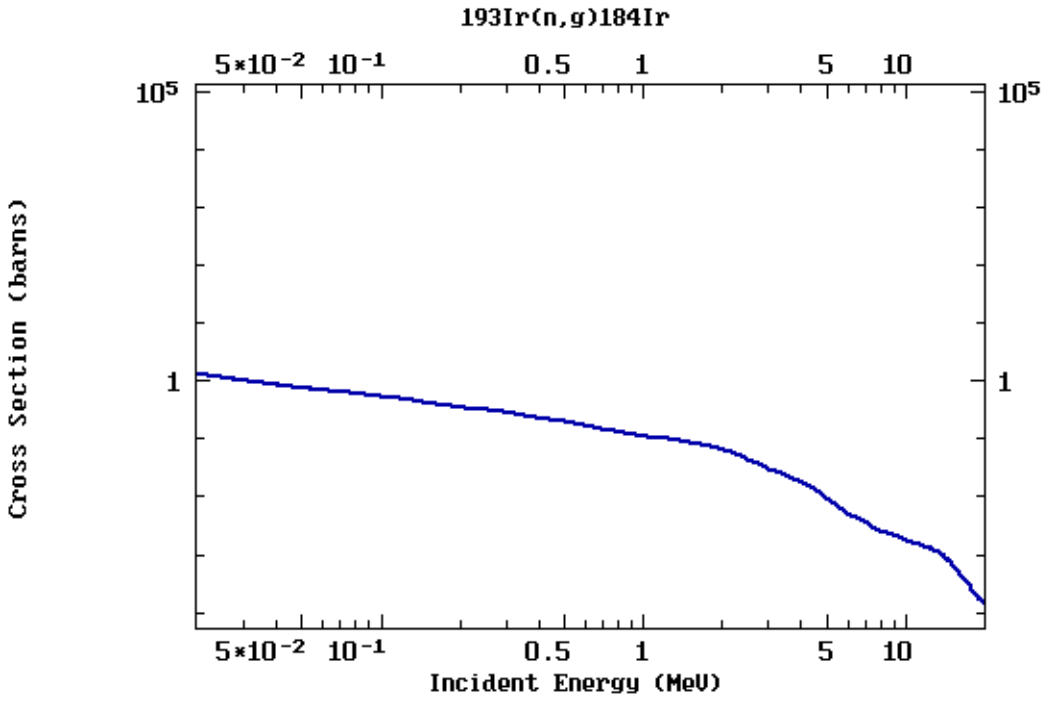

Figure 40 – Ir Cross Section (log/log)

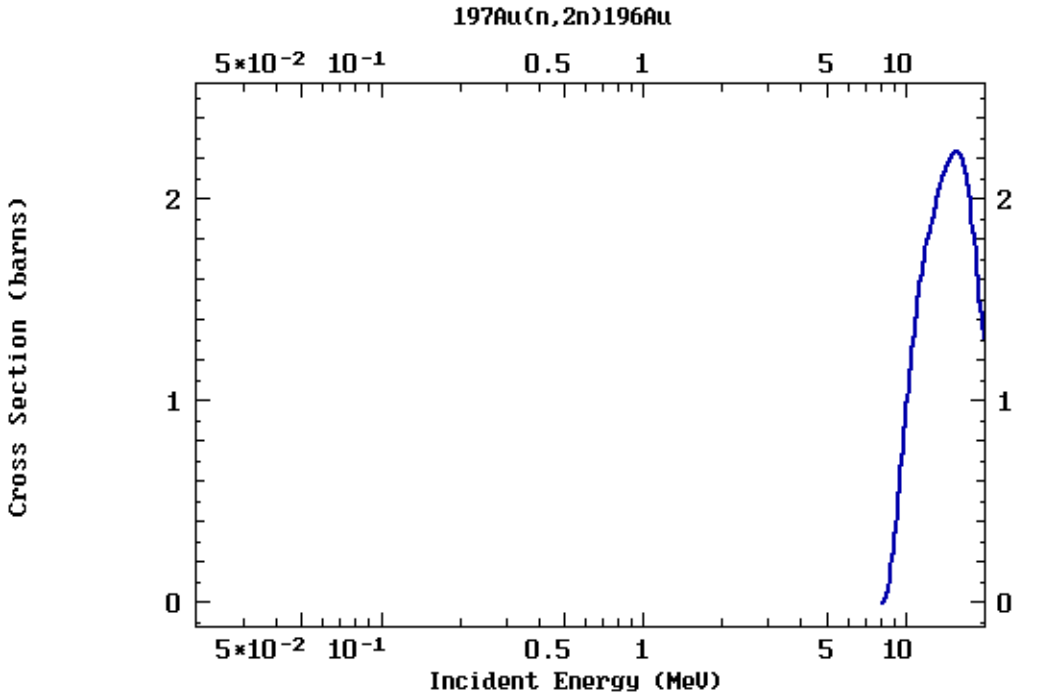

Figure 41 – Au (Threshold Reaction) Cross Section (lin/log)

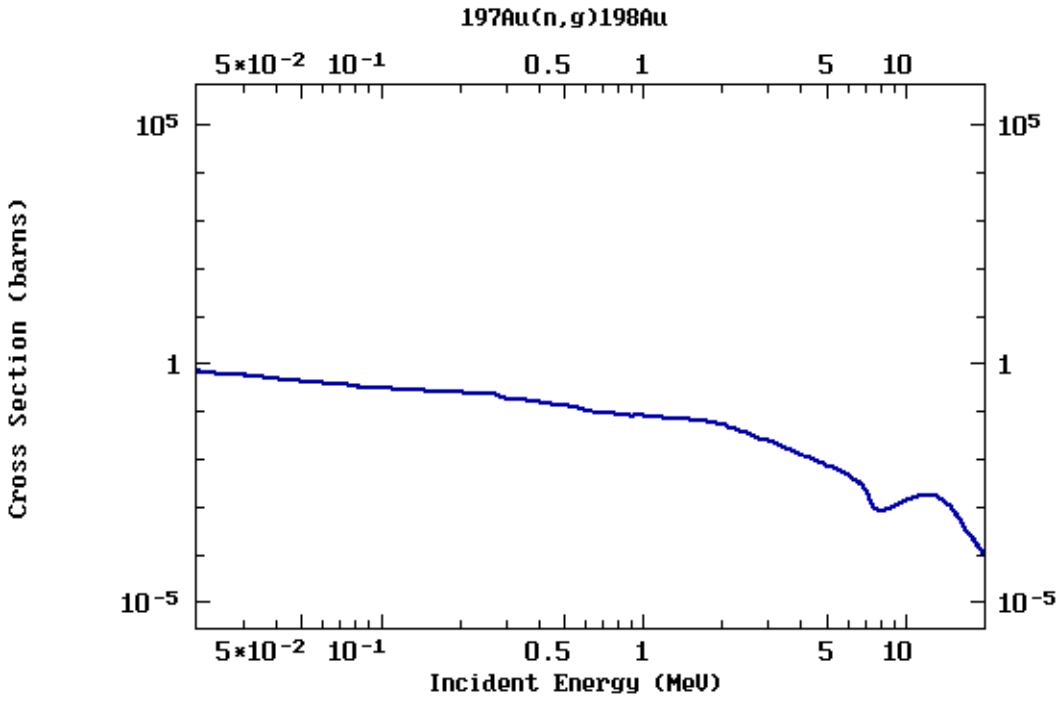

Figure 42 – Au (No Threshold Reaction) Cross Section (log/log)

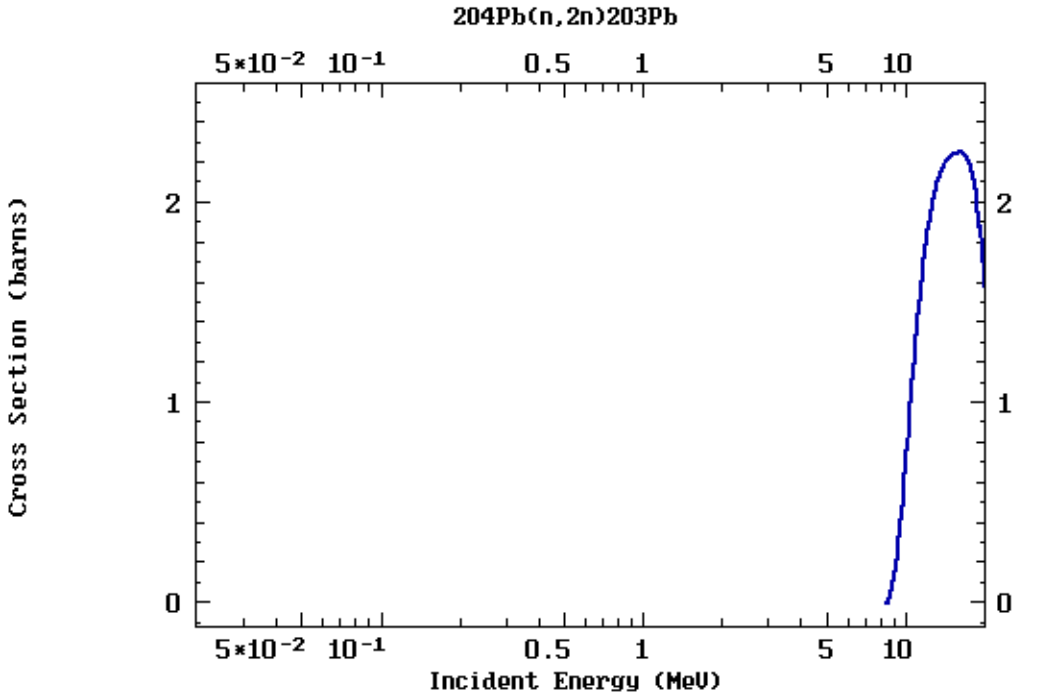

Figure 43 – Pb Cross Section (lin/log)

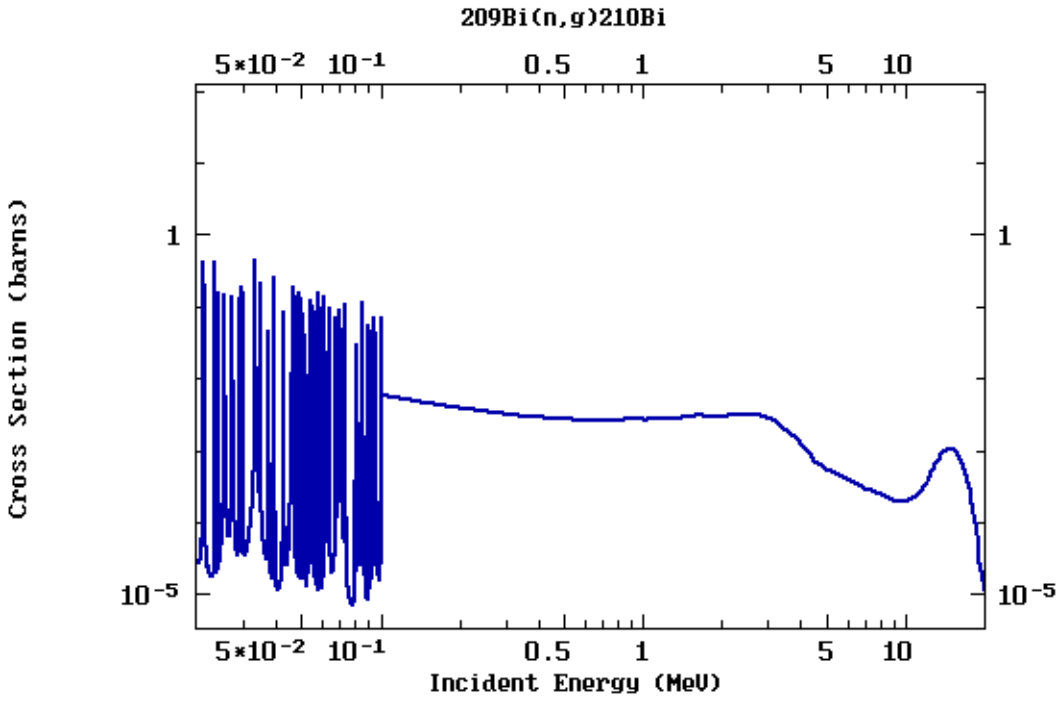

Figure 44 – Bi Cross Section (log/log)

REFERENCES

[1] White House, "National Security Strategy," United States Government, Washington, D.C., 2015.

[2] J. O. Johnson, "Development of Activation Foil Integrated Detector System," Oak Ridge National Laboratory, Oak Ridge, TN, 2015.

[3] ASTM International, "ASTM E261," 2016. [Online]. Available: www.astm.org.

[4] ASTM International, "ASTM E526," 2017. [Online]. Available: www.astm.org.

[5] E. William C. Roesch, "US – Japan Joint Reassessment of Atomic Bomb Radiation Dosimetry in Hiroshima and Nagasaki, Dosimetry System 1986 (DS86), Volumes 1 and 2," Radiation Effects Research Foundation – a Cooperative Japan – United States Research Organization, Japan, 1987.

[6] R. W. Young and G. D. Kerr, "Reassessment of the Atomic Bomb Radiation Dosimetry for Hiroshima and Nagasaki -- Dosimetry System 2002," Radiation Effects Research Foundation, 2005.

[7] K. Kato, M. Yamamoto, T. Kumamaru, Y. Yamamoto, M. Habara, T. Aoyama and Y. Yoshizawa, "Euoprium Isolation from Silicate Rock Samples Exposed to Hiroshima Atomic Bomb Neutrons," *Analytical Sciences,* vol. 3, pp. 493-497, 1987.

[8] D. E. Peplow, Z. W. Bell and S. P. Hamilton, "Identification of Leakage Spectra from Neutron Activation in Glass/Cherenkov Detectors," in *ANS RPSD 2014 - 18th Topical Meeting of the Radiation Protection & Shielding Division of ANS*, Knoxville, 2014.

[9] B. E. Watt, "Energy Spectrum of Neutrons from Thermal Fission of U-235," *Phys. Rev.,* vol. 87, no. 6, pp. 1037-1041, 1952.

[10] J. E. Lepstone, "Watt Parameters for the Los Alamos Model: Subroutine getab," Los Alamos National Laboratory, Los Alamos, 2007.

[11] D. E. Cullen, "Sampling ENDL," Lawrence Livermore National Laboratory, Livermore, 2004.

[12] N. P. M. Laboratory, "XCOM: Photons Cross Section Database," 11 12 2018. [Online]. Available: https://www.nist.gov/pml/xcom-photon-cross-sections-database. [Accessed 11 12 2018].

[13] H. Hirayama, "Lecture Note on Photon Interactions and Cross Sections," in *International Conference on the Monte Carlo 2000*, Lisbon, Portugal, 2000.

[14] Cross Section Evaluation Working Group, "ENDF Database," Brookhaven National Laboratory, Upton, 2018.

[15] US Government, Nuclear Matters Handbook, Washington: US Goverment, 2016.